ISTANBUL TECHNICAL UNIVERSITY ★ GRADUATE SCHOOL

ADSORPTIVE REMOVAL OF HEAVY METAL IONS FROM AQUEOUS SOLUTION USING METAL ORGANIC FRAMEWORK

Ph.D. THESIS

FADHIL ABID ELAIWI

Department of Chemical Engineering

Chemical Engineering Programme

MAY 2021

ISTANBUL TECHNICAL UNIVERSITY ★ GRADUATE SCHOOL

ADSORPTIVE REMOVAL OF HEAVY METAL IONS FROM AQUEOUS SOLUTION USING METAL ORGANIC FRAMEWORK

Ph.D. THESIS

FADHIL ABID ELAIWI

(506162004)

Department of Chemical Engineering

Chemical Engineering Programme

Thesis Advisor: Prof. Dr. Ahmet SİRKECİOĞLU

MAY 2021

ISTANBUL TEKNİK ÜNİVERSİTESİ ★ LİSANSÜSTÜ EĞİTİM ENSTİTÜSÜ

SULU ÇÖZELTİDEN AĞIR METAL İYONLARININ METAL ORGANİK KAFES KULLANARAK ADSORPSİYON YOLUYLA UZAKLAŞTIRILMASI

DOKTROA TEZİ

FADHIL ABID ELAIWI
(506162004)

Kimya Mühendisliği Bölümü

Kimya Mühendisliği Programı

Tez Danışmanı: Prof. Dr. Ahmet SİRKECİOĞLU

MAYIS 2021

FADHIL ABID ELAIWI, a Ph.D. student of ITU Graduate School student ID 506162004, successfully defended the thesis/dissertation entitled "ADSORPTIVE REMOVAL OF HEAVY METAL IONS FROM AQUEOUS SOLUTION USING METAL ORGANIC FRAMEWORK", which he prepared after fulfilling the requirements specified in the associated legislations, before the jury whose signatures are below.

Thesis Advisor: **Prof. Dr. Ahmet SİRKECİOĞLU** .....
Istanbul Technical University

Jury Members: **Prof. Dr. Mehmet Göktuğ AHUNBAY** .....
Istanbul Technical University

Prof. Dr. Fatma Seniha GÜNER .....
Istanbul Technical University

Assoc. Prof. Dr. Alper UZUN .....
Koç University

Prof. Dr. Sibel SARGUT .....
Marmara University

Date of Submission : 24 March 2021

Date of Defense : 7 May 2021

FOREWORD

First and foremost, I would like to thank Almighty God for reasons too numerous to mention. , and especially for giving me the confidence and strength to pursue my ambition in postgraduate studies.

I owe my deepest gratitude with my sincere appreciation to Prof. Ahmet Sirkecioğlu for his kind supervision, motivation, great suggestions, his guidance in writing up this thesis, and for introducing me to this interesting field of Metal Organic Frameworks.

My deepest gratitude and thanks to Jury members for their scientific guidance and support.

Additionally, I would like to extend my great appreciation to all members of the chemical engineering department, chemistry metallurgy faculty. graduate school, Istanbul technical university for their help and support.

I would like to convey my sincere appreciation to all the staff of Al-Furat Al-Awsat technical university, Iraq for their support and encouragement.

I am also thankful to the secretaries and administrative staff in the technical college /Al-Mussiab, Babylon, Iraq who were always ready to assist me when I needed help.

I wish to express gratefulness to all my colleagues in the power mechanics techniques engineering department, technical college /Al-Mussiab. Babylon, Iraq for their continual guidance.

My heartfelt thanks to the spirits of my parents, sisters, and brothers; they have provided me the benefits in my whole life.

Finally, I would like to thank my wife, and my daughters, for their patience, support, encouragement, and sacrifice to fulfill my ambitions.

MAY 2021

FADHIL ELAIWI
(Assistant lecturer)

TABLE OF CONTENTS

Page

ABBREVIATIONS

FT-IR **:** Fourier Transform Infrared
MIL **:** Materials of Institute Lavoisier
MOFs **:** Metal-organic Frameworks
PSM **:** Post-synthetic Modification
PXRD **:** Powder X-ray diffraction
SEM **:** Scanning Electron Microscopy
TGA **:** Thermogravimetric analysis

SYMBOLS

A	**:** The Integrated Area Under Breakthrough	**-**
B	**:** Langmuir Isotherm Constant	L/mg
C	**:** Value Of Intercept In intra-Particle Diffusion Kinetic Model	mg/g
$\mathbf{C_{ads}}$	**:** Metal Adsorbed Concentration	mg/l
$\mathbf{C_e}$	**:** Metal ion Concentration At Equilibrium	mg/L
$\mathbf{C_o}$	**:** Initial Metal Ion Concentration	mg/L
H	**:** Height of adsorbent in the fixed bed	cm
$\mathbf{k_1}$	**:** Rate Constant of Pseudo-First Kinetic Model	min^{-1}
$\mathbf{K_2}$	**:** Rate Constant Pseudo-Second Order Kinetic Model	mg/g.min
$\mathbf{K_F}$	**:** Freundlich Constants (Capacity Uptake)	-
$\mathbf{K_{id}}$	**:** Rate Constant Of Intra-Particle Diffusion Kinetic Model	$mg/gm.\ min^{1/2}$
$\mathbf{K_s}$	**:** Sips constant	L/mg
$\mathbf{k_{th}}$	**:** Thomas Kinetic Constant	mL/min.mg
$\mathbf{k_{YN}}$	**:**Yoon-Nelson rate constant	min^{-1}
M	**:** Mass Of Adsorbent	g
n	**:** Freundlich Constants (Adsorption Intensity)	-
Q	**:** Rete Of Flow	mL/min
$\mathbf{Q_e}$	**:** Adsorption Capacity At Equilibrium State	mg/g
$\mathbf{q_e}$	**:** Adsorption Capacity (flow system)	mg/g
$\mathbf{q_o}$	**:** Maximum Equilibrium Column Capacity	mg/g
$\mathbf{Q_m}$	**:** Mono-layer Uptake Capacity	mg/g
$\mathbf{Q_t}$	**:**Adsorption Capacity At Time t	mg/g
$\mathbf{q_{total}}$	**:** Total mass of ions moved through the packed column	mg
RE%	**:** Percentage Of The Removing Efficiency	/
$\mathbf{t_b}$	**:** Time of breakthrough	min
$\mathbf{t_e}$	**:** Time of exhusted	min
V	**:** Volume Of Solution	L

Greek symbols

τ	**:** Time Consumed To 50% Of Adsorbate Breakthrough Time, min

LIST OF TABLES

Page

LIST OF FIGURES

Page

ADSORPTIVE REMOVAL OF HEAVY METAL IONS FROM AQUEOUS SOLUTION USING METAL ORGANIC FRAMEWORK

SUMMARY

Industrialization and rapid increase in human population are the cause of increase in wastewater generation. Depending on the source, these wastes may contain hazardous pollutants such as heavy metals, toxic organic compounds, dissolved inorganic solids and etc. Heavy metals are the serious threat to environmental and human health. Due to their toxicity and carcinogenic effects, close attention must be paid to heavy metals containing wastewaters. Even very small amounts of heavy metals can result in severe physiological and neurological damages. Therefore, numerous processes have been developed to treat wastewater minimize this health hazard potential. These processes include membrane filtration, ion exchange, adsorption, chemical precipitation, nanotechnology treatments, electrochemical and advanced oxidation processes.

Ion exchange and adsorption are both physicochemical methods used to treat heavy metal containing wastewaters. In both cases high surface are plays an important role. As a new generation of crystalline porous materials, metal-organic frameworks (MOFs) possess high surface area, tunable pore structure and functionalizable surfaces. With these attributes, MOFs have an essential role in several fields, including wastewater treatment.

Based on the affinity of amino groups in chelating sites for heavy metal ions, a porous metal-organic framework (MOF) [ED-MIL-101(Cr)] were synthesized as an adsorbent for lead, copper, and cadmium ions. Hydrothermal method was used to synthesize the MOF samples.

The functionalized MOF samples were characterized by powder X-ray diffraction (PXRD) to investigate the functionalization process and compare the synthesized MOF with the pristine MIL-101(Cr) samples. Fourier Transform Infrared (FT-IR) spectroscopy was used to analize the functional groups of the adsorbent before and after the treatment process which can be useful in estimating the mechanism for the recovry process and assess the relationship between the ions and the adsorbents sites. Scanning electron microscopy (SEM) and thermogravimetric analysis (TGA), were also performed to investigate crystal structure and the thermal stability of the MOFs in a specified temperature range, respectively. Finally, the surface characteristics of the samples and the particles size distribution were investigated with N_2 adsorption-desorption conducted at 77 K.

In order to investigate the adsorption performances of ED-MIL-101(Cr) for the chosen heavy metal cations (Pb(II), Cu(II), and Cd(II) ion), batch experiments were conducted with single, binary, and ternary metal solutions. During these experiments the effect of experimental conditions such as pH, adsorbent dosage, initial concentration, were investigated.

With the aim of evaluation of conditions for removing of the three metal ions using ED-MIL-101(Cr), several isotherm models were tested to choose the best fit model with the experimental data. Normal and extended forms of Freundlich, Langmuir, and Sips isotherms were adopted to analyze the adsorption behavior of the MOF samples. ED-MIL-101(Cr) exhibits maximum adsorption capacities (mg/g) of 82.55, 69.9 and 63.15 mg/g for Pb(II), Cu(II) and Cd(II), respectively. The experimental data revealed that the adsorption capacity of the adsorbent for the different metal ions at the same concentration mainly depends on the affinity of the adsorbent which was in the order of Pb(II) >Cu(II) > Cd(II) in single ion solution. This selectivity order is governed mainly by ionic features such as ionic radius, electronegativity, and hydrated ionic radius.

The influence of ionic interaction between the competitive ions in a multi-ion solution namely interaction factor is quantitatively studied and tabulated its values for multi-ion systems. For further studies, kinetics models applied to investigate the Pb(II), Cu(II), and Cd(II) ions adsorption mechanism on ED-MIL-101(Cr). Also, rate-control steps were determined using kinetic method. Linear forms of pseudo-first order, pseudo-second order, and intra-particle diffusion equations were used to interpret the kinetic data. It was observed that the kinetic data that obtained with batch adsorption processes were well fitted with pseudo-second-order model. Also the regeneration process for exhausting ED–MIL–101(Cr) was carried out to assess the recyclability of ED-MIL-101(Cr) for adsorption of lead, copper, and cadmium ions. It was observed that there was an insignificant change in the adsorption efficiency of ED-MIL-101(Cr) samples after three adsorption-regeneration cycles.

In order to simulate the real-life experience adsorption experiments conducted also in dynamic system. For this part of the experimental work, a fixed bed of ED-MIL-101(Cr) was prepared for the continuous removal of Pb(II), Cu(II), and Cd(II) ions from the aqueous solutions.

A series of experiments were carried out in the fixed bed system to obtain the breakthrough curves data for the adsorption of single and ternary metal ions. The effects of different operating conditions such as static bed height (2, 4, and 6 cm), flow rate (10, 15, and 20 mL/min), and initial concentration of heavy metal ions (50, 75, and 10 mg/L) on the removal efficiency were investigated. The experimental breakthrough data of three metal ions were fitted well with the theoretical model. The breakthrough curves for single and multiple systems showed that Pb(II) has the longest breakthrough time compared with other metals indicating a high affinity toward this ion while Cd(II) had the shortest breakthrough time.

Thomas Model and Yoon-Nelson models were used to evaluate the breakthrough curves and evaluate the dynamic data. The results from these two models suggest that the maximum adsorption capacity of the investigated heavy metal ions from single aqueous solutions are in the order of Pb(II) > Cu(II) > Cd(II). These results are in agreement with the experimental data which are also related to the affinity of the adsorbent for the

adsorbed ions. Comparably, Yoon-Nelson model is the best model for the data obtained for the metal adsorption experiments conducted with various bed lengths.
It can be concluded that amino-functionalized MIL-101(Cr) was found to be a promising candidate for metal ion removal from the aqueous environment.

SULU ÇÖZELTİDEN AĞIR METAL İYONLARININ METAL ORGANİK KAFES KULLANARAK ADSORPSİYON YOLUYLA UZAKLAŞTIRILMASI

ÖZET

Sanayileşme ve insan nüfusundaki hızlı artış, atık su üretiminin artmasına yol açmaktadır. Bu atıklar, kaynağına bağlı olarak ağır metaller, toksik organik bileşikler, çözünmüş inorganik katılar vb. gibi tehlikeli kirleticiler içerebilir. Ağır metaller çevre ve insan sağlığı için ciddi bir tehdittir. Toksisiteleri ve kanserojen etkileri nedeniyle ağır metal içeren atıksulara çok önem verilmelidir. Çok küçük miktarlardaki ağır metaller bile ciddi fizyolojik ve nörolojik hasarlara neden olabilir. Bu nedenle, atık suyu arıtmak için bir başka deyişle bu sağlık tehlikesi potansiyelini en aza indirmek için çok sayıda proses geliştirilmiştir. Bu işlemlere membran filtrasyonu, iyon değişimi, adsorpsiyon, kimyasal çöktürme, nanoteknolojik işlemler, elektrokimyasal ve ileri oksidasyon gibi prosesler örnek olarak verilebilir.

İyon değişimi ve adsorpsiyon, ağır metal içeren atık suları arıtmak için kullanılan fizikokimyasal yöntemlerdir. Her iki durumda da yüksek yüzey alanı önemli bir rol oynar. Yeni nesil kristal gözenekli malzemeler olan metal-organik kafesler (MOF'ler), yüksek yüzey alanına, ayarlanabilir gözenek yapısına ve fonksiyonelleştirilebilir yüzeylere sahiptir. Bu özellikleriyle MOF'ler, atık su arıtımı da dahil olmak üzere birçok alanda kullanım alanı bulabilmektedirler.

Bu çalışmada atık sulardan ağır metallerin uzaklaştırılmasında kullanılabilecek adsorban sentezlenmiştir. Sulu çözeltilerdeki ağır metal iyonları için şelatlama bölgelerindeki amino gruplarının afinitesi göz önünde bulundurularak, kurşun, bakır ve kadmiyum iyonları için adsorban olarak krom bazlı gözenekli bir metal-organik kafes (MOF) [ED-MIL-101(Cr)] hazırlanmıştır. MOF numunelerinin sentezlenmesinde hidrotermal yöntem kullanılmıştır.

Fonksiyonelleştirilmiş MOF örnekleri, fonksiyonelleştirme sürecini izlemek için fonksiyonelleştirilmemiş MOF örneği de sentezlenmiştir. Her iki örneğin kristaliniteleri toz X-ışını kırınımı (PXRD) ile belirlenmiştir. Adsorbanın fonksiyonelleştirme öncesi ve sonrasındaki fonksiyonel gruplarını analiz etmek için Fourier Dönüşümü Kızılötesi (FT-IR) spektroskopisi yönteminden yararlanılmıştır. FT-IR yönteminden aynı zamanda metal adsorpsiyonunun mekanizmasını belirlemekte, ve metal katyonları ile adsorpsiyon merkezleri arasındaki ilişkiyi değerlendirmede de yararlanılmıştır. MOF'ların kristal yapısını ve belirli bir sıcaklık aralığındaki ısıl kararlılığını belirleyebilmek için sırasıyla taramalı elektron mikroskobu (SEM) görüntülerinden ve termogravimetrik analiz (TGA)

yönteminden yararlanılmıştır. Son olarak, 77 K'de gerçekleştirilen N_2 adsorpsiyon-desorpsiyonu ile numunelerin yüzey özellikleri ve gözenek açıklığı dağılımı belirlenmiştir.

ED-MIL-101(Cr) örneğinin seçilen ağır metal katyonlar (Pb(II), Cu(II) ve Cd(II) iyonu) için adsorpsiyon performanslarını araştırmada tekli, ikili, ve üçlü metal çözeltileri ile deneyler gerçekleştirilmiştir. Bu deneylerde pH, adsorban dozajı, başlangıç konsantrasyonu gibi deneysel koşulların etkisi araştırılmıştır.

ED-MIL-101(Cr) kullanılarak Pb, Cu ve Cd katyonlarının adsorpsiyon yoluyla uzaklaştırılmasında elde edilen deneysel veriler Freundlich, Langmuir ve Sips Modelleri kullanılarak değerlendirilmiştir. Hazırlanan ED-MIL-101(Cr) örneklerinin, Pb(II), Cu(II) ve Cd(II) adsorpsiyon kapasiteleri sırasıyla, 82.55, 69.9 ve 63.15 mg/g olarak saptanmıştır. Kesikli sistemde gerçekleştirilen tek katyonlu adsorpsiyon deneylerinden katyon MOF örneklerinin katyon seçiciliğinin Pb(II) >Cu(II) > Cd(II) sırasıyla değiştiğini göstermiştir. Bu sıralamanın oluşmasında katyonların iyonik yarıçapı, elektronegativitesi ve sulu iyonik yarıçapını gibi iyonik özelliklerin büyük rol oynadığı gözlenmiştir.

Çok iyonlu bir çözeltide rekabetçi iyonlar arasındaki iyonik etkileşimin etkisi, etkileşim faktörü nicel olarak incelenmiştir. Çalışmanın sonraki aşamalarında, sürekli ortamda ED-MIL-101(Cr) üzerinde Pb(II), Cu(II) ve Cd(II) iyonlarının adsorpsiyon mekanizmasını araştırmak için kinetik modeller test edilmiştir. Ayrıca bu modeller kullanılarak adsorpsiyonda hız kontrol adımları belirlenmiştir. Bu verilerin yorumlanmasında yalancı birinci dereceden, yalancı ikinci dereceden ve parçacık içi difüzyon denklemlerinin lineer formları kullanılmıştır. Kesikli adsorpsiyon deneylerinden elde edilen verileri açıklamakta, test edilen modellerden yalancı ikinci dereceden modelin en iyi model olduğu belirlenmiştir. Kurşun, bakır ve kadmiyum iyonlarının adsorpsiyonu için ED-MIL-101(Cr)'nin geri dönüştürülebilirliğini değerlendirmek için ED-MIL-101(Cr)'nin rejenerasyon işlemi gerçekleştirilmiştir. Üç adsorpsiyon-rejenerasyon döngüsünden sonra ED-MIL-101(Cr) numunelerinin adsorpsiyon verimliliğinde önemsiz bir değişiklik olduğu gözlenmiştir.

Gerçek hayattaki deneyimleri benzeştirmek için dinamik sistemde de adsorpsiyon deneyleri gerçekleştirilmiştir. Deneysel çalışmanın bu kısmı için, sulu çözeltilerden Pb(II), Cu(II) ve Cd(II) iyonlarının sürekli olarak uzaklaştırılması için sabit bir ED-MIL-101(Cr) yatağı hazırlanmıştır.

Tekli ve ikili metal iyonların adsorpsiyon dönüm noktası eğrileri için sabit yatak adsorpsiyon kolonu kullanılarak bir dizi deney yürütülmüştür. Adsorpsiyon verimliliği üzerinde statik yatak yüksekliği (2, 4 ve 6 cm), akış hızı (10, 15 ve 20 mL/dak) ve ağır metal iyonlarının başlangıç konsantrasyonu (50, 75 ve 10 mg) gibi farklı çalışma koşullarının etkileri araştırılmıştır. Pb, Cu, ve Cd katyonlarının adsorpsiyon dönüm noktası eğrilerine farklı adsorpsiyon modelleri uygulanmıştır. Tekli ve çoklu katyon sistemlerinde elde edilen izotermler, MOF örneklerinin diğer metal katyonlara kıyasla Pb(II) iyonuna karşı yüksek bir afinite sahip olduğu belirlenmiştir. Sabit yatakta gerçekleştirilen adsorpsiyon deneyleri MOF örneklerinin en yüksek kapasiteyi Pb içeren sulu çözeltilerle, en düşük kapasiteyi ise Cd içeren sulu çözeltilere karşı sergilemiştir.

Dönüm noktası eğrilerini ve dinamik verileri değerlendirmek için Thomas Modeli ve Yoon-Nelson modellerinden yararlanılmıştır. Bu iki modelden elde edilen sonuçlar, tekli sulu çözeltilerden incelenen ağır metal iyonlarının maksimum adsorpsiyon kapasitesinin Pb(II) > Cu(II) > Cd(II) sırasıyla değiştiğini göstermiştir. Bu sıralama adsorbanla adsorbat

arasındaki çekimle açıklanabilmektedir. Benzer şekilde, Yoon-Nelson modelinin, çeşitli yatak uzunlukları ile gerçekleştirilen adsorpsiyon deneylerinden elde edilen verileri açıklayan en iyi model olduğu saptanmıştır.
Amino-fonksiyonelleştirilmiş MIL-101(Cr)'nin sulu ortamdan metal iyonlarının uzaklaştırılması için umut verici bir aday olduğu sonucuna varılabilir.

1. GENERAL INTRODUCTION

1.1 Introduction

The growth and the development in the global industries have resulted in the production of a significantly high-level concentration of contaminants in the effluents of these industrial activities. [1,2]. The most harmful elements among these contaminants are the heavy metals that were observed in released water from many sources such as mining, textile, Battery manufacturing, pharmaceutical industries, electroplating, and petroleum refining [3]. The heavy metals term is used to describe metals that have a molecular weight in the range of 63.5 to 200.6 and mass density higher than 5 g/cm^3 [4]. Common types of heavy metals are copper, cobalt, cadmium, zinc, lead, mercury and iron, etc. Since heavy metal ions are non-biodegradable and can accumulate in the living tissues they are considered toxic, carcinogenic, and led to detrimental effects for living organisms, and human beings [5-7].

Among the ions of heavy metals, the lead ion is considered highly toxic, an enzyme inhibitor, and a general metabolic poison that can accumulate in the brain, kidney bones and destroy these particular organs [8]. The water content of lead in an amount higher than the permissible limit can cause several diseases such as hepatitis, anemia, kidney disease, encephalopathy, and mental retardation [9].

Copper is one of the most commonly used heavy metals which is often found in the raw wastewater of many industries such as metal finishing, mining, and electroplating. The presence of copper ion in a concentration higher than the permitted level produces allergic contact dermatitis, corneal opacity, and neurological abnormalities [1]. Also, exposure to high concentrations of cadmium can cause severe health problems for human beings such as erythrocyte destruction, renal dysfunction, emphysema, and chronic pulmonary problems [10]. From the previous details, great efforts should be devoted to reducing the content of lead, copper, and cadmium ions in the water ecosystem to acceptable levels. Substantial analysis and development work has been allotted in the event of sturdy

technology for the remedy of heavy metals pollution. Thus far, various treatment strategies including ion exchange, chemical precipitation, membrane separation, chemical oxidation, electrochemical treatment, floatation, and adsorption, as well as biological approaches have been investigated to varying extents to figure out the most suitable method that is cost-effective, efficient, and demand less energy for its operation for remediation of heavy metals contaminations in waste product [11]. The applications, description, and economics of common methods for heavy metal ions removal were shown in Table 1.1 [12,13].

Among the previous-mentioned processes, adsorption is considered as the most extensively used method which has been employed for a wide variety of aquatic pollutants including heavy metals [14]. It exhibits significant advantages such as efficiency, wide availability, profitability, and simplicity in operation [15].

In general, the adsorption process describes a phenomenon that happens once a liquid solute or gas accumulates on a solid surface (adsorbent), forming a film of atoms or molecules (adsorbate). The adsorption of ions at the solid-liquid interface and its influence on ions mobility in the adsorption media is directly controlled by the diverse properties of the adsorbate and adsorbent. Adsorbents with a relatively high surface area, suitable pore volume and morphology, specific adsorption sites, electrostatic charge, and functional groups are capable of adsorbing pollutants from water [16]. Traditional adsorbents that have been extensively inspected and developed to date include those permanently porous substances such as activated carbons (AC), zeolites, carbon nanotubes (CNTs), metal oxide nanoparticles, etc. [17].

MOF-type materials have recently emerged as a special group of crystalline porous hybrid materials, are constructed from metal ions or clusters coordinated with organic ligands [18]. The particular interest of these classes of materials due to their inherent structural characteristics such as low densities, considerably large surface area, easy tenability, and modifiable pores [19–22]. Because of their unique properties, MOFs porous materials have significant applications in the fields of drug delivery [23], catalysis [24], adsorption [25] , separation, and gas storage [26]. However, their usage in the liquid phase investigation is relatively rare [27].

Table 1.1: Treatment processes for heavy metals removal.

Treatment process	Description	Economic	Types of wastes	Example applications
Precipitation	The chemical reaction produced solid material which settles	Relatively high costs	Lime slurries	Metal plating; wastewater treatment
Ion-exchange	Waste stream flows through resin bed where ions are selectivity exchanged	Relatively high costs	Heavy metals aqueous solutions	Metal plating
Reverse osmosis	Separation of dissolved materials from the liquid through a membrane	Relatively high costs	Heavy metals; organics; inorganic aqueous solutions	Seldom used industrially
Electrolysis	Separation of positively charged Materials by application of electric current	Dependent on concentrations	Heavy metal ions from aqueous solutions.	Metal plating
Ultrafiltration	Separation of molecules by size using membrane	Relatively high costs	Heavy metals aqueous solutions	Metal coating applications
Flocculation	Agent added to aggregate solids together to facilitate separation	Relatively high costs	Aqueous solutions with finely divided solids	Refinery oil/ Water Mixtures, paper wastes, mineral industry
Electrodialysis	Separation based on differential rates of diffusion through membranes	Moderately expensive	Separation/Concentration n of ions from aqueous streams	Separation of acids and metallic solutions
Evaporation	Solvent recovery by boiling of solvent	Energy-intensive	Organic/ Inorganic aqueous streams	Rinse waters from Metal plating waste
Adsorption	Physical or chemical interaction between solid and adsorbed substance	Relatively low costs	Organic/ Inorganic aqueous streams	Metal plating, Mineral industry, Water Mixtures, Wastewater treatment

Recently, it was stated that many investigations had been done for the application of MOFs to adsorption various polluted components such as organic dyes [28], aromatic compounds [29], and pharmaceuticals [30].

1.2 Hypothesis

Among MOFs-type porous materials, chromium terephthalate MOF MIL-101(Cr) ((MIL, Material of Institute Lavoisier) has the unit formula $Cr_3F(H_2O)_2O[(O_2C)–C_6H_4–(CO_2)]_3 \cdot nH_2O$, regarded as a novel adsorbent with high surface area, large pore volume and considerable chemical stability in the aqueous solution [31]. Based on the previous merits, MIL-101(Cr) has some application as a novel adsorbent for aromatic compounds, organic dyes, and pharmaceuticals [32]. Some reports suggested that MIL-101(Cr) can be modified by post-synthetic technique or pre-synthetic modification (ligand modification) to produce functionalized MOF with new physical and chemical features for adsorption of heavy metal ions [27,33]. Based on the activity of amino groups in providing chelating sites for ions such as heavy metal ions, MIL-101(Cr) can be functionalized with amino moieties by pre-ligand functionalization to modifying the pores of MIL-101(Cr). The resulting grafted MOF can be tested as an adsorbent for heavy metal ions.

1.3 Objectives

The main objectives of this study involve:

1. Synthesize the Amino-functionalized of Cr-based MOFs [ED-MIL-101(Cr)] and characterize their crystal structures, morphologies, functional groups, and surface area.
2. Investigation of the adsorption behavior of as-synthesis amino-grafted MOFs in a single, binary and ternary systems of Pb(II), Cu(II), and Cd(II) ions
3. Determination of the adsorption models to the isotherms after conducting single and multi-ions adsorption experiments.
4. Analyze the kinetic data and estimate which model will be suitable to describe the mechanism of the adsorption process.

5. Evaluate the breakthrough analysis of contaminated water remediation using continuous flow adsorption processes.

2. ADSORPTION TECHNOLOGIES

2.1 Introduction

Theoretically, adsorption is a phase operation that is extensively used in practice to extract substances from fluid phases (liquids or gases) and produces an enriched surface of a liquid or a solid in chemical species from the fluid phase [34,35]. In the field of water treatment, adsorption technology has been evidenced as an efficient removal process for various types of solutes. Mainly, molecules or ions are removed from the aqueous solution onto solid surfaces. The availability of active, energetic sites on the solid interface represents the driving force to interacting with solutes in the adjacent aqueous phase as well as to the specific chemical or physical properties.

The basic definitions used in the studies of the adsorption process are shown in Figure 2.1 [36]. The adsorbent referred to the solid material which provides the adsorption sites at its surface. The constituents that are to be adsorbed are called adsorbate. By altering the properties of the aqueous phase, *e.g.* temperature, concentration, pH, *etc.*, the adsorbed particles can be moved back into the liquid phase and released from the solid surface. This opposite process is called desorption.

Since adsorption is a surface operation, the surface area is a key adsorbent performance parameter. Adsorbents with a relatively high surface area, suitable pore volume and geometry, specific active adsorption sites, functional groups, and electrostatic charge are capable of attracted contaminants from aqueous media [37,38]. The large surface of the typical adsorbent is due to the internal cages constituted by the pore walls rooted in the material's high porosities [15].

2.2 Types of Adsorption

The process of adsorption is mainly controlled by the interaction category at the solid-liquid interface. The adsorption could occur because dissolved species are attracted to the adsorbent surface which has a net electrical charge or replacements in the crystal lattice of the adsorbent or chemical dissociation reaction at the solid surface. Depending on this exploration, the adsorption operation can be categorized into the below sorts [39,40].

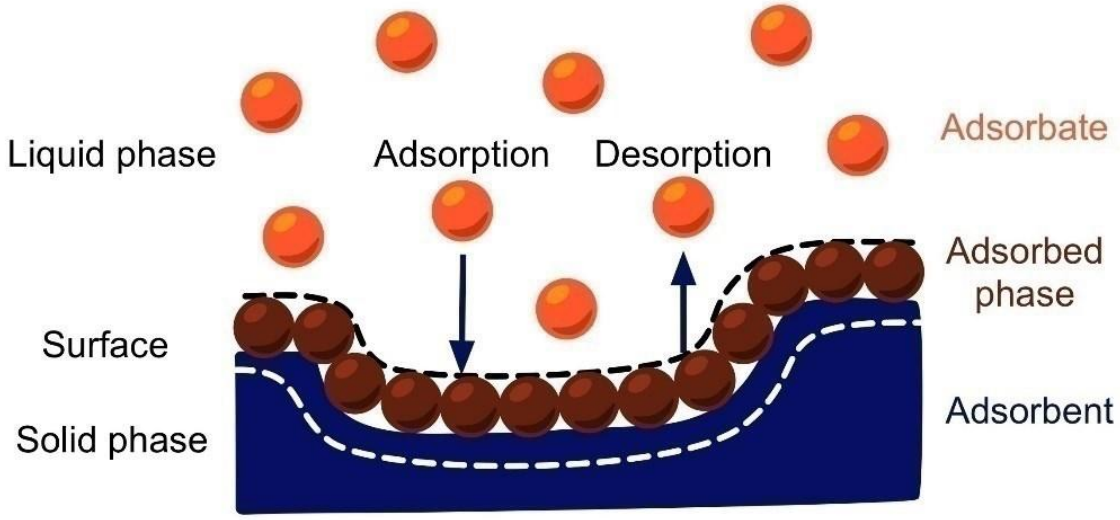

Figure 2.1: Basic terms of adsorption illustration [36].

2.2.1 Physical adsorption

Physical adsorption occurs between solid molecules and the species to be adsorbed as a consequence of Vander Waal attraction forces (dipole-dipole interactions, induction forces, dispersion forces) which are fairly weak [41,38]. Physical adsorption reversibility depends on the strength of attractive bonds between the solid phase and adsorbate. If these forces are weak, desorption is directly affected [42,35]. The adsorbed molecule is not bound to a particular site on the substrate in physical adsorption but is rather free to undergo translational motion within the interface. Physical adsorption arises rapidly and may be a mono-molecular layer (monolayer), or multi-molecular layers thick (multilayer).

When the size of the molecules is close to the pores, then the capillary condensation occurs, and pores fill with adsorbed particles. Usually, physical adsorption predominates at low temperatures and is characterized by relatively low adsorption energy. The heat of the physical adsorption for the reaction is 40 kJ / mol of the adsorbed species [43].

2.2.2 Chemical adsorption

This kind of adsorption includes the presence of a chemical reaction between the adsorbed species and the adsorbent in a monolayer [44]. Chemisorption exhibits high adsorption energies because the adsorbent forms tight localized bonds at the adsorbent's active sites. In this case, by moving on the surface or within the interface, molecules are considered not free [45,46]. This type is often irreversible and the adsorption heat is substantially higher than for the physical type of adsorption, ranging from 40 to 400 kJ / mol [47]. Table 2.1 tabulates the most important characteristics of physical and chemical sorption [48].

2.2.3 Exchange adsorption

Exchange adsorption is a mechanism where ions of one adsorbate material accumulate on an adsorbent surface as a result of electrostatic attraction to charged sites on the adsorbent surface. Electrical attraction forces between the adsorbate ions and the adsorbent surface characterize this type of adsorption [49].

Both the electronegativity and hydrated ionic radius control this type of adsorption in a multi-ion system, the ion which has a higher level of electronegativity will display more attractive forces to active sites on the adsorbent than the other present competitive ions in the system. Also, the ion with a smaller ionic radius can penetrate through more fine pores in the adsorbent surface, consequently shows larger affinity and a higher extent of removal efficiency [48].

2.3 Functional Adsorbents for Water Decontamination

When employing adsorption for remediation processes of pollutants, the adsorbent materials play a key factor in the investigation of the efficacy of the treatment process. In general, most solids tend to adsorb species from gasses or liquids to their surface.

However, only some materials have a satisfactory selectivity and capacity to make them feasible.

Table 2.1: Important properties of chemical and physical adsorption.

Physisorption	Chemisorption
The heat of adsorption usually in the range of 20-40 kJ mol^{-1}.	The heat of adsorption in the range of 40-400 kJ mol^{-1}.
Van der Waal's forces are the driving forces.	Chemical bond forces are the driving forces.
It frequently takes place at low temperatures and decreases with increasing temperature.	It takes place at a higher temperature.
It is reversible.	It is irreversible.
It is related to the case of liquefaction of the gas.	The extent of adsorption is approx. not related to the liquefaction of gas.
It is not very specific.	It is highly specific.
It forms multi-molecular layers.	It forms mono-molecular layers.
It does not require any activation energy.	It requires activation energy.

The adsorbent materials should possess the following properties [50]:

- High porous solid structure with large pore volume which is accessible by substances being adsorbed from fluids. These materials may be inorganic or organic, natural or synthetic occurring, and in certain conditions may have molecular sieving properties.
- Suitable mechanical properties such as good attrition resistance and high strength.
- Reasonable kinetic properties permit for transferring of adsorbing particles rapidly to the active sites in the adsorbent.
- High surface area Structure with multiple functionalities.

- The applicability and efficiency of the regeneration process without losing substantial adsorptive sites.

In regards to cationic species removal and especially for heavy metal ions, an abundant variety of adsorbent materials have been developed in the past decades, including carbon-based materials, biological materials, metal oxides, and synthetic functional materials (layered double hydroxides and zeolites) [11,37,51]. Herein, a general survey on the respective categories of materials is provided below:

2.3.1 Carbon-Based material

Carbon-based materials such as activated carbons and charcoals represent the oldest types of adsorptive materials used in the contaminants treatment process. It ordinarily works as a universal adsorbent that has been broadly used as an all-purpose adsorbent since the 1930s [52]. These carbonaceous materials possess a suitable potential for the recovery of organic and inorganic from polluted fluids. The activated carbon can be prepared from petroleum coke, pistachio shell, bone-char, and agricultural sources such as coconut shells, lignin, peat, rice hulls, peanut husks, nutshells, sugarcane bagasse, hazelnut, pistachio shell, and so on [53]. The large mesopores and microspores volumes and the resulting high particle surface area are the chief advantages associated with the activated carbon adsorbents.

Extensive investigations have been conducted to assess the capability of activated carbon (AC) for removing heavy metal ions like copper, lead, zinc, cadmium, etc. from contaminated water [54–56].

Furthermore, new novel types of carbon-based materials such as carbon nanotubes (CNTs), graphene, and graphene oxide have recently been developed, and they have been tested for heavy ions removal from wastewater [57,4]. But, the manufacturing cost for these types of novel carbon materials is considered relatively high for widespread applications in wastewater treatment [58].

2.3.2 Biomaterials

Significant attention recently has been devoted to treatment techniques for contaminated solutions by heavy metal ions using biomass-based materials (biosorbents) as a new promising type of cost-effective adsorbent. There are three sources for preparing the

boisorbents as follows: (1) dead biomass such as lignin, bark, krill, crab shell, etc.; (2) algal biomass; (3) microbial biomass, e.g. fungi, bacteria, and yeast [59]. Cu(II), Cd(II), Pb(II), Zn(II), and other heavy metal ions have also been reported to be removed using different biosorbents [60 – 62].

2.3.3 Zeolite

Zeolites are an important type of practical adsorbent materials with a wide variety of porous crystalline solid structures. It consists of hydrated aluminosilicate materials of a porous structure with valued physicochemical properties, which make them play a significant role in many synthesis and treatment processes such as catalysis, ion exchange, adsorption, and molecular sieving. The structures of zeolite are based mainly on consecutive networks of corner-sharing SiO_4 and AlO_4 tetrahedra which encompass cavities and channels [63]. Although those zeolites are naturally occurring but also economical to be manufactured and functionalized. The cations present in the zeolites like, calcium, sodium, and potassium ions are exchangeable with co-existence cations in the aqueous solutions like heavy metal ions. Some researchers have been worked on the removal of heavy metal ions using zeolite [64].

Nowadays, great efforts have been devoted to reducing the content of heavy metal ions in the water ecosystem to acceptable levels. For these targets, metal-organic frameworks (MOFs) due to their intriguing features are considered as a promising candidate in the adsorption process of heavy metals from polluted water.

2.4 Metal-Organic Frameworks (MOFs)

MOF-type materials have recently emerged as a special group of crystalline porous organic-inorganic hybrid materials. Owing to 3D-network structural characteristics of MOF materials and the possibility to modify their pores surface with various functional groups [20–22,65], these materials have significant applications in the fields of drug delivery [23], catalysis [24], adsorption [25], separation, and gas storage [26].

In general, MOFs are defined as the crystalline materials constructed by inorganic metal ions or clusters coordinated with organic ligands (linkers) to form a high-order uniformity

structure over three dimensions as shown in Figure 2.2 [66]. The number of organic linkers which coordinated with metal cluster represented by the specific coordination numbers (CNs). These organic ligands are classically di, tri, or tetravalent linkers. The shape and pore size of these MOF materials can easily be modified by changing the organic linkers and metal ions [16].

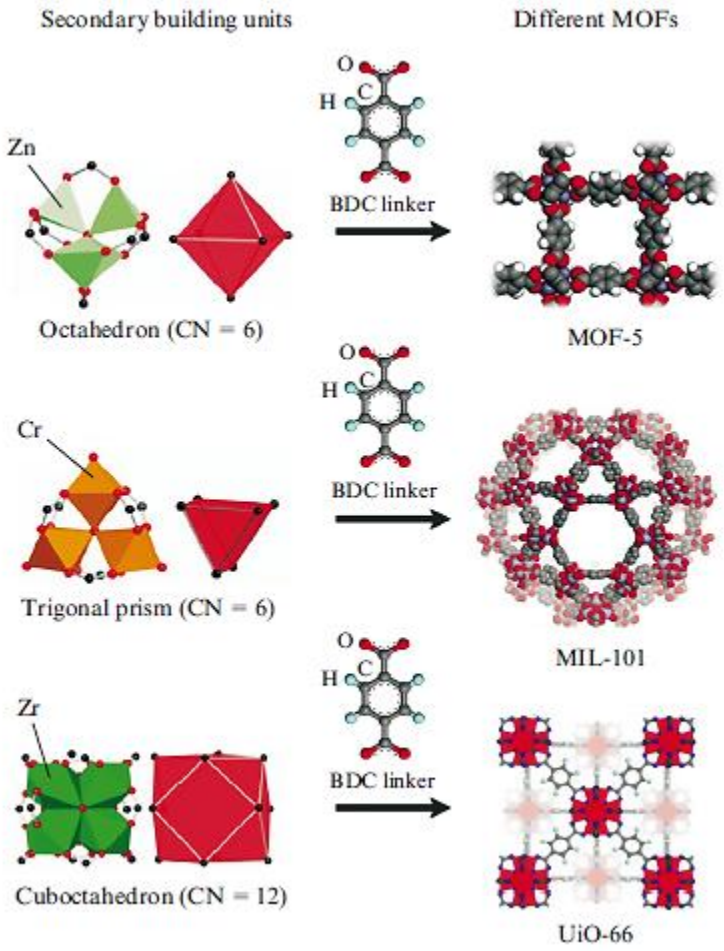

Figure 2.2: Structures of different MOFs with the terephthalate (BDC) dianion as a linker [66].

2.5 Metal-Organic Materials in Adsorption

As a newly developed sort of porous crystalline material, MOF materials have exhibited great attention in their potential adsorption-related applications compared with the other conventional porous materials like activated carbon, aluminosilicate zeolites, and metal oxides. Besides, as a hybrid of inorganic and organic materials, MOFs are associated with

a milder synthesis condition. With a great availability of various configurations and structures via post-synthetic modification (PSM), as well as higher porosity and surface area, MOF is expected to be a high-capacity adsorbent.

The use of MOF adsorbents in removing contaminants from water is a developing area of research and this section will emphasize the recent developments in heavy metal removal [67– 69].

Grouped by heavy metal, the removal effectiveness of MOFs that have been manufactured and tested to date will be explained. Details of each framework and its properties, to give a broader picture of the merits and drawbacks of each material, are also included.

2.6 Heavy Metal Uptake in MOFs

MOFs adsorbents that have been tested for the heavy metal ions uptake from contaminated water are overviewed. The studies are summarized and showed in Table (2.2) with key details exhibited in the specified literature papers and presented below in sub-paragraphs with the discussion of outcomes presented by researchers of these reports.

Wang et al. studies in 2015 the manufacturing process of $Cu_3(BTC)_2$-SO_3H framework by treatment of $Cu_3(BTC)_2$ with sulfonic acid using post-synthetic modification and ox--idation in sequential order. The adsorption process assessment of cadmium (II) using $Cu_3(BTC)_2$-SO_3H framework adsorbent was conducted. It has been proposed that the cadmium(II) was chelated to sulfonic groups within $Cu_3(BTC)_2$-SO_3H framework in the removal process (Figure 2.3). The incorporation of a sulfonic group into the modified MOF enhances the Cd(II) selectivity over other ions probably because of coordination modes and binding sites of the SO_3H^{-1} group [67].

In 2015, Chakraborty et al. synthesized AMOF-1 and reported being a potential cadmium (II) adsorbent. This material was based on the zinc (II)-based metal ions combined with versatile tetracarboxylic linkers. The maximum value for cadmium ions adsorption was determined to be 41 $mg.g^{-1}$ and 24 hr was the required time to reach the equilibrium [68].

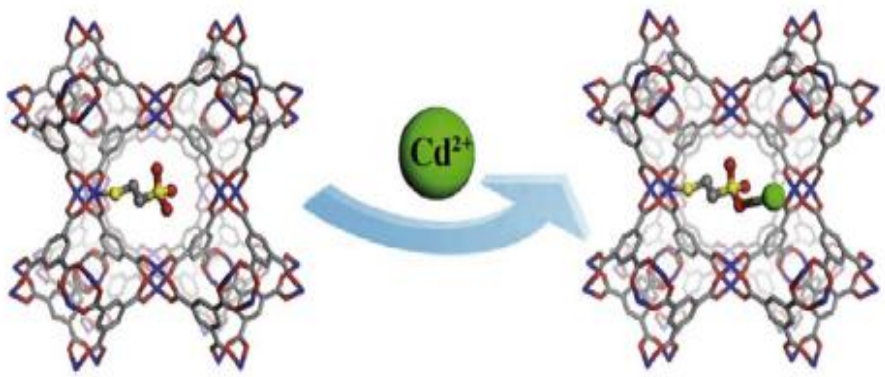

Figure 2.3: Schematic illustration of Cadmium (II) adsorption mechanism onto the $Cu_3(BTC)_2$-SO_3H MOF [117].

Another MOF-type adsorbent for cadmium (II) removing, PCN-100- was synthesized by Fang et al. in 2010, manufactured from TATAB ligands (i.e. 4,4′,4″-s-triazine-1,3,5-triyl tri-p-amino-benzoate) and $Zn_4O(CO_2)_6$ SBUs (secondary building units). Herein the metal ions were encapsulated by chelating coordination mode within the linkers supplied by the MOF. The indicated uptake value of the cadmium(II) adsorption was 1.6Cd(II) per formula unit [118].

Saleem et al. studied in 2015 the effect of incorporation of a sulfur-containing group by post-synthetic modification of zirconium-based MOF, UiO-66-NH_2 to synthesis UiO-66-NHC(S)NHMe, the last modified MOF was tested as an adsorbent for heavy metal removal. The result of this work indicates that the maximum uptake for Pb^{2+}, Cd^{2+}, Hg^{2+}, and Cr^{3+} was determined to be 232, 49,769, and 117 mg/g respectively. These outcomes reveal that incorporation of thiourea groups dramatically increases the heavy metal removal efficiency of UiO-66 frameworks in comparison with parent MOF due to the high affinity of sulfur-containing links for heavy metal ions [119].

Abbasi et al. in 2015, tested another MOF-type adsorbent for Cd(II) removal, a 3D cobalt and TATAB based MOF (3D Co(II) MOF), which was produced using hydrothermal synthesis or ultrasound irradiation method to give nano-sized particles. A comparison study revealed that the maximum adsorption capacities of nanostructure of this MOF were higher than those for 3D Co (II) MOF. Whereas the optimal pH value for each type was about 6. The reduction of adsorption in acidic conditions was suggested to be caused by protonation of available active -NH groups.

Table 2.2: Key information on the MOFs used in adsorption sorted according to metal ions.

Metal	MOF	Adsorption capacity (mg g^{-1})	Metal ion source	Equilibri--um time (min)	Optimal pH	Refs.
As	UiO-66	303 As(V)	$Na_2HAsO_4 \cdot 7H_2O$	2880	2	[69]
	C; F–S; D ZIF	127; 108;118 As(III)		600	8.5	[70]
	MIL-53(Al)	106 As(V)	$Na_3AsO_4 \cdot 12H_2O$	660	8	[71]
	ZIF-8	50 As(III); 60 As(V)	$NaAsO_2$; $Na_3AsO_4 \cdot 12H_2O$	420 for As(V); 780 for As(III)	7	[72]
	MOF-808	25 As(V)	Na_3AsO_4	30	8	[73]
	MIL-53(Fe)	21 As(V)	n/d	90–120	6–7	[74]
	Fe-BTC	12 As(V)	Na_3AsO_4	10	4	[75]
Cd	Manganese MOF	176Cd(II)	$Cd(NO_3)_2 \cdot 4H_2O$	60	5	[76]
	Cu-terephthalate MOF	100Cd(II)	Cd salt/Sungun wastewater	120	-	[77]
	HS-mSi@MOF-5	98Cd(II)	n/d	30	6	[78]
	$Cu_3(BTC)_2$-SO_3H	89Cd(II)	$CdCl_2 \cdot 2H_2O$	10	6	[68]
	UiO-66-NHC(S)NHMe	49Cd(II)	n/d	240	-	[79]
	TMU-5	43Cd(II)	$Cd(NO_3)_2 \cdot 4H_2O$	15	10	[80]
	AMOF-1	41Cd(II)	n/d	1440	-	[81]
	HKUST-1-MW@$H_3PW_{12}O_{40}$	33Cd(II)	n/d	80	7	[82]
	3D Co(II) MOF or (1)	70% Cd(II)	$Cd(NO_3)_2 \cdot 4H_2O$	100	6	[83]
	PCN-100	1.6Cd(II) per formula (ICP)	$Cd(NO_3)_2$	2880	-	[79]
Cr	MOR-1-HA	280 (±19) Cr(VI	Cr_2O_7 solution	60	3	[84]
	ZJU-101	245 Cr(VI)	Cr_2O_7 solution	10	-	[85]
	TMU-30	145 Cr(VI)	K_2CrO_4	10	5.6	[86]
	TMU-5	123 Cr(III)	$Cr(NO_3)_3 \cdot 9H_2O$	15	10	[80]
	UiO-66-NHC(S)NHMe	117 Cr(III)	n/d	240	-	[87]
	Chitosan-MOF	94 Cr(VI)	$K_2Cr_2O_7$	480	2	[88]
	Cu-BTC	48 Cr(VI)	$K_2Cr_2O_7$	-	7	[89]
	1-NO_3	37 Cr(VI)	$K_2Cr_2O_7$	240	5	[90]
	PCN-100	1.4 Hg(II)	$HgCl_2$	2880	-	[79]

Table 2.2 (continued): Key information on the MOFs used in adsorption sorted according to metal ions**.**

Metal	MOF	Adsorption capacity (mg g^{-1})	Metal ion source	Equilibri--um time (min)	Optimal pH	Refs.
Cr	Fe_3O_4@MIL-100(Fe)	18 Cr (VI)	n/d	120	2	[91]
	ZIF-67	15 Cr(VI)	$K_2Cr_2O_7$	20-60	5	[92]
Pb	MnO_2-MOF	917 Pb(II)	Pb(NO3)2	60	5	[76]
	MOF-5	659 Pb(II)	n/d	30	5	[93]
	MIL-53(Al@100aBDC)	492 Pb(II)	Pb(NO3)2	360	-	[94]
	HS-mSi@MOF-5	312 Pb(II)	n/d	30	6	[78]
	TMU-5	251 Pb(II)	Pb(NO3)2	15	10	[80]
	UiO-66-NHC(S)NHMe	232 Pb(II)	n/d	240	-	[79]
	HKUST-1-MW@$H_3PW_{12}O_{40}$	98 Pb(II)	n/d	10	7	[82]
	Cu-terephthalate MOF	80 Pb(II)	Pb salt/Sungun wastewater	120	7	[77]
	AMOF-1	71 Pb(II)	n/d	1440	-	[81]
	Dy(BTC)(H_2O)$(DMF)_{1.1}$	5 Pb(II)	$Pb(NO_3)_2$	10	6.5	[95]
	3D Co(II) MOF or (1	70% Pb(II)	$Pb(NO_3)_2$	100	6	[96]
Hg	BioMOF	900 $HgCl_2$; 166 CH_3HgCl	$HgCl_2$; CH_3HgCl	30 to 120	7	[97]
	UiO-66-NHC(S)NHMe	769 Hg(II)	n/d	240	-	[79]
	Thiol-HKUST-1	714 Hg(II)	$HgCl_2$	120	-	[98]
	$[Ni(3\text{-}bpd)_2(NCS)_2]_n$	713 Hg(II)	$HgCl_2$	120	-	[99]
	FJI-H12	440 Hg(II)	$Hg(NO_3)_2$	60	7	[100]
	LMOF-263	380 Hg(II)	$HgCl_2$	30	4-10	[101]
	Zn(hip)(L)·(DMF)(H_2O)	333 Hg(II)	$Hg(NO_3)_2$	60	5	[102]
	Fe_3O_4@SiO_2@HKUST-1	264 Hg(II)	$HgCl_2$	10	3	[103]
	SH@SiO_2/Cu$(BTC)_2$	210 Hb(II)	n/d	60	5.5	[104]
	AMOF-1	78 Hg(II)	n/d	1440	-	[81]
	MOF-74-Zn	63 Hg(II)	$Hg(NO_3)_2$	90	6	[105]
	MIL-101-Thymine	52 Hg(II)	$HgCl_2$	200	6	[106]

Table 2.2 (continued): Key information on the MOFs used in adsorption sorted according to metal ions**.**

Metal	MOF	Adsorption capacity (mg g^{-1})	Metal ion source	Equilibri--um time (min)	Optimal pH	Refs.
Hg	ZIF-90-SH	22 Hg(II)	$HgCl_2$	1440	-	[107]
	Zr-DMBD	100% Hg(II)	$Hg(NO_3)_2$; $HgCl_2$	720	-	[108]
	Cr-MIL-101-AS	99% Hg(II)	n/d	360	-	[109]
	3D Co(II) MOF or (1)	70% Hg(II)	$Hg(NO_3)_2$	100	6	[96]
	PCN-100	1.4 Hg(II)	$HgCl_2$	2880	-	[79]
Others						
Al	3D Co(II) MOF or (1)	90% Al(III)	$AlCl_3$	100	6	[96]
Fe	3D Co(II) MOF or (1)	100%	$FeCl_3$	80	6	[96]
	Cu-terephthalate MOF	115 Fe(III)	Fe salt/Sungun wastewater	120	7	[110]
Mn	Cu-terephthalate MOF	175 Mn(II)	Mn salt/Sungun	120	7	[110]
Zn	Cu-terephthalate MOF	150 Zn(II)	Zn salt/Sungun wastewater	120	7	[110]
Ag	MIL-53(Al)	183 Ag(I)	$AgNO_3$	180	-	[111]
	HKUST-1	±100% NP	$AgNO_3$	10	6-7	[112]
Ni	Chitosan-MOF	60 Ni(II)	$Ni(NO_3)_2{\cdot}6H_2O$	480	5	[88]
Co	TMU-5	63 Co(II)	$Co(NO_3)_2{\cdot}6H_2O$	15	10	[80]
Cu	ZIF-8	800 Cu(II)	$Cu(NO_3)_2$	30	4	[113]
	MOF-5	290 Cu(II)	n/d	30	5.2	[114]
	Cu-terephthalate MOF	225 Cu(II)	Cu salt/Sungun wastewater	120	7	[110]
	Cd-MOF-74	190 Cu(II)	$Cu(NO_3)_2$	10	6-7	[115]
	TMU-5	57 Cu(II)	$Cu(NO_3)_2{\cdot}3H_2O$	15	10	[80]
	Chitosan-MOF	51 Cu(II)	$CuSO_4{\cdot}5H_2O$	480	5	[88]
	UiO-66(Zr)-2COOH	11 Cu(II)	$Cu(NO_3)_2{\cdot}3H_2O$	60	6	[116]
	$Dy(BTC)(H_2O)(DMF)_{1.1}$	5 Cu(II)	$Cu(NO_3)_2{\cdot}3H_2O$	10	6.5	[95]
	ZIF-8	3.5 mmol/g	$CuCl_2{\cdot}2H_2O$	20	-	[117]

PXRD analysis indicated that the material's crystallinity remained intact during adsorption, as no substantial signs of degradation were observed after the spent adsorbent was examined [118].

Zhang et al. in 2016, successfully modified a zinc-based metal-organic framework material (MOF-5) by thiol modification in the layer of silica gel as a medium to obtain a thiol-functionalized MOF material (HS-mSi@MOF-5), and later used to adsorb cadmium and lead ions from aqueous media. Batch adsorption experiments revealed that the saturated uptake capacity of HS-mSi@MOF-5 for lead and cadmium ions is 312 and 98 mg g−1, respectively, whereas MOF-5 adsorbent exhibits lower values which were only 211and 43.6 mg g−1, respectively with shorter equilibrium time for modified MOF adsorbent than for MOF-5. A proposed removal mechanism of lead and cadmium ions on HS-mSi@MOF-5 adsorbent is potentially attributed to thiol coordination interaction and the electrostatic attraction as displayed in Figure 2.4 [96].

In 2014, Tahmasebi et al. successfully manufactured three types of zinc-based MOFs (TMU-4), (TMU-5), and (TMU-6) which functionalized with azine and amine groups using mechano-synthesis routine. Adsorption studies were performed to assess these MOFs as adsorbents for extraction and removal of some types of heavy metal ions including Cd(II), Co(II), Cr(III), Cu(II), and Pb(II) from polluted samples. The influence of the basicity of these MOFs adsorbents on the efficiency of adsorption was tested. The obtained results from these tests revealed that the removal efficiency for metal ions for TMU-5 and TMU-4 were nearly the same values, whereas their removal efficacies are higher values than that of TMU-6 because of the smaller basicity of the nitrogen atoms on the TMU-6 pore boundaries as compared to azine groups on the TMU-5 and TMU-4 pores [120].

Rahimi and Mohaghegh reported in 2015 on the adsorption capability of heavy ions by using the magnetic Copper terephthalate MOF, as an effective adsorbent. The removal of metal ions takes place through chemical adsorption that is greatly enhanced by the carboxylate groups that are readily available within the MOF. The uptake process was enhanced by increasing the solution pH because of the stronger electrostatic interactions between the metal ions and the anionic MOF pore surface.

the maximum adsorption capacities were found to be around 225, 100, and 80 mg g^{-1} for Cu(II), Cd(II), and Pb(III) respectively, at an optimal pH of 7 and with equilibrium being reached within 120 min for all three ions [80].

In 2013, Zou et al. described an efficient synthesis process for chemically functionalized HKUST-1-MW and HKUST-1-MW@H3$PW_{12}O_{40}$ MOFs under microwave irradiation**.** An assessment of heavy ions adsorption in an aqueous solution using (HKUST-1-MW@$H_3PW_{12}O_{40}$) as a kind of novel adsorbent material was performed. Even though it exhibited no Hg^{2+} adsorption, an equilibrium capacity and high selectivity of 98.18 mg.g^{-1} for $Pb^{2+}$and 32.45 mg.g^{-1} for Cd^{2+} was detected [110].

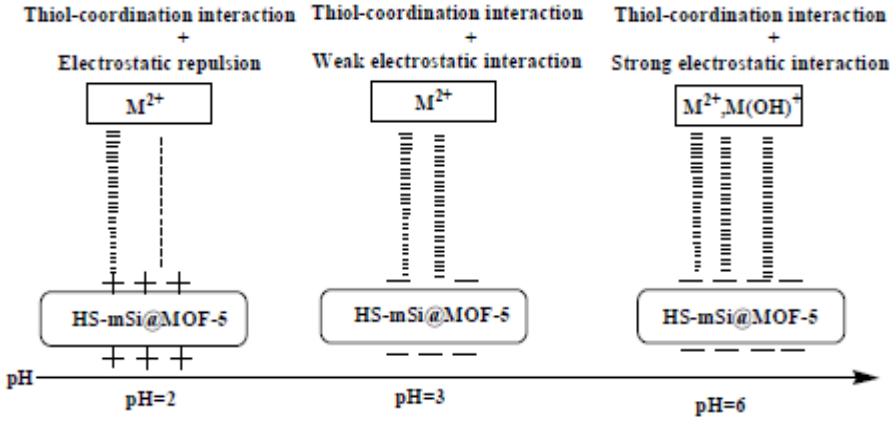

Figure 2.4: Adsorption mechanism of Cd(II) and Pb(II) at different pH over HS-mSi@MOF-5 substrate [95].

Yang et al. reported in 2016 about the removal of Cr(IV) ions from aqueous solution by using magnetic microspheres of Fe_3O_4@MIL-100Fe as an adsorbent. In this study Fe_3O_4, particle seeds were used to grow the MIL-100(Fe) shell in situ (via hydrothermal reaction), on which the MOF was based(Figure 2.5) The adsorption results reveal that the maximum value for uptake capacity was noted at 18 mg.g^{-1} at pH value at 2, with a period of 2 h to reach the adsorption equilibrium. Also, it was found that the electrostatic interactions between chromium ions ($HCrO_4^-$) and the adsorbent (Fe_3O^+) were enhanced at acidic conditions and so adsorption efficiency increased with decreasing pH of solution [121].

Chitosan- MOF (UiO-66) composite was manufactured firstly via microwave irradiation process in 2016 by Wang et al. then assessed in adsorption tests of polluted water which containing heavy metal ions. The results of adsorption tests reveal that the adsorption capacity of Cr(VI), Cu(II), and Ni(II) reached) (93.6, 50.6, and 60)mg.g^{-1}, respectively after 8 h of adsorption. These values for uptake are much higher than the results of previous investigations of chitosan (78mg.g $^{-1}$) [122] for Cr(VI) removal or modified chitosan for Cu(II) (34.5 mg.g $^{-1}$) [123] and Ni(II) (15.3 mg.g $^{-1}$) removal [124]. The higher values of uptake capacities for metal ions on chitosan- MOF (UiO-66) composite adsorbent ascribed to the firmly electrostatic attraction between the heavy ions and oxygen atoms or the linkers of -NH_2 group [91].

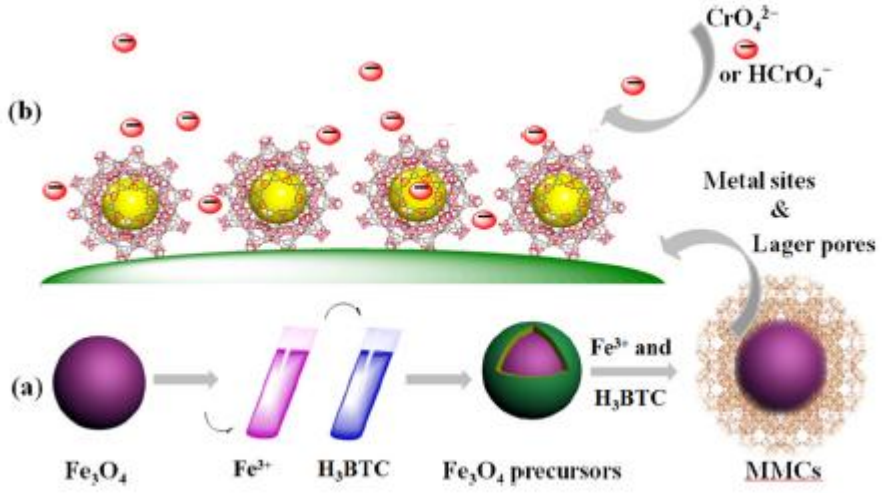

Figure 2.5: An illustration of (a) synthesis of the Fe3O4@MIL-100Fe magnetic microspheres and (b) adsorption process of chromium (VI) onto the microspheres [121].

Zhang et al. reported in 2016 on the ability to use the silica-coated, thiolated MOF-5 derivative, [HS-mSi@MOF-5], as an effective adsorbent for lead (II) removal. This MOF exhibits high removal capacity of about 312mg.g^{-1} and a relatively short period consumed to reach equilibrium (30 min) which makes it an active adsorbent [96].

2.7 Porous Chromium Terephthalate MIL-101

Considerable efforts to discover a new type of crystalline porous materials have been continuously done to overcome drawbacks of conventional types of zeolites such as limited incorporation of the metal element and limited pore sizes to prompt diffusion

problem [125,126]. As a result, there has been a tremendous increase in the synthesis of non-aluminosilicate-based crystalline porous materials during the past period.

As such, some researchers have recently initiated a universal study of the trivalent metal carboxylate systems, which has led to the discovery of the chromium (III) carboxylate with giant pores labeled as MIL- 101 [125]. MIL-101 structure is essentially fabricated from hybrid super tetrahedral (ST) building units built up from linkage of 1,4- benzene dicarboxylate (BDC) ligands and trimeric chromium (III) octahedral clusters (Figure 2.6 a). Octahedra are related through the μ_3O oxygen atom to form the trimeric building unit. The ST building unit is shaped by rigid terephthalate ligands and trimeric chromium (III) octahedral clusters. The four vertices of the ST are engaged by the trimers, and the organic linkers are located at the six edges of the ST (Figure 2.6 b). The linking between the ST is established through vertices to ensure a 3D network of supertetrahedra (Figure 2.6 c). The STs are microporous (with a $\approx$ 8.6 A˚ free aperture for the windows), and the resulting framework delimits two types of mesoporous cages occupied with guest elements. These two cages, which are present in a 2:1 ratio, are delimited by 20 and 28 ST with internal free diameters of $\approx$ 29A˚ and 34A˚, respectively (Figure 2.6 d, e) [126,127].

2.7.1 Hydrothermal synthesis and purification

The hydrothermal process accomplishes the synthesis processes of MIL-101 via a cooperative ionic interaction between terephthalate ligands and trimetric chromium (III) octahedral clusters, which form the skeleton of crystal frameworks together with solvent as a template. Some researchers such as Loiseau and Ferey established using a mineralizing agent like fluorine or sodium ions to increase the crystallinity and favors the formation of highly crystalline phases in MIL-101 [128]. Due to the presence of a significant amount of non-reacted terephthalic acid in outside and within the pores of MIL-101, leading to a decrease of its pore volume as well as the surface area, so recently developed an effective purification method to produce MIL-101 with high BET surface area. This method comprises three-step processes such as double filtration using two different filters, solvent treatments using hot ethanol, water, and fluoride–anion exchange

using aqueous NH_4F or DMF solutions to remove the residual unreacted raw materials that present in the pores of MIL-101 [126].

2.7.2 Surface functionalization with amine grafting

The search for a new modification method to functionalize pore channels and cavities in MOFs is a crucial procedure for spreading the application of these new hybrid materials. Moreover, the introduction of functionality into the channel of MOF materials may spread its diverse importance in catalysis, adsorption, encapsulation of metal nanoparticles, and

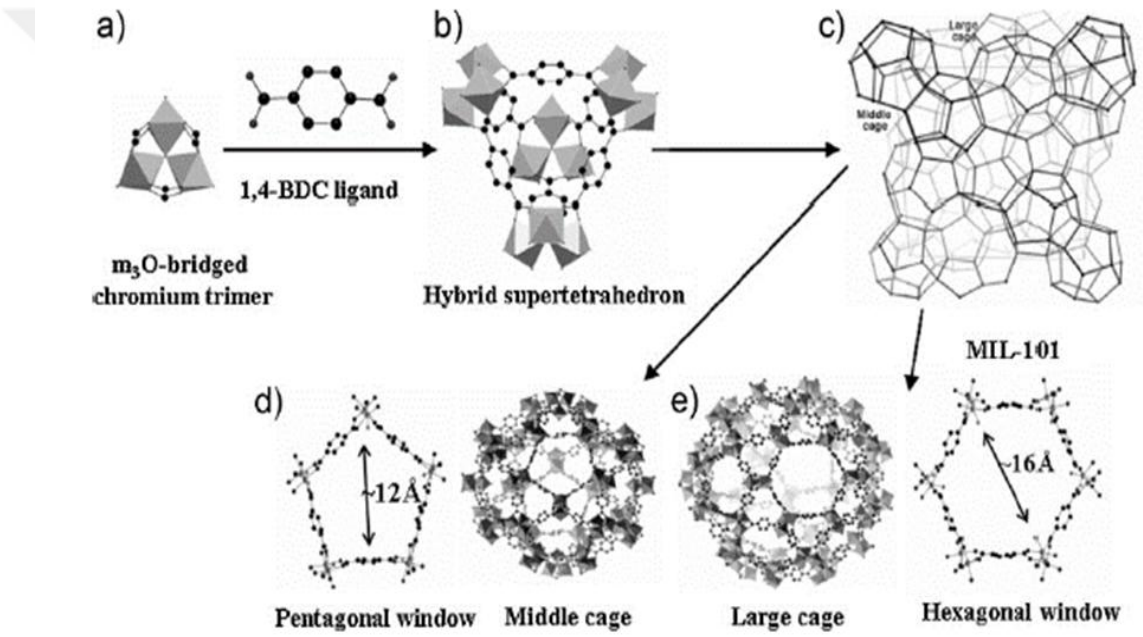

Figure 2.6: Basic building units and crystal structure of MIL-101 [126].

functionalized thin surface films. Regarding the functionalization of MOFs, there have been so far three approaches: a) pre-modification of organic linkers with functionalized ligands, b) post-covalent modification with functionalization of organic ligands or linker sites, and c) post- grafting of CUS with chelating agents or electron-rich molecules [129, 130]. Post-synthetic modification of a ligand in IRMOF-3 was covalently functionalized by acetylation [131]. It has been also reported that the cavities of MOFs can be easily modified by chemical modification without change of the original crystal structure. For the selective post-synthetic functionalization of CUS in the MIL-101, some reports

suggested using a grafting reagent with multifunctional chelating groups, such as ethylenediamine (ED). As illustrated in (Figure 2.7), when one amine group of ED is linked to CUS of Cr(III) in MIL-101 by direct ligation [132].

The concept of amine grafting onto CUS can be extended to sulfonic acid grafting, which is useful for solid acid catalysis. Some researchers have succeeded in the encapsulation of noble metals, such as Pd, Pt, and Au over the amine-grafted MIL-101 according to the procedure depicted in (Figure 2.7). This encapsulation process reveals the activity of amine groups to react with cations that present in contact with them [132,130].

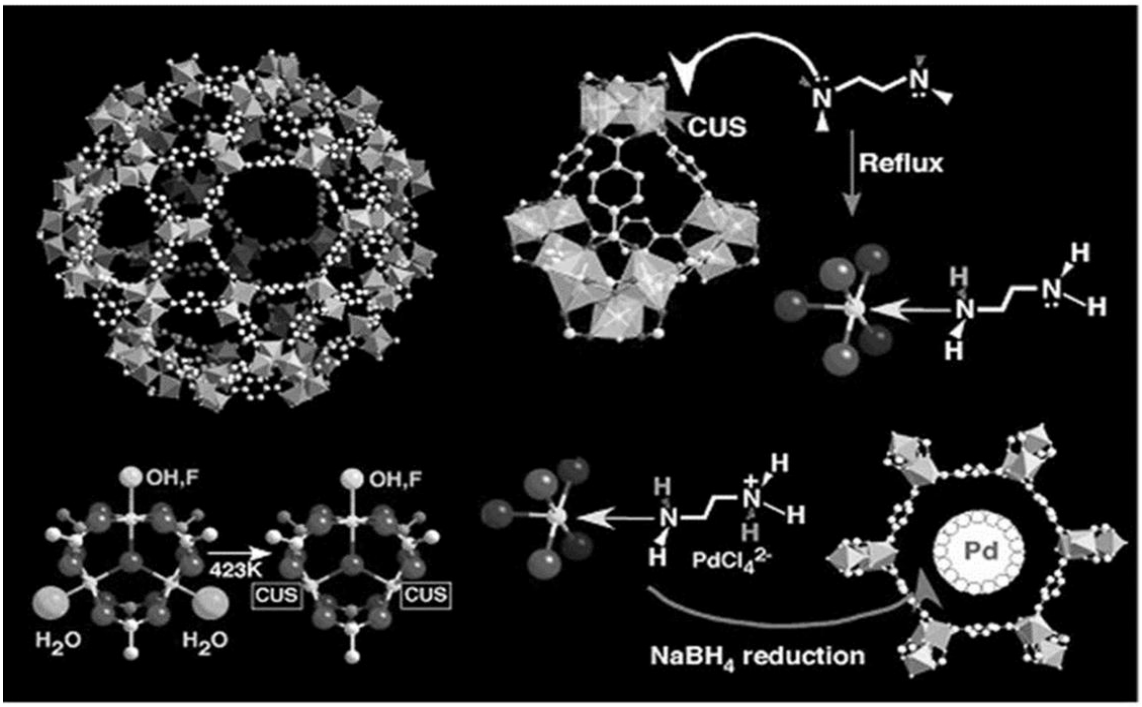

Figure 2.7: Schematic views of surface functionalization of MIL-101 [132].

3. THEORIES AND EXPERIMENTAL WORK

3.1 Adsorption Systems

The contact manner between the solid and the liquid phase can be categorized as batch and continuous contact systems [133].

3.1.1 Batch adsorption system

In the adsorption process, the dissolved solute (adsorbate) such as metal ions or gas atoms, will diffuse from the fluid to the solid phase to attain the equilibrium state between the concentrations of the solute in the two phases.

The adsorbed amount of metal ions in single and multi-ions systems can be calculated by the difference between their initial and final concentrations. For any system at equilibrium conditions, a mass balance states the amount of solute (adsorbate) adsorbed onto the solid phase (adsorbent) must be equal to the amount of solute extracted from the solution, or in mass balance formula:

Amount of adsorbed	=	Initial amount of adsorbate present	-	Final amount of adsorbate present

The previous terms can be rewritten in mathematical representation as:

$$Q_e m = C_o V - C_e V \qquad (3.1)$$

Equation (3.1) can be re-arranged as follows:

$$Q_e = \frac{C_o - C_e}{m} \times V \quad (3.2)$$

Where Q_e is the amount of material adsorbed at equilibrium state (adsorption capacity), *V* is the volume of solution and m is the mass of the adsorbent.

It is well known that Q_e is sometimes more conveniently expressed in units of mass (or mole) of solute per unit mass of the solid phase [133], however, in this investigation, the mass of solute per unit mass of the solid phase was selected. For this reason, the initial metal ion concentration C_o and the metal ion concentration at equilibrium C_e are expressed in mg solute per liter, Q_e is presented on mg/g basis, m in (g) mass of adsorbent, and V in a liter (L) of the treated metal ion solution.

The percentage of removing efficiency (RE %) can be expressed as follows:

$$RE\% = \frac{C_o - C_e}{C_o} \times 100 \quad (3.3)$$

3.2. Adsorption Isotherm Models

The adsorption isotherm expresses the relation between the quantity of material adsorbed (Q_e) and their concentration in the solution (C_e) at equilibrium condition. Usually, the amount of material adsorbed is related as a function of the concentration at a constant temperature, and the obtaining function is called adsorption isotherm [134,135]. Some typical isotherm profiles are shown as arithmetic diagrams [136] as displayed in (Figure 3.1). The linear isotherm goes through the origin and the amount of adsorbed is proportional to the concentration in the fluid. Isotherm that is convex upward is called favorable because a relatively high loading can be obtained at a low concentration in the fluid. The limiting case of a very favorable isotherm is irreversible adsorption, where the amount adsorbed is independent of concentration down to very low values. An isotherm that concaves upward is called unfavorable because a relatively low solid loading is obtained and because it leads to quite a long mass transfer zone in the bed [137]. From

these patterns of curves, it will be noted that adsorption is a specific property corresponding to the nature of the adsorbate and adsorbent system [138].

3.2.1. Single component system

Langmuir isotherm

The Langmuir model can be considered as the most extensively applied sorption isotherm model. It has produced a good agreement with a wide variety of investigational data. Langmuir model suggests that the monolayer adsorption occurs on a homogeneous surface [139].

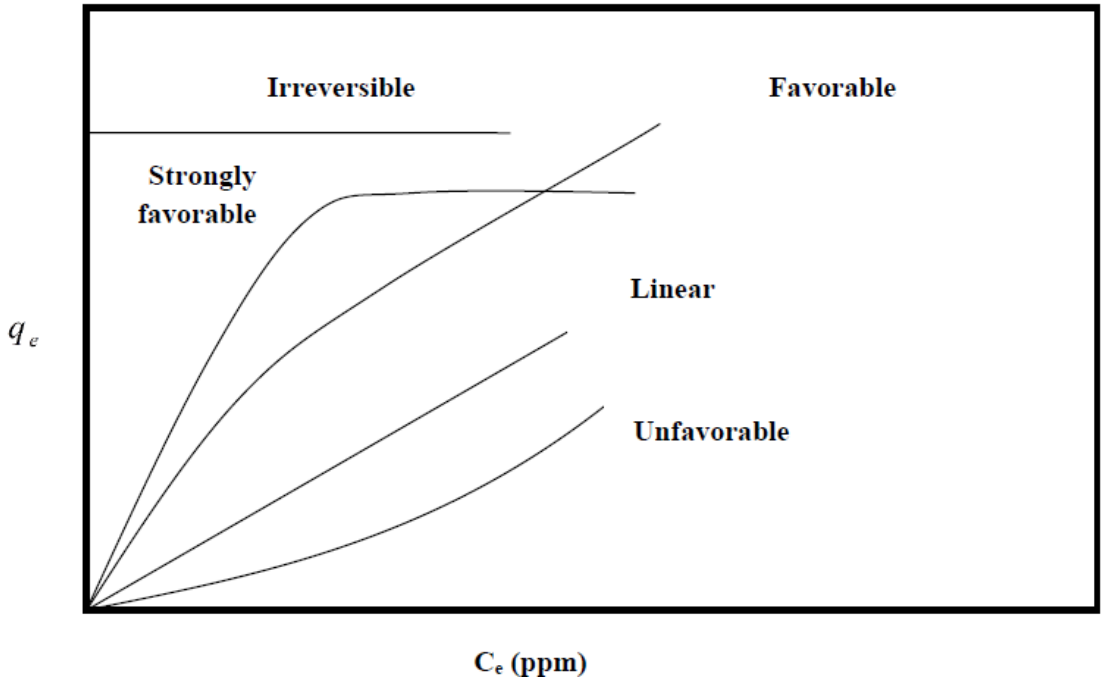

Figure 3.1: Adsorption isotherm [136].

Langmuir isotherm was developed in 1916 by Irving Langmuir with the below assumptions [140]:

- The surface of the adsorbents is uniform, that is, all the adsorption sites are equivalent.

- There is no interaction between molecules adsorbed on neighboring sites.
- All adsorption occurs through the same mechanism
- Molecules are adsorbed at the defined sites on the adsorbent surface.

At equilibrium, a saturation of adsorptive sites is observed which is graphically characterized by the plateau. Langmuir model is shown below in Equation (3.4) [27,141]:

$$Q_e = \frac{Q_m b C_e}{1 + b C_e} \tag{3.4}$$

Equation (3.4) can be re-arrange to linearized form:

$$\frac{C_e}{Q_e} = \frac{1}{Q_m} C_e + \frac{1}{b Q_m} \tag{3.5}$$

Where, Q_e (mg/g) denotes the adsorption capacity, Q_m (mg/g) denotes the mono-layer uptake capacity, C_e (mg/L) represent the equilibrium concentrations, *b*, represents the Langmuir isotherm constant in (L/mg) is corresponding to the affinity between the dissolve ion and solid adsorbent. The values of the Langmuir constants Q_m and b can be calculated by plotting C_e/Q_e versus C_e.

Freundlich isotherm model

Freundlich in 1906 suggested an empirical adsorption isotherm equation for non-ideal systems [142]. The Freundlich model assumes that the adsorption occurs as a multilayer on a heterogeneous surface; the Freundlich model is stated as Equation (3.6) [141]:

$$Q_e = K_F C_e^{1/n} \tag{3.6}$$

And the equation (3.6) can be linearized by taking the logarithms of two sides as follows:

$$\log(Q_e) = \log(K_F) + \frac{1}{n}\log(C_e) \quad (3.7)$$

Where the Freundlich constants corresponding to adsorption intensity and capacity uptake are represented with n (dimensionless) and K_F, respectively. The constants in the Freundlich isotherm formula can be calculated by plotting Log (Q_e) vs. Log (C_e).

Sips isotherm model

The Sips isotherm is a three parameters isotherm model involving the combination of the Langmuir and Freundlich isotherms to overcome the application limits of these two isotherms and predict the heterogeneity of the adsorption systems. This model is valid for localized adsorption without adsorbate-adsorbate interactions [143]. The non-linear expression for the Sips model is expressed as.

$$Q_e = \frac{Q_m K_s (C_e)^m}{1 + K_s (C_e)^m} \quad (3.8)$$

By re-arranging of Equation (3.8) to obtain the linearized form as shown below:

$$\log\left(\frac{Q_e}{Q_m - Q_e}\right) = m\log(C_e) + \log(K_s) \quad (3.9)$$

Where Q_e depicts the equilibrium adsorption capacity (mg/g), C_e the equilibrium concentration of component (mg/L), Q_m the maximum adsorption capacity (mg/g), K_s the Sips isotherm constant (L/mg), and m the dimensionless Sips model exponent which can also be employed to describe the heterogeneity of the system. When C_e approaches a high value, the Sips isotherm efficiently reduces to Langmuir monolayer sorption behavior, while at low C_e value, it shows the Freundlich isotherm model [144,145].

3.2.2. Multi components system

Extended Langmuir model

The Langmuir model can be extended to simulate the isotherm of a binary system which can be expressed with the following equation [146] :

$$Q_{e,i} = \frac{Q_{m,i} b_i C_{e,i}}{1+\sum_{K=1}^{N} b_K C_{e,k}} \quad (3.10)$$

In this equation $C_{e,i,}$ and $Q_{e,i}$ represent the concentration and uptake of the metal ion (i) in a competitive ions system at the equilibrium condition, respectively. $Q_{m,i,}$ and b_i are the Langmuir parameters for single component *i*.

Extended Freundlich model

The empirical Freundlich model can be extended for mixtures of species as shown by an expression given below [147]:

$$Q_{e,i} = \frac{K_i C_{e,i}^{n_i+x_i}}{C_{e,i}^{x_i}+\sum_{j=1}^{N} K_j C_{e,j}^{nj}} \quad (3.11)$$

Where the parameters Ki ($mg.g^{-1}$) $(L.mg^{-1})^{1/n}$ and ni are calculated from the particular Freundlich model for the substance i.

Extended Sips model

The model is applied for the competitive adsorption of component (i) in a solution containing (N) components. The adsorption capacity of a component i can be calculated when it is present in association with other components. The modified sips isotherm for the multicomponent system is shown below [144,145]:

$$Q_{e,i} = \frac{Q_{m,i} K_{s,i} (C_{e,i}^{m_i})}{1+\sum_{j=1}^{N} K_{s,j} (C_{e,j}^{mj})} \quad (3.12)$$

$Q_{e,i}$ denotes to the equilibrium adsorption capacity for component i (mg/g), $C_{e,i}$ the equilibrium concentration of component i (mg/L). $Q_{m,i}$ the maximum uptake capacity for component i (mg/g). The Sips constants are taken from the isotherm data of individual components. At a lower pollutant concentration for (m) value of 0, the model approaches Freundlich isotherm. For higher adsorbate concentration for value m approaching 1, the model can be modified to Langmuir isotherm.

3.3 Adsorption Kinetics

The adsorption kinetics laws describe the rate of solute uptake which in sequence controls the residence time of sorbate at the solid–solution contact surface. Therefore, it is essential manner to be able to estimate the rate at which sorbate is recovered from aqueous media to design efficient sorption treatment processes [148].

3.3.1 Pseudo-First order kinetic model

The pseudo-first order model (Lagergren rate equation) is suggested as the first-rate equation for the adsorption of liquid/solid systems based on solid capacity [149]. This equation is one of the most extensively applied rate relations for the adsorptive removal of a solute from a liquid phase. It can be represented as:

$$\frac{dQ}{dt} = K_1(Q_e - Q_t) \tag{3.13}$$

By integrating equation (3.13) between the boundary conditions (Qt = 0) at (t= 0) and (Qt = Q*e*) at (t = t) and rearranged to obtain a linear form:

$$\ln(Q_e - Q_t) = \ln(Q_e) - K_1 t \tag{3.14}$$

Where Qe and Qt are the amount of component adsorbed at equilibrium and at time t (mg/g); respectively. While k_1 is the equilibrium rate constant of pseudo-first sorption (1/min).

3.3.2 Pseudo-Second order kinetic model

This model based on the following assumptions [150]:

- Formation of a monolayer from adsorbed material on the solid surface.
- The equal amount of adsorption energy for each adsorbent and independent of the pattern of surface coverage.
- There are no interaction effects between the adsorbed compounds on the active sites of the adsorbent surface.

The equation for the pseudo-second order kinetic rate is written as shown below:

$$\frac{dQ}{dt} = \mathrm{K}_2(Q_e - Q_t)^2 \quad (3.15)$$

Where K_2 (mg/g.min) is the rate constant of the 2nd order model. For the same boundary conditions of the first order kinetic rate model, the integrated form of equation 3.9 becomes [151]:

$$\frac{\mathrm{t}}{\mathrm{Q_t}} = \frac{\mathrm{t}}{\mathrm{K_2 Q_e^2}} + \frac{\mathrm{t}}{\mathrm{Q_e}} \quad (3.16)$$

The parameters in the equation (3.10) can be specified graphically from the plot of t/Qt vs. t.

3.3.3 Weber and Morris intra-particle diffusion model

Weber and Morris suggested a kinetic model based on intra-particle diffusion and can be written as [152]:

$$\mathrm{Q_t} = \mathrm{K_{id}} \mathrm{t}^{0.5} + \mathrm{C} \quad (3.17)$$

Where Kid (mg/gm. $min^{1/2}$) is the rate constant of intra-particle diffusion, *C* is the value of intercept which gives an idea about the boundary layer thickness, i.e. the larger intercept; the greater is the boundary layer effect. If the plots of Qt versus $t^{1/2}$ give a linear relationship, then the intra-particle diffusion step controls the rate of adsorption. Otherwise, this process is not the only determining mechanism; also other mechanisms such as electrostatic interaction, ion exchange may be operating to different extents.

3.1.2 Dynamic adsorption system

The assessment of the dynamic response and Analysis of the adsorption data of continuous flow systems are essential characteristics for determining the feasibility of a real industrial adsorption process [153]. The breakthrough curve was revealed and indicated the adsorbent effectiveness of the continuous flow adsorption system operated at certain conditions [154]. The breakthrough curves are typically expressed in graphs of time or effluent volume versus the concentration of heavy ions in the effluent stream (C_t)

normalized to that in the influent stream (C_o). The total quantity of adsorbed ions (q_{total}, mg) can be determined by equation (3.18) shown below:

$$q_{total} = \frac{QA}{1000} = \frac{Q}{1000}\int_{t=0}^{t=t_{total}}(C_{ads})dt \quad (3.18)$$

Where Q is denoted to flow rate in (mL/min), and (A) is the integrated area under the plot of the adsorbed concentration (C_{ads}) versus the flow time (t).

The total mass of the metal ions moved through the grafted MOFs packed in the column m (mg), and the adsorption capacity q_e (mg/g) at the equilibrium condition can be determined using the following relationships, respectively:

$$m = \frac{C_o Q\, t_{total}}{1000} \quad (3.19)$$

$$q_e = \frac{q_{total}}{w} \quad (3.20)$$

Where (w) represents the mass of MOFs in the column (g).

3.4. Mathematical Adsorption Models of Column Data

3.4.1 Thomas model

Several theoretical models were applied to estimate the breakthrough curve of the packed column to determine the maximum adsorbent capacity and the kinetic constants of the column. Among these models, the Thomas model is applied to describe the adsorption column performance and predicting the column breakthrough curves owing to its higher accuracy compared with the other models. This model assumes that a reversible reaction of second-order represents the control driving force in the adsorption steps in the absence of axial dispersion [155].

The expression of the Thomas model in the linearized form is shown below in equation (3.21):

$$\ln\left(\frac{C_o}{C_t}-1\right)=\frac{K_{th}q_o w}{Q}-K_{th}C_o t \quad (3.21)$$

In Thomas model equation, k_{th} and q_o denoted to Thomas Kinetic constant (mL/min.mg) and maximum equilibrium column capacity (mg/g) respectively, their values can be specified from the graph of $\ln[(C_o/C_t)-1]$ versus the time at certain operating conditions.

3.4.2 Yoon-Nelson model

Yoon–Nelson model is suitable and applicable for a single adsorbate system, this model includes fewer column factors and data as displayed in equation (3.22) [156]:

$$\ln\left(\frac{C_t}{C_o-C_t}\right)=K_{YN}t-\tau K_{YN} \quad (3.22)$$

The factors k_{YN} and (τ) in this form represent the Yoon-Nelson rate constant (min^{-1}) and time consumed to 50% of adsorbate breakthrough time (min). From the plot of ln [Ct/(Co - Ct)] against time(min), The values of k_{YN} and (τ) can be determined.

3.5 Experimental Work

3.5.1 Characterization

Prepared samples were characterized by powder X-ray diffraction (PXRD) which were performed by using X'Pert pro diffractometer (Cu Kα, 45 kV, 20 ma, λ= 1.54060A°). To characterize the functional groups in samples, Fourier Transfer Infrared (FT-IR) spectrometer (Perkin Elmer, Germany) was used. A scanning electron microscope (JSM-6390LV) was used to depict the morphology of samples. The surface characteristics of the samples were analyzed with N_2 adsorption-desorption conducted at 77 K using Micromeritics ASAP 2020. A TGA (Thermal Gravimetric Analyzer PYRIS Diamond

TG/DTE, Perkin Elmer) work was performed to study the stability of the MOFs. ca. 5 mg samples were heated to (550°C) at a rate of 10°C / min under N_2 flow.

Metal ion concentrations were measured with an optical emission spectrometer (Optima 2100, Perkin Elmer, Germany) at a wavelength of 220.351, 327.396, and 228.802 nm for Pb^{2+}, $Cu^{2+,}$ and Cd^{2+} respectively.

3.5.2 Synthesis of ED-MIL-101

ED-MIL-101 was synthesized by following the routine of the hydrothermal process reported by Lin et al. [158]. Typically, 3.2 g of chromic nitrate nonahydrate ($Cr(NO_3)3{\cdot}9H_2O$, Sigma-Aldrich, 99%) and 1.44 g of (aminoterephthalic acid) (Sigma-Aldrich, 99%) were added slowly to a solution consists of 0.8 g NaOH and 60 mL of water. The mixture was then stirred for 30 min at room temperature and then transferred to a Teflon-lined stainless steel autoclave. The autoclave was heated for 12 hr at 150°C in an oven. After cooling to room temperature, the solid constituents were separated by centrifuging at 7000 rpm for 5 min. The green product was washed with water, DMF(N, N-dimethylformamide, C_3H_7NO, Guang Zhou, 99.5%), and hot ethanol(Nanjing, China) respectively, then dried overnight at 100°C. The final product, functionalized MOF, was designated as ED-MIL-101(Cr).

3.5.3 Preparation of heavy metal solutions

Stock solutions (200 mg/l) of copper and cadmium ions were prepared by dissolving a suitable amount of $Cu(NO_3)_2.3H_2O$ and $Cd(NO_3)_2.4H_2O$ in de-ionized water. The pH of the stock solution was measured to be (5.2±0.2) and (5.3± 0.4) for Cu(II) and Cd(II) solutions, respectively.

3.5.4 Adsorption experiments

First of all, all the experiments were conducted at 25 ° C. Several experiments were performed to figure out the optimum value of pH for the Cu(II) and Cd(II) uptake by ED-MIL-101(Cr) with dosage 1 g/L. Before the single and binary adsorption experiments, the amount of adsorbent was determined by treating the various amount (0.2-2 g/L) of adsorbent in 50 mL of related salt solution with a concentration of 100 mg/L. Not only was the amount of adsorbent determined, but the equilibrium time also determined, which

180 minutes was. For single and binary adsorption isotherms**,** a dosage amount of 1.2 g/L of MOF was used and stirring in 50 mL of related metal ion solution with concentrations in the range of 10 to 300 mg/L until reaching the equilibrium. The pH value of the solutions was kept at a constant value of 6 to get evenly the effect of hydrogen ions during adsorption experiments, pH was adjusted by using 0.1 mol/L of NaOH or HCl, depending on the initial pH value of the solution. Fully loaded MOFs were then separated by centrifuging.

For a multi ions system, the mixture was prepared by using an equal amount from the parent initial solutions.

3.5.5 Kinetic experiments

The experiments for kinetic investigation were conducted by mixing 600 mg of ED-MIL-101(Cr) with 500 ml with a concentration of 200 mg/L of (Pb^{2+} / Cu^{2+} / Cd^{2+}) ions with continuous stirring at room temperature (25^{o}C). After a certain time interval, samples were withdrawn from the solution to measuring the remaining concentration of metal ions under inspection. The models of pseudo-first order, pseudo-second order, and Weber and Morris intra-particle diffusion have been used to describe the kinetic data.

3.5.6 Packed bed column set-up

The dynamic downward flow experiments were conducted using a column of borosilicate glass with an inner diameter of 2.4 cm and a length of 50 cm. Glass wool was placed at the bottom of the column to prevent the loss of adsorbent during the process. A certain amount of ED- MIL-101(Cr) adsorbent was packed into the column. Beforehand the test start, deionized water was pumped through the pack to soaking the adsorbent and get rid of the air entrapped between the particles. To regulate and control the flow rate of the test solution through the column a peristaltic pump was used. After a certain time interval, the effluent solution was collected for measuring the content of the heavy metal ions.

Effect of bed height

For the assessment of the adsorption efficiency of decorated MOF (ED-MIL-101(Cr)), column experiments were conducted at different heights (2, 4, and 6 cm). The single-ion

solution of Pb(II), Cu(II), and Cd(II) with a concentration of 75 mg/L and flow rate of 15 ml/min was feed in the down flow direction into the backed column. Samples of effluent solutions were taken out at adequate analytical periods for analysis purposes.

Effect of influent flow rate

The flow rate of the influent solution of heavy ions affected the contact time between the adsorbent and metal ions, which is consequently influenced the service time of the backed column. In this work, the flow rate of single ion for Pb(II), Cu(II), and Cd(II) were controlled to be 10, 15, and 20 mL/min. while and the adsorbent height of ED-MIL-101(Cr) was 4 cm and the initial

Effect of influent initial concentration

The adsorption efficiency of functionalized adsorbent (ED-MIL-101(Cr)) for removal of Pb(II), Cu(II), and Cd(II) ions from a single ions solution was investigated for various initial ion concentrations (50, 75, 100 mg/L) for 75 mg/L flow rate and 4cm packed height of the adsorbent. After each experiment. Suitable amounts of Effluent solution were gathered at an adequate period to determine their metal ion content.

4. RESULTS AND DISCUSSIONS

4.1 Introduction

Nowadays, developing high-efficient porous MOFs adsorbents to heavy metal removal has attracted growing attention because a variety of hazardous metal ions have been often detected in various aquatic environments. Most MOFs materials are based on divalent metal ions (i.e.Cu^{+2}, Ni^{+2}, Zn^{+2}). However, based on recent studies show that chemical stability, especially toward hydrolysis can be enhanced by using trivalent metal ions as an alternative for divalent ions [157].

For the experimental work of this study, ED-MIL-101(Cr) was synthesized using a pre-ligand functionalization routine for MIL-101(Cr), also the physicochemical properties of the manufactured functionalized MOF were characterized. The potential application of the functionalized MIL-101(Cr) in the removal of (pb^{2+}/ Cu^{2+} / Cd^{2+}) from single, binary, and ternary aqueous solutions in batch and dynamic adsorption processes were performed. For the batch adsorption experiments, isotherm and kinetics models were investigated. Finally, for the dynamic system, breakthrough curves and kinetics models were also conducted.

4.2 Characterization of Synthesized ED-MIL-101(Cr)

4.2.1 X-ray diffraction

To make sure the prepared material is functionalized MIL-101(Cr), unfunctionalized MOF was also prepared (Figure 4.1). displayed X-ray diffraction patterns of the original and functionalized MOF. The reflection planes corresponding to Miller indices [(202), (311), (400),…(753)] as shown in (Figure 4.2) are indexed for the MIL-101 and these are compatible with the reported values [31,159]**.** It can be observed that characteristic peaks

of the synthesized ED-MIL-101 material match well with those of MIL-101. However, a slight difference in the intensity, which can be attributed to the new functional group inclusion, is observed in the case of ED-MIL-101. Also, the degree of crystallinity was calculated which was 71.25%. These observations are all in agreement with the one reported in the literature [160].

4.2.2 Sorption of nitrogen gas and pore size distribution:

The N_2 adsorption-desorption isotherm of ED-MIL-101was shown in (Figure 4.3). It can *be* seen that the isotherm categorizes as type I according to the classification of IUPA. A small step observed at $P/P_o \sim 0.2$ indicates the existence of micropores and mesopores structures [31], which can be observed in (Figure 4.4). The measurement of surface area and pore volume of ED-MIL-101 show a decrease in both of them compared with pristine MIL-101. The BET surface area and pore volume for ED-MIL-101 were 766.5 m^2/g and 0.47 cm^3/g, respectively.

The value of surface is within the range (347-1270 m^2/g) which is reported in the literature [161]. Substantial variations in surface area in MOFs, for instance, MOF-101(Cr) and ED-MIL-101(Cr) in the reported results even for the same synthetic procedure. Several possible reasons for the variations in the reported values include phase purity, degree of functionalization, crystal defects, and the presence of guest molecules (contaminants) still in pores after the purification of prepared ED-MIL-(Cr). The BET's parameter (C) for MIL-101and ED-MIL-101 was 72.78 and 158.9 respectively.

The functionalization mechanism involves the formation of coordination bond of open metal sites or coordinatively unsaturated sites (CUSs) and the amine group in the ligand that render the cages of MIL-101(Cr) will be equipped by the amine group and blockage some of the pores in the MIL-101(Cr), consequently result in a reduction in the porosity of the grafted MOFs. In addition to the reason, the morphology of crystals suffers from a slight distortion during the modifying process as depicted in the SEM image leads to losing some voids between the MOFs particles.

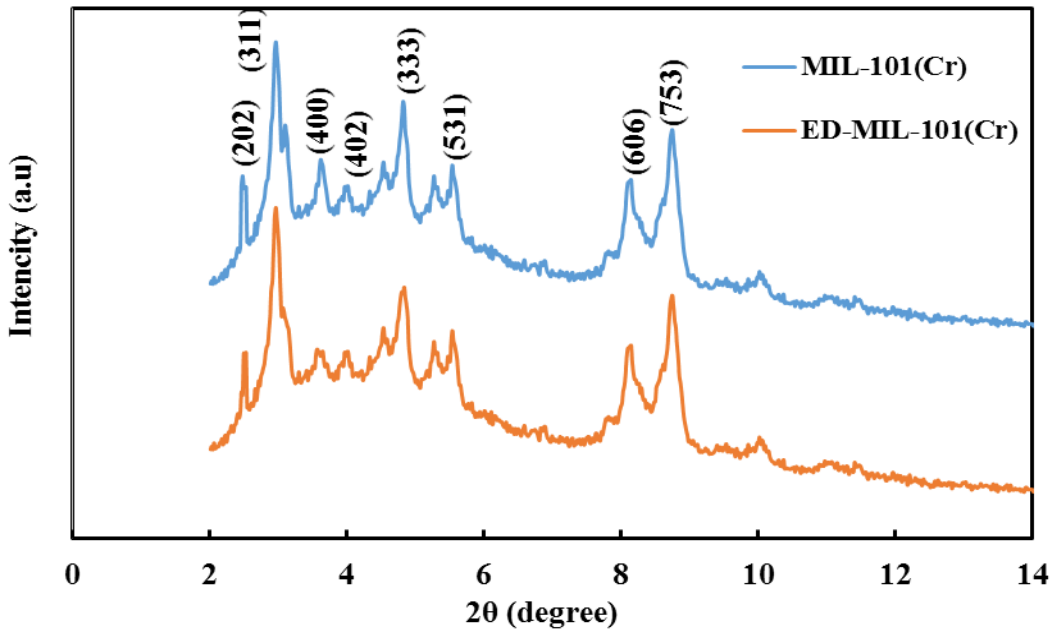

Figure 4.1: X-ray diffraction curves for MIL-101 and ED-MIL-101.

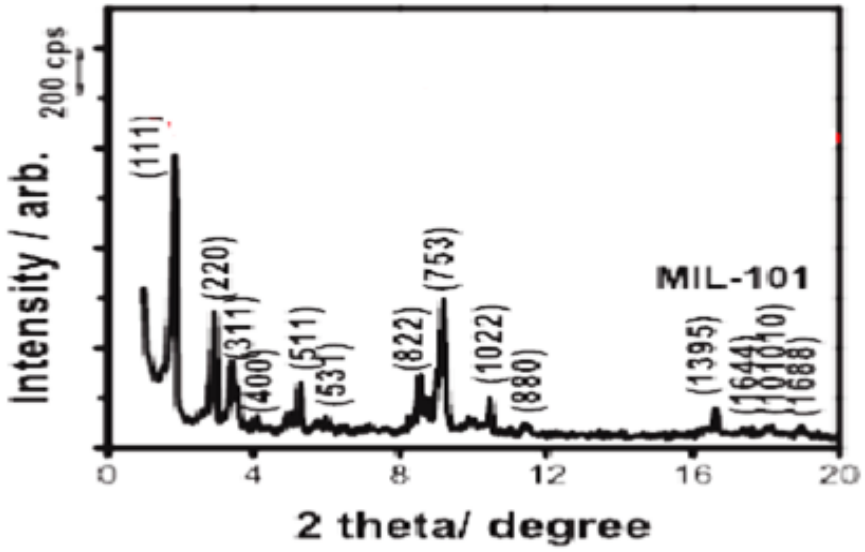

Figure 4.2: X-ray diffraction curves for MIL-101 [31].

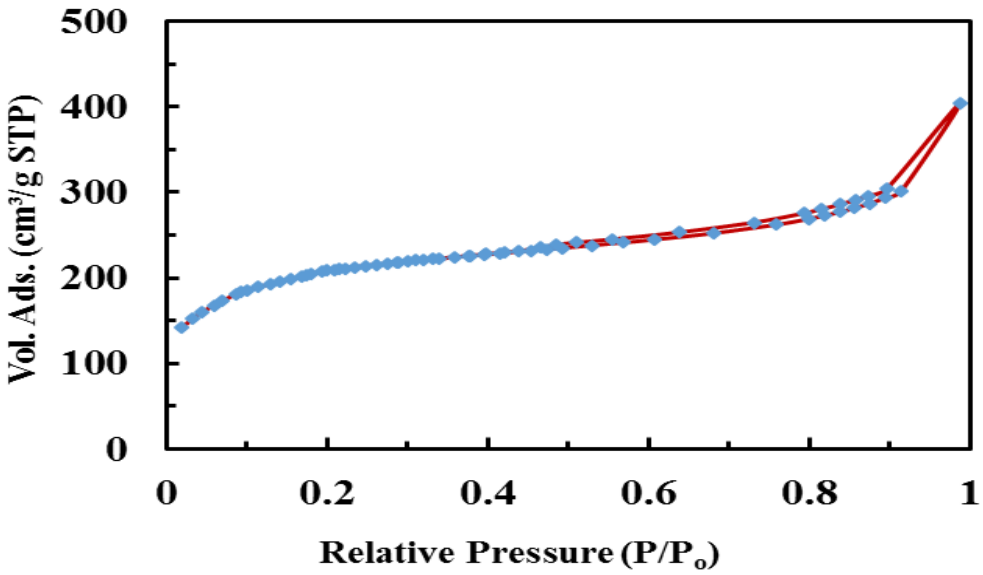

Figure 4.3: Adsorption-desorption isotherms of N_2 on ED-MIL-101.

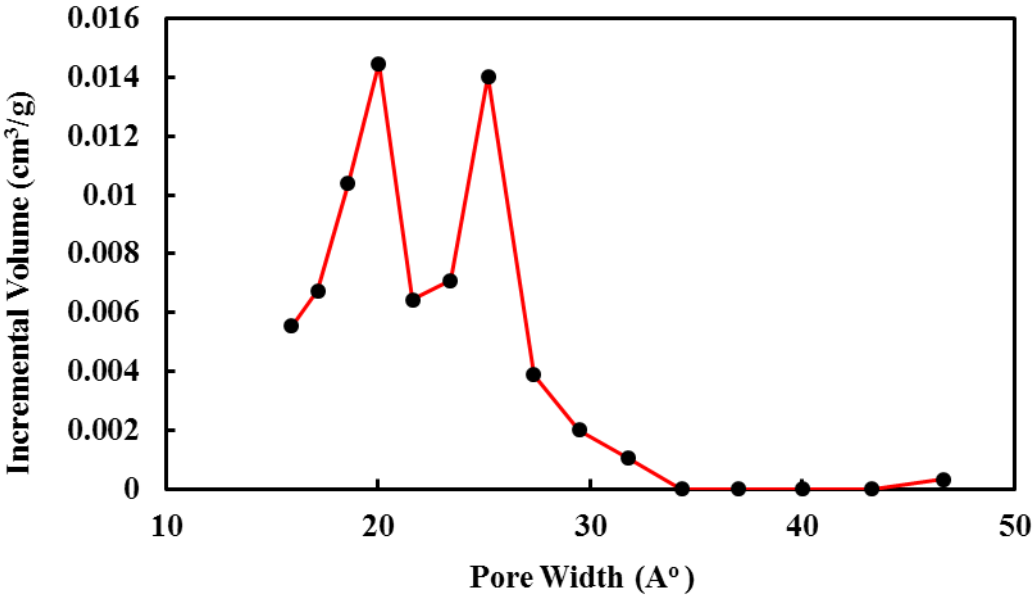

Figure 4.4: Pore size distribution of ED-MIL-101.

4.2.3 Scanning electron microscopy

The morphologies of the prepared samples were analyzed by scanning electron microscopy (Figure 4.5). It can be observed that after the functionalization process the structure of ED-MIL-101 tends to be irregular and rougher while the pristine MOF has a more uniform shape.

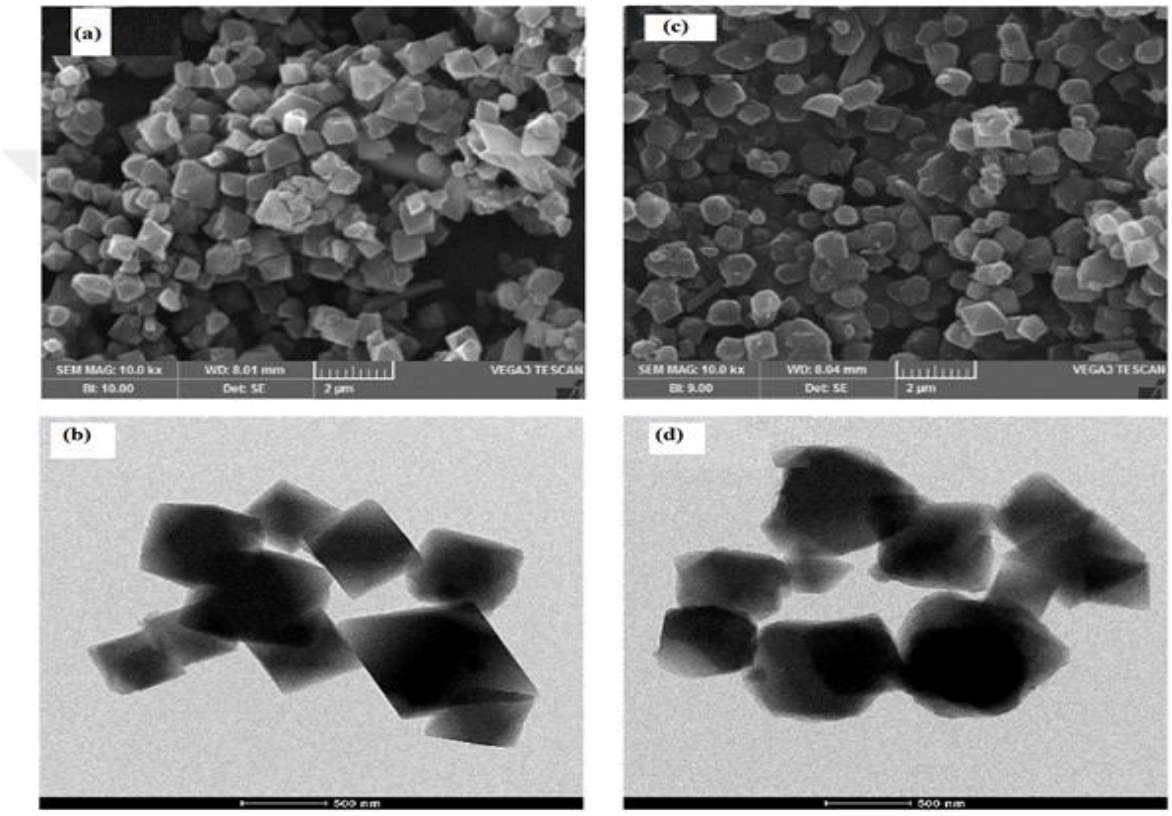

Figure 4.5: SEM images: (a) and (b) for MIL-101. (c) And (d) for ED-MIL-101.

4.2.4 Thermogravimetric analysis (TGA)

The thermal stability of prepared ED-MIL-101 and MIL-101 are shown in the thermogravimetric analysis curve (Figure 4.6). The curves reveal that modification of the pristine MOF with ED decreases slightly the thermal stability of MIL-101. While the ED-MIL-101 framework is still stable up to 300°C.

4.2.5 Fourier transforms infrared (FTIR) spectroscopy

Figure 4.7 exhibits the spectrums of FT-IR for grafted and untreated materials. For grafted MIL-101, the $-NH_2$ plane stretching and C−N stretching frequency can be related to beaks at 882 and 1051 cm^{-1}, [162,65] respectively. Moreover, the peak at 1581 cm^{-1} can be ascribed to the N−H bond stretching [163]. Furthermore, the stretched bands at 3434 cm^{-1} and 2900 cm^{-1} belong to planes of −NH and−CH groups, respectively [164]. All these observations show the success of the functionalization of MIL-101(Cr).

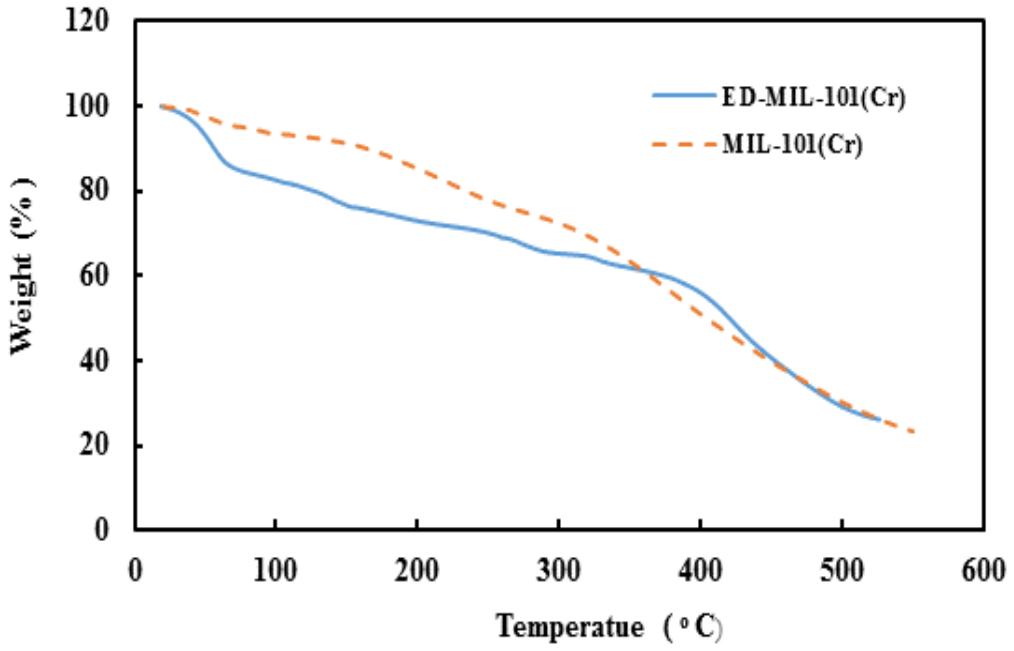

Figure 4.6: Thermogravimetric (TG) curves of MIL-101(Cr) and ED-MIL-101(Cr).

4.3 Batch System Adsorption Experiments:

4.3.1 Influence of pH:

The effect of pH solution on removal efficacy at various initial pH values for a single heavy ions system is displayed in (Figure 4.8). It can be observed that the percentage recovery for each ion was increased with increasing pH till 6 pH value which approximately represents the limit of precipitation and metal hydrolysis except the value for Cd(II) which is greater than 8. For a single ion system, the maximum values of removal efficiency for Pb(II), Cu(II), and Cd(II) ions onto ED-MIL-101(Cr) adsorbent were about 72.15%, 63.5%, and 58.15% respectively at pH 6.

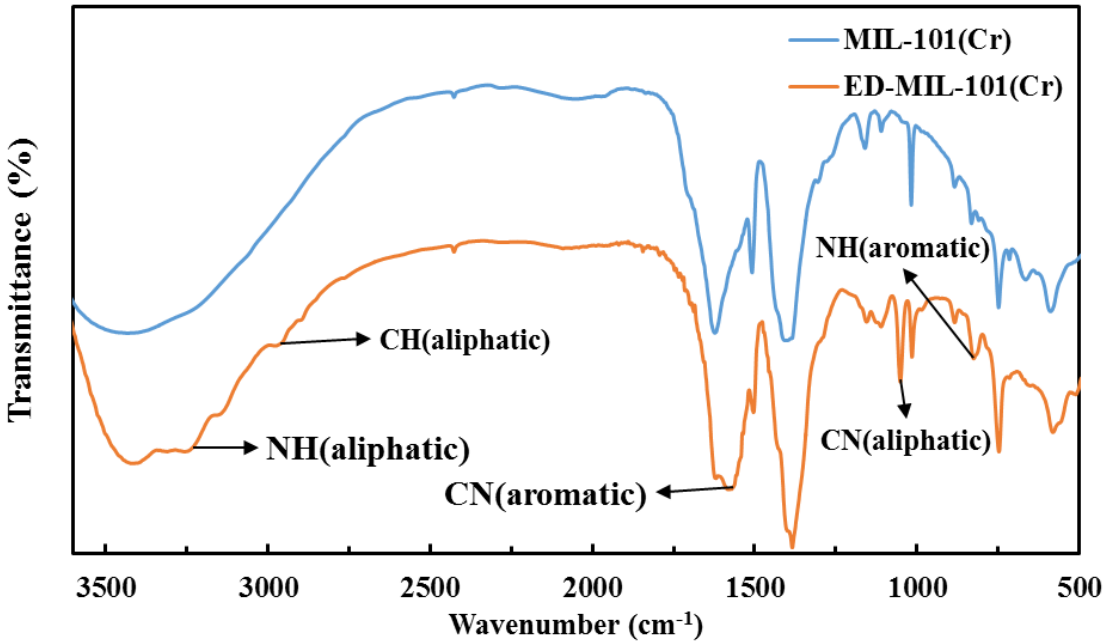

Figure 4.7: FT-IR spectrums of MIL-101 and ED-MIL-101.

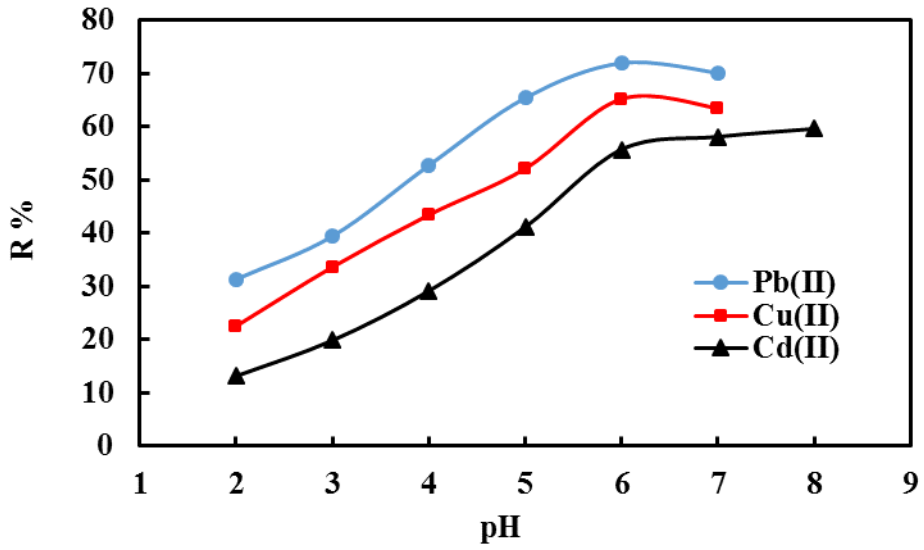

Figure 4.8: Effect of pH on the removing efficiency of single adsorption of Pb(II), Cu(II), and Cd(II) on ED-MIL-101(Cr) at (Co=100 mg/L, m=1g/L).

The low value of ions uptake at low pH attributed to competition between the protons and cation of lead, copper, and cadmium ions in the solution which leads to protonation

of chelating sites at ED-MIL-101(Cr). With increasing the pH values, metal removal from the solution is enhanced substantially. The main reason is that the protonation of carboxyl groups and amino groups is relatively weakened and most of them chelated with Pb(I),Cu(II), and Cd(II) ions. A pH value of 6 was chosen for all adsorption tests in both single and multi-ion systems.

4.3.2 Effect of adsorbent dosage in single-ion systems:

With the motivation of calculation the sufficient amount of adsorbent. A dosage of ED-MIL-101 in the range of (0.2 to 1.8) g/L was used to adsorb a solution with a concentration of 100 mg/L from (Pb(II)/Cu(II)/Cd(II)) ions. As can be detected from the results shown in (Figure 4.9), the uptake amount of Pb(II), Cu(II), and Cd(II) ions were increased with increasing the adsorbent dosage until reaching a plateau value at 1.2 g/L.

This behavior was expected because of the abundant number of active sites provided by the MOF adsorbent at constant ions concentration of the aqueous solution. After exceeding the optimum amount of adsorbent material, there is no noticeable influence of additional quantities due to reaching the equilibrium state in which the solute is uniformly distributed between the liquid and solid phases. Therefore, (1.2) g/L of ED-MIL-101 will be taken as the optimum amount for the next runs. Furthermore, the removal efficiency was in the order Pb(II)>Cu(II) >Cd(II), this attributed to the affinity of ED-MIL-101 toward the adsorbed ions, the electronegativity of ions, and hydrated ionic radius which also affects the uptake capacity as displayed briefly in the next section. These results match the observations in reported literature [165–168].

4.3.3 Adsorption isotherms:

Adsorption isotherm experiments were performed in the various initial concentration of Pb(II), Cu(II), and Cd(II) ions to determine the maximum capacity of ED-MIL-101. Results were shown in (Figure 4.10), The results reveal that the capacities of ED-MIL-101 at equilibrium for each component increase significantly in a low concentration zone with the increasing concentration, then increase gradually until reaching the upper limit of adsorption capacity of grafted MOF. It can be noticed that high concentration can enhance and support the driving force to overcome the resistance of mass transfer between

the aqueous phase and the adsorbent phase [169,170]. Furthermore, it is also observed that ED-MIL-101 has adsorption capacity with order Pb(II)>Cu(II)> Cd(II) (II) ion. These capacities were observed to be 82.55, 69.9, and 63.15 mg/g for Pb, Cu, and Cd ions, respectively.

Several studies stated that the adsorption capacity of the adsorbent for the different metal ions at the same concentration mainly depends on the affinity of the adsorbent which is almost affected by main ionic features such as the ionic radius, electronegativity, and hydrated ionic radius [171,173]. The main ionic properties of Pb(II), Cu(II), and Cd(II)ions are given in Table (4.1) [1]. It is found that the amount of Pb(II) ions bonded to the adsorbent is higher than the other ions owing to the greater electronegativity of lead ions. As stated in the literature the metal ion which has more electronegativity is more strongly bonded with the active sites at the adsorbent surface [174,175]. Also, there is another reason for the difference in uptake capacity which is attributed to the hydrated radius of the ions. The ion which has the smaller hydrated ionic radius can easily penetrate the smaller pores without steric hindrance which means more sites are available for adsorption [171,176]. Therefore it was observed that the adsorbed amount of Pb(II) ions higher than cupper and cadmium ions since it has a smaller hydrated ionic radius.

Table 4.1: Basic Properties of Pb^{2+}, $Cu^{2+,}$ and Cd^{2+} ions.

Metal ion	Electronegativity	Ionic radius (A^o)	Hydrated ionic radius (A^o)
Pb(II)	2.33	1.32	4.01
Cu(II)	1.90	0.73	4.19
Cd(II)	1.69	0.95	4.26

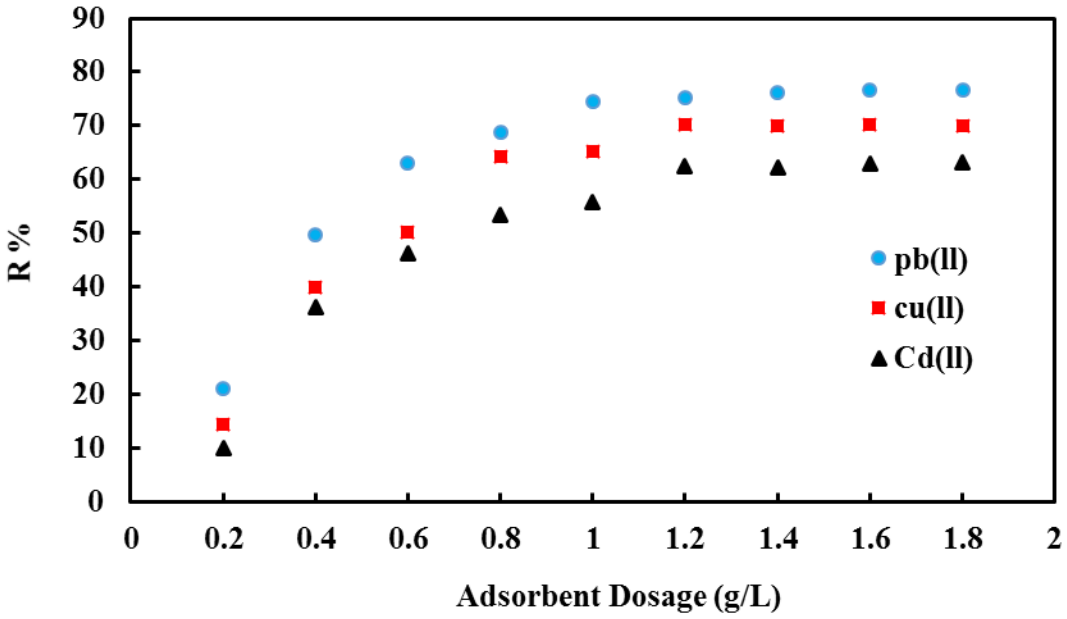

Figure 4.9: Removing efficiency for Pb(II), Cu(II), and Cd(II) in a single ion system (Co=100 mg/L, pH=6).

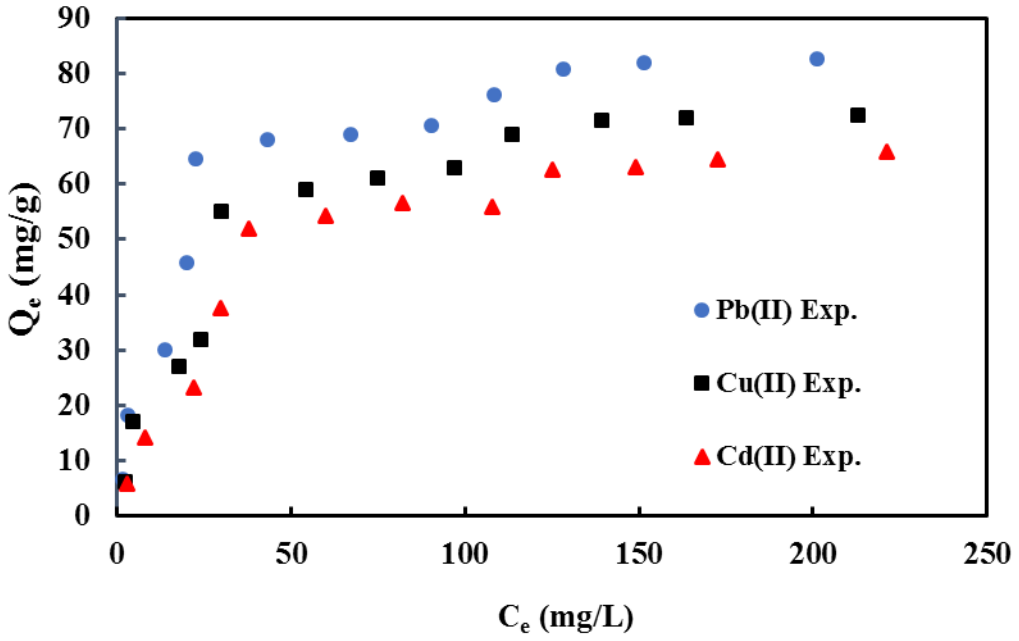

Figure 4.10: Experimental isotherms for Pb(II), Cu(II), and Cd(II) in a single system. (m=1.2g/L, pH=6).

4.3.4 Adsorption in binary and ternary systems

In a system for binary and ternary ions of Pb(II), Cu(II), and Cd(II) the adsorption characteristics of adsorbent and the potential interaction effects between the coexisting ions were studied. Herein, multi-ion solutions containing an equal amount of examined ions were used in the experiments. The concentration ranged from 10 mg/L to 200 mg/L. pH and temperature were maintained at 6 and 298 K, respectively. The results are shown in (Figures 4.11 to 4.14). It can be noticed that the single uptake amounts in the binary system are approximately the same values at low initial content f (Figure 4.15). This result reveals that the interaction between the ions is negligible. When the concentrations of co-existence ions increased to high values, there will be competition between these ions for the active site of the adsorbent on the surface. This behavior matched the results obtained for a single ion system. Table 4.2 shows the values of the adsorption capacity of ED-MIL-101 single and binary ion systems. It can be concluded that the uptake amounts at a low concentration of the two ions are approximately the same amount. As mentioned previously these results can be explained by the number of active sites that participate in the adsorption process and the weak interaction between the competing ions [173,177].

The influence of ionic interaction between the competitive ions in a multi-ion solution can be expressed by the ratio of adsorption capacity for the metal ion in the multi-ion system (Q_e^{mix}) to that in a single ion system (Q_e). This ratio is named interaction factor which can be classified in three cases [178]. As are given as shown:

(1) $Q_e^{mix}/Q_e > 1$; the interaction of the other ions had a positive effect and enhanced the adsorption,

(2) $Q_e^{mix}/Q_e = 1$; negligible interaction,

(3) $Q_e^{mix}/Q_e < 1$; adsorption was suppressed by the coexisting ions,

Based on the results of ionic interaction given in Table 4.2 the adsorption of copper ion was influenced by the presence of cadmium ion because of the competition between the coexisting ions to adsorb to the active sites at the adsorbent surface.

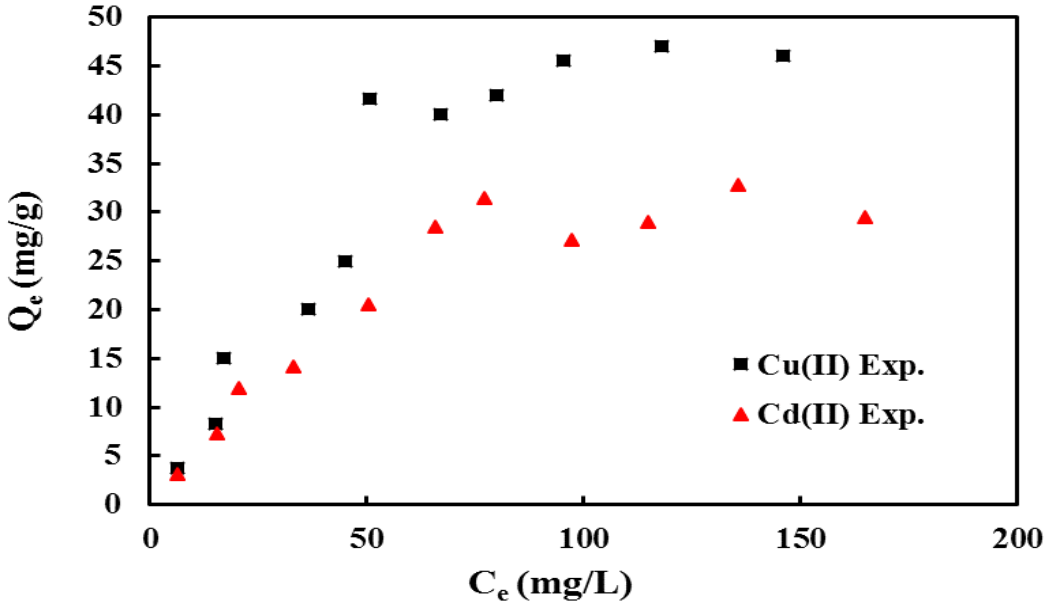

Figure 4.11: Experimental isotherms for Cu(II) and Cd(II) in binary solution.(m=1.2g/L, pH=6).

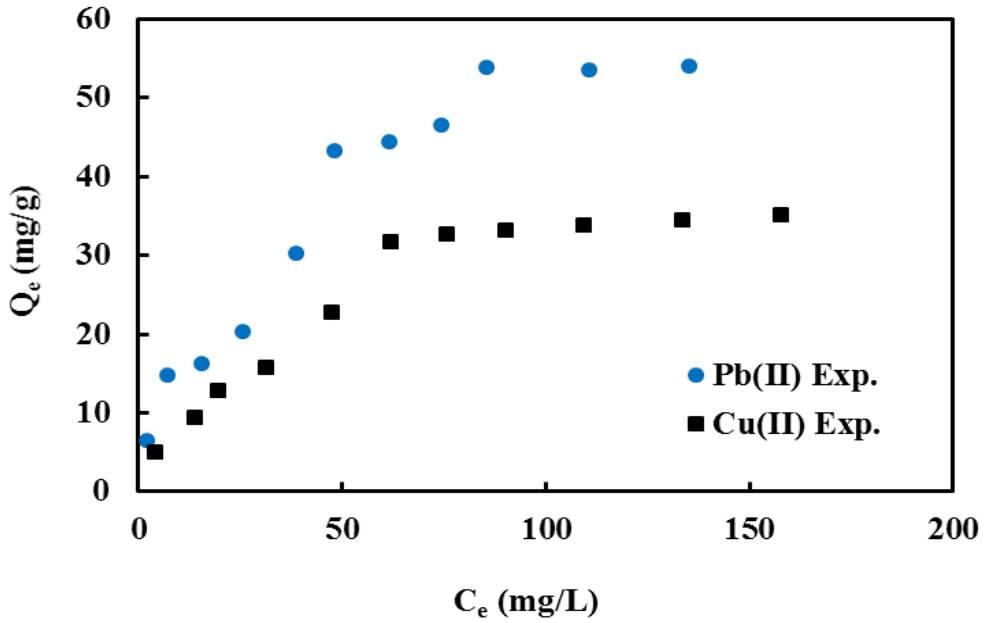

Figure 4.12: Experimental isotherms for Pb(II) and Cu(II) in binary solution.(m=1.2g/L, pH=6).

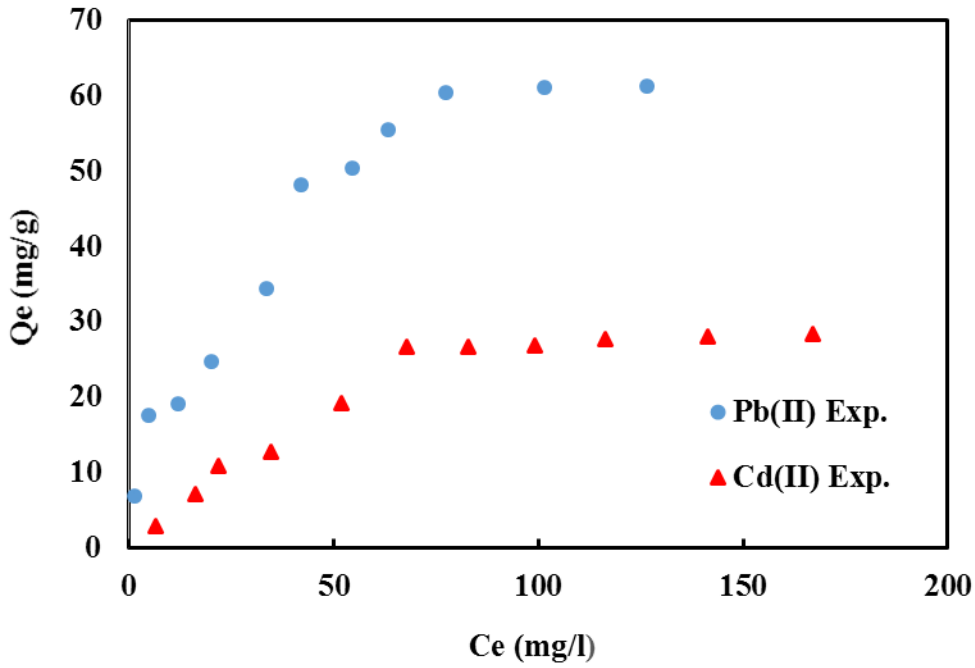

Figure 4.13: Experimental isotherms for Pb(II) and Cd(II) in binary solution.(m=1.2g/L, pH=6).

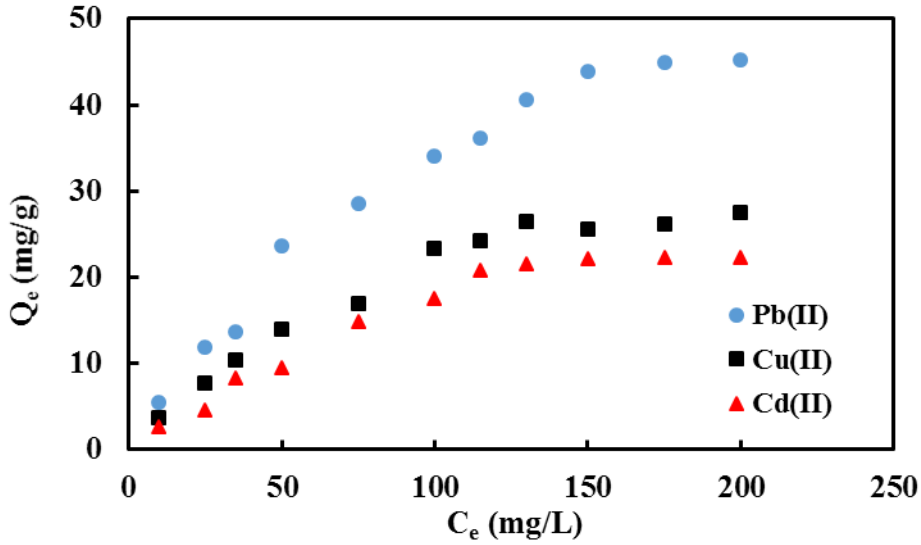

Figure 4.14: Experimental isotherms for Pb(II), Cu(II) and Cd(II) in ternary solution (m=1.2g/L, pH=6).

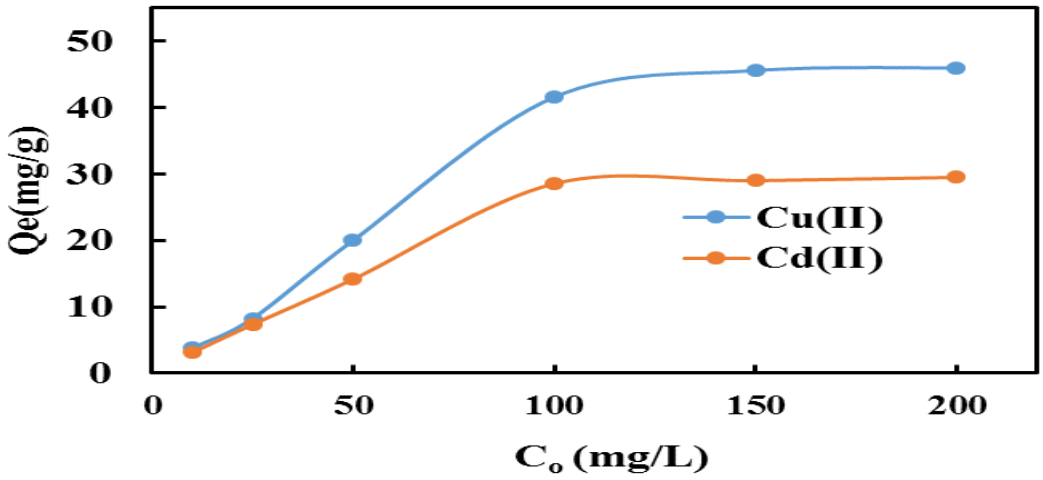

Figure 4.15: Adsorption capacity for binary system at various initial concentration of Cu(II) and Cd(II) .(m=1.2 g/L, pH=6).

Table 4.2: Adsorption capacities of ED-MIL-101 in single-and binary-ion systems (dosage=1.2g/L, pH=6).

C_o (mg/L)	Single ion system (Q_e)(mg/g)		Binary ion system (Q_e) (mg/g)		The interaction ion factor in binary ion system	
	Cu(II)	Cd(II)	Cu(II)	Cd(II)	Cu(II)	Cd(II)
10	6.25	5.80	3.37	3.10	0.54	0.53
25	17.0	14.1	8.25	7.34	0.49	0.52
50	27.0	23.3	20.0	14.15	0.74	0.61
100	55.0	51.9	41.6	28.55	0.76	0.55
150	62.5	60.0	45.6	29.0	0.73	0.48
200	72.0	62.5	46.0	29.5	0.64	0.47

4.3.5 Isotherm models

In this study, to present the distribution way of the studied ions between the solid and liquid phase, Langmuir, Freundlich, and Sips models were used to analyze the various adsorption data of the adsorbed ion. The parameters of these isotherm models and the

correlation coefficient (R^2) values are summarized in Table (4.3) for the single-ion system. It can be seen from (Figures 14.24, 14.25, and 4.26) that the Langmuir and Sips models are fit better than the Freundlich model for single ion adsorption of adsorbed ions on ED-MIL-101.this result proved the high values of the regression coefficients (R^2) calculated for the well correlated models. These results indicate the homogeneity of the adsorbent surface in the absence of competitive ions which is proved by the values of m nearest to unity in the sips model parameters. Also it can notice that the similarity between Langmuir and sips model when increasing the concentration of each studied ion this behavior is evidence by the slight difference in the calculated values of Q_m for adsorbed ions. On the other hand, as can be observed from Figures related to the adsorption process in binary and ternary ions (Figure 4.19 to 4.30). The Freundlich model is proved to be the better model to represent the adsorption of heavy ions from their solutions on grafted MOF adsorbent.

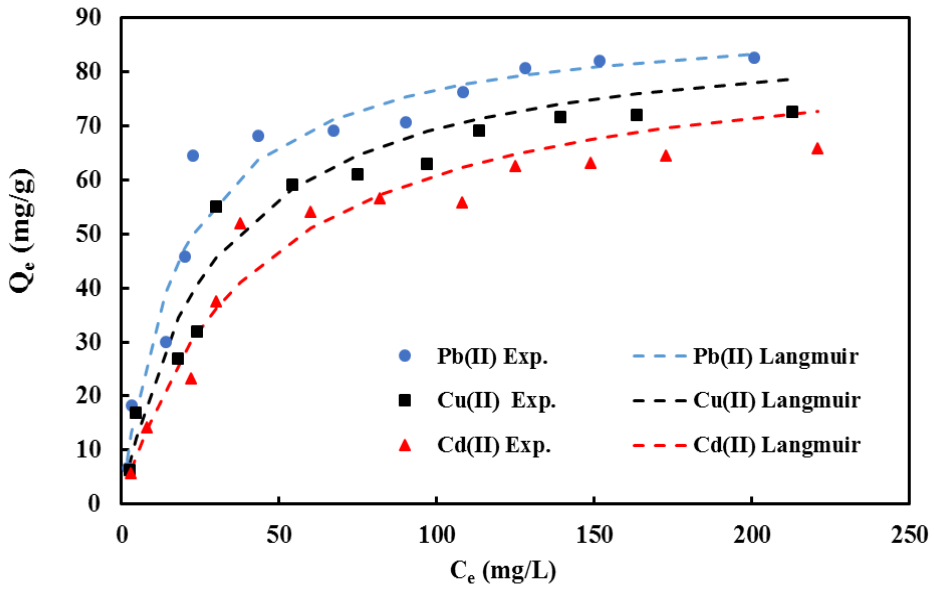

Figure 4.16: Experimental and Langmuir isotherms for Pb(II), Cu(II), and Cd(II) in a single system (m=1.2g/L, pH=6).

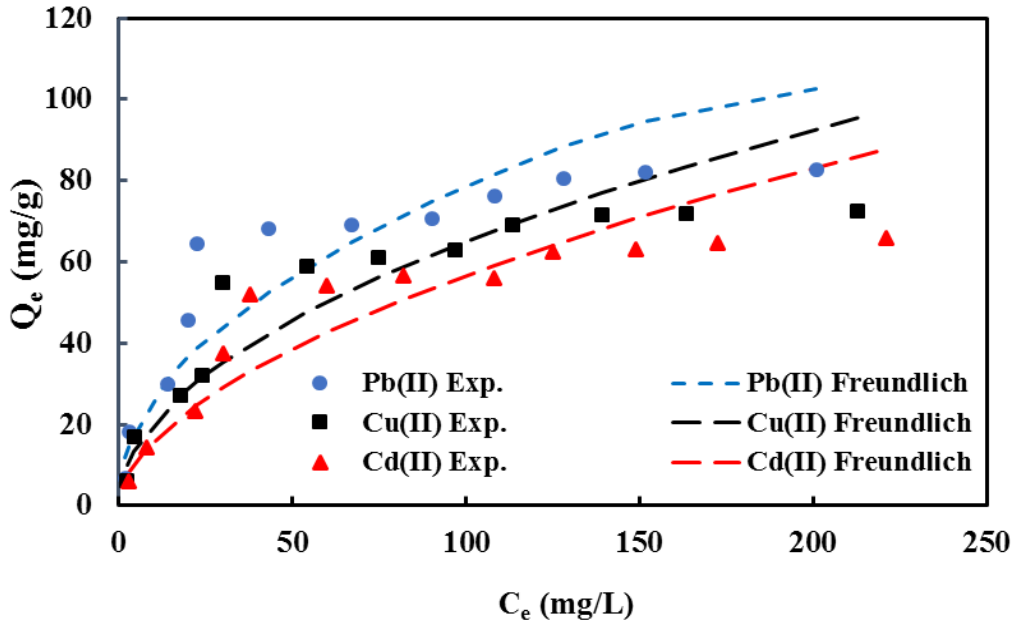

Figure 4.17: Experimental and Freundlich isotherms for Pb(II), Cu(II) and Cd(II) in a single system(m=1.2g/L, pH=6).

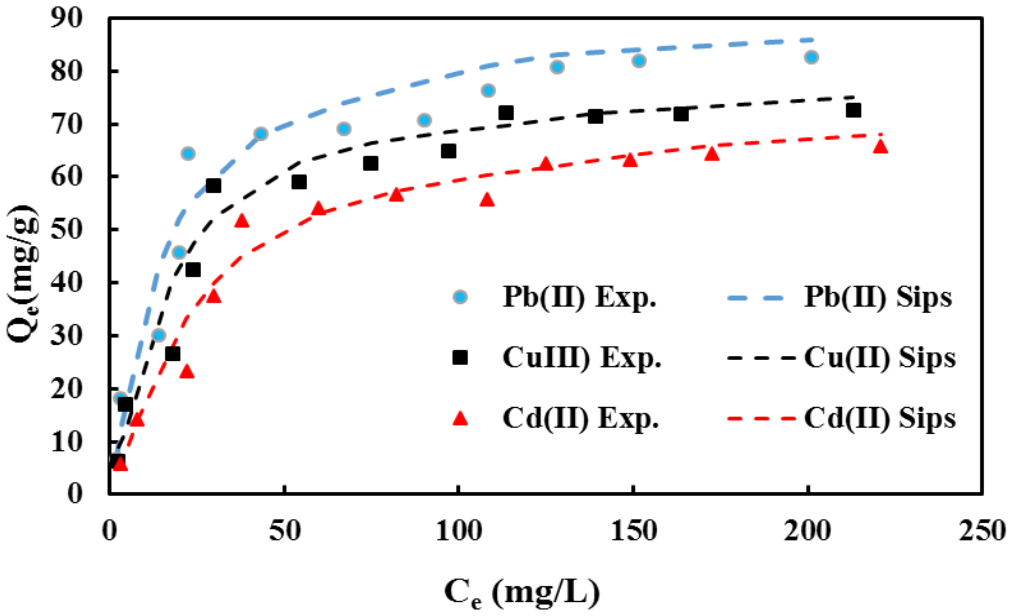

Figure 4.18: Experimental and Sips isotherms for Pb(II), Cu(II), and Cd(II) in a single system (m=1.2g/L, pH=6).

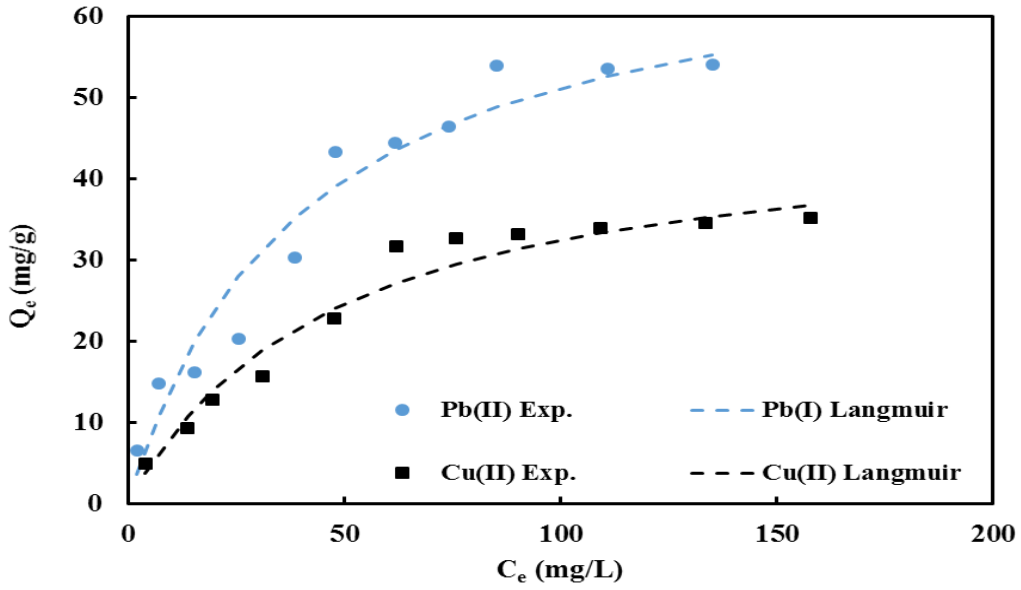

Figure 4.19: Experimental and Langmuir isotherms for Pb(II) and Cu(II) in binary system (m=1.2g/L, pH=6).

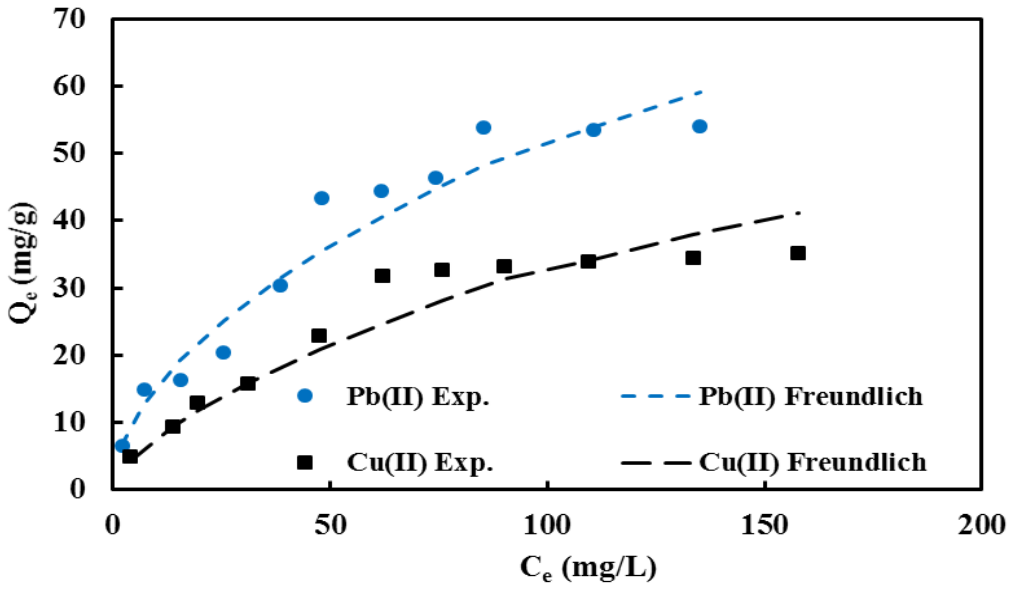

Figure 4.20: Experimental and Freundlich isotherms for Pb(II) and Cu(II) in a binary system(m=1.2g/L, pH=6).

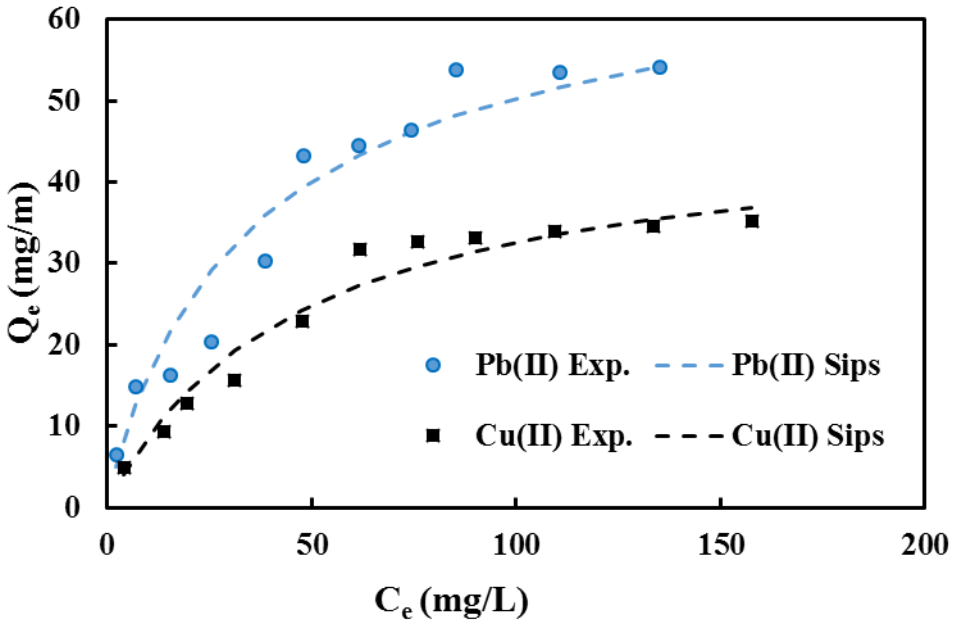

Figure 4.21: Experimental and Sips isotherms for Pb(II) and Cu(II) in a binary system (m=1.2g/L, pH=6).

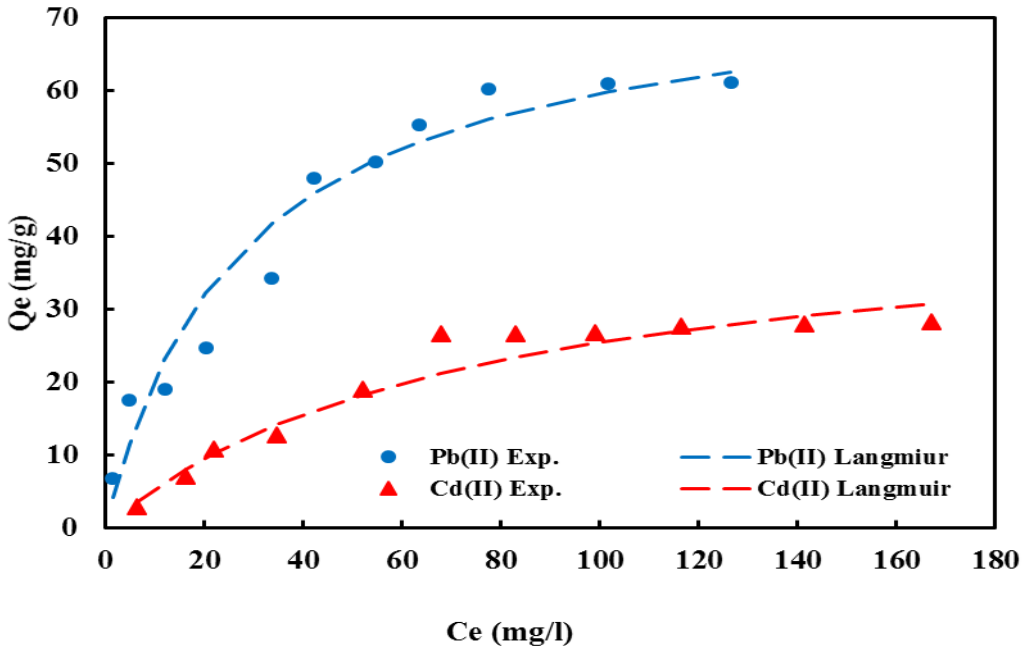

Figure 4.22: Experimental and Langmuir isotherms for Pb(II) and Cd(II) in a binary system (m=1.2g/L, pH=6).

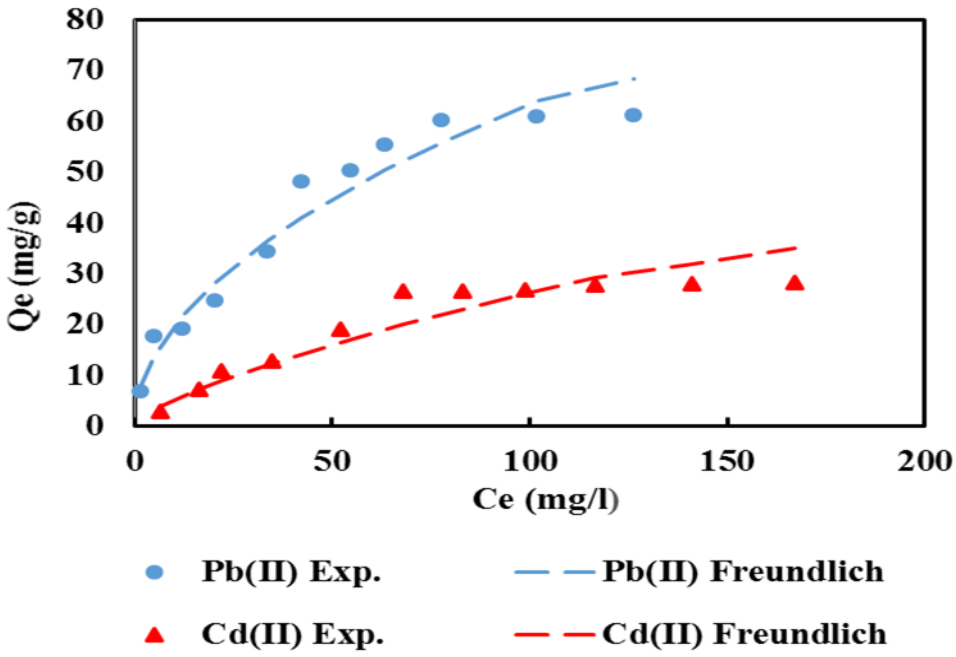

Figure 4.23: Experimental and Freundlich isotherms for Pb(II) and Cd(II) in binary system (m=1.2g/L, pH=6).

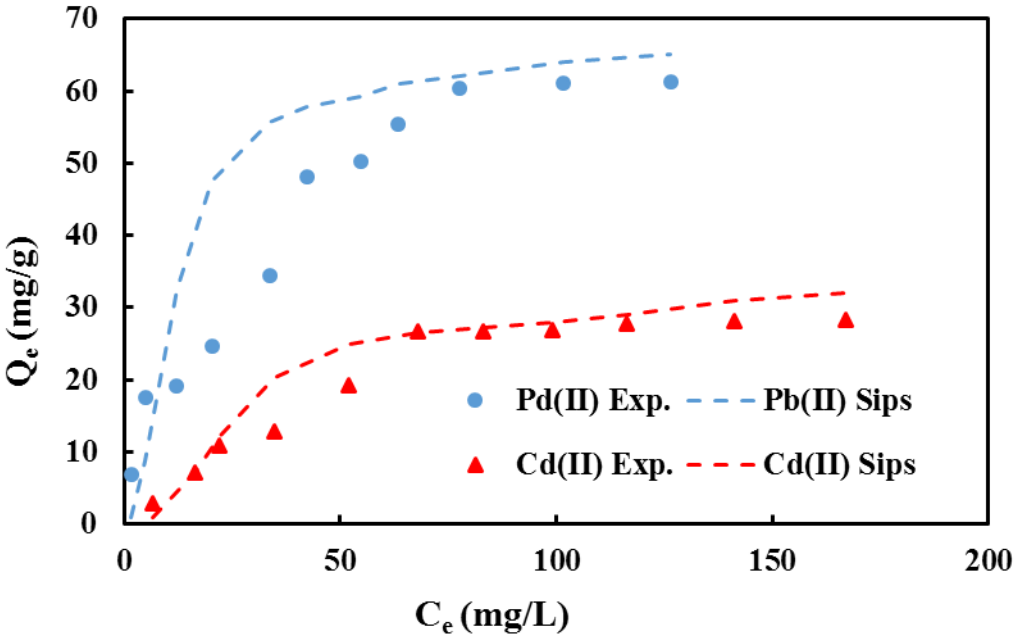

Figure 4.24: Experimental and Sips isotherms for Pb(II) and Cd(II) in a binary system (m=1.2g/L, pH=6).

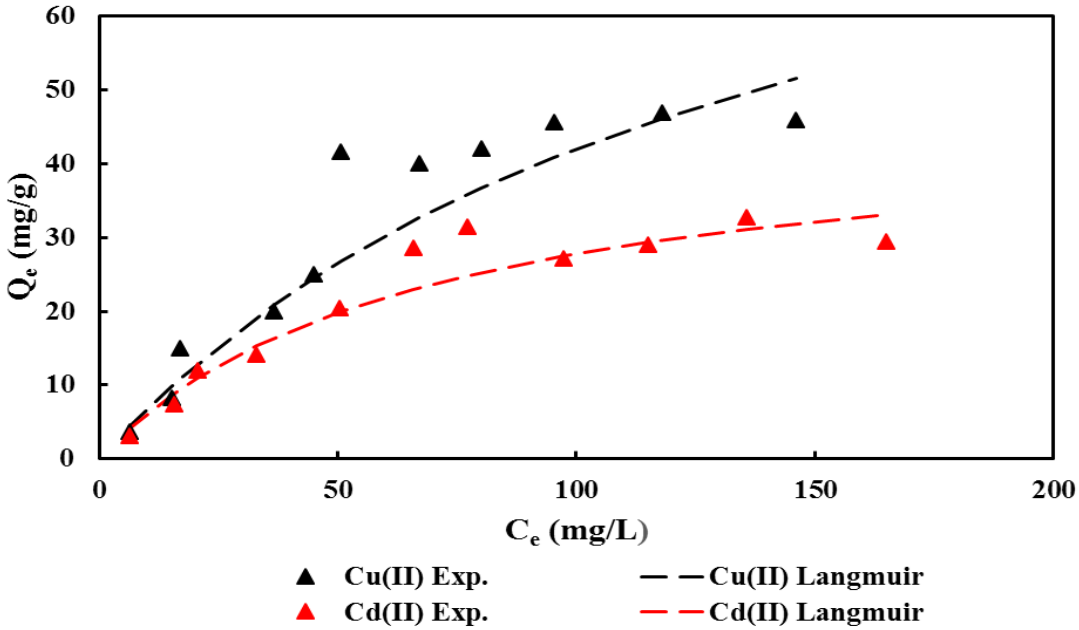

Figure 4.25: Experimental and Langmuir isotherms for Cu(II) and Cd(II) in a binary system (m=1.2g/L, pH=6)

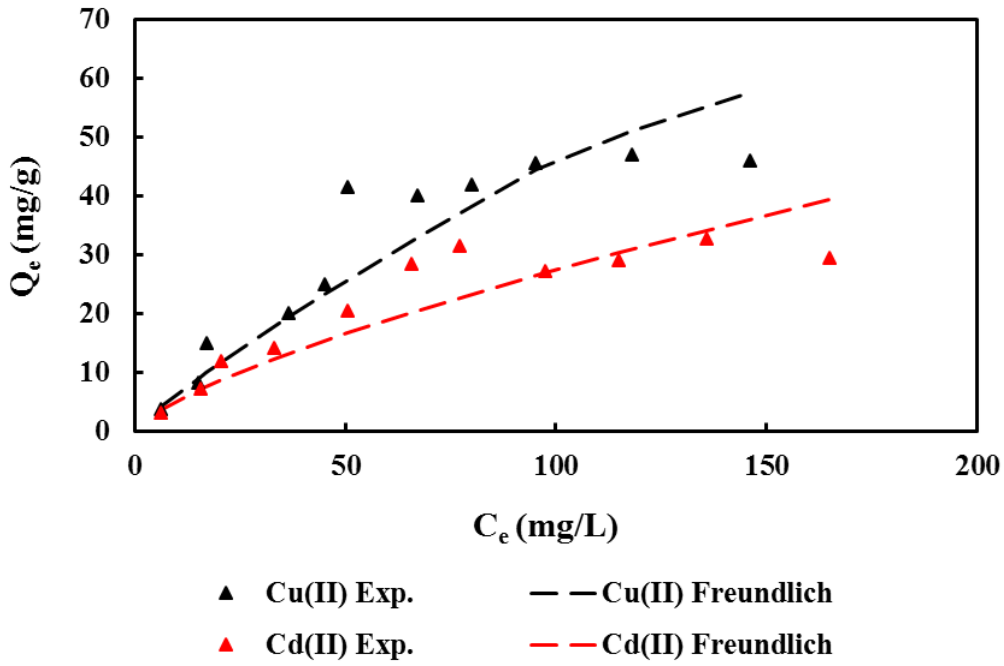

Figure 4.26: Experimental and Freundlich isotherms for Cu(II) and Cd(II) in binary system (m=1.2g/L, pH=6).

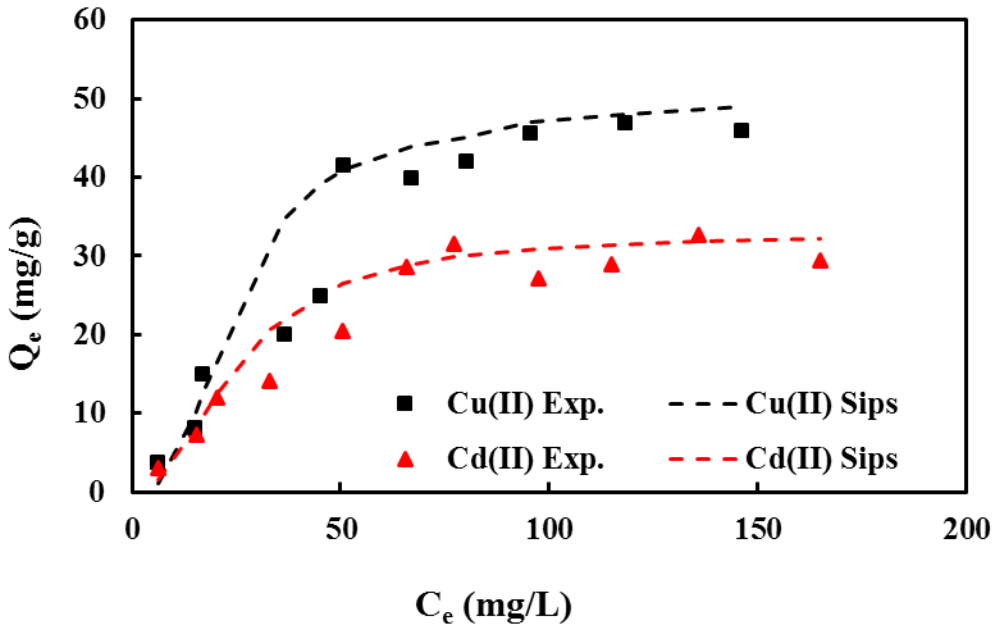

Figure 4.27: Experimental and Sips isotherms for Cu(II) and Cd(II) in a binary system (m=1.2g/L, pH=6).

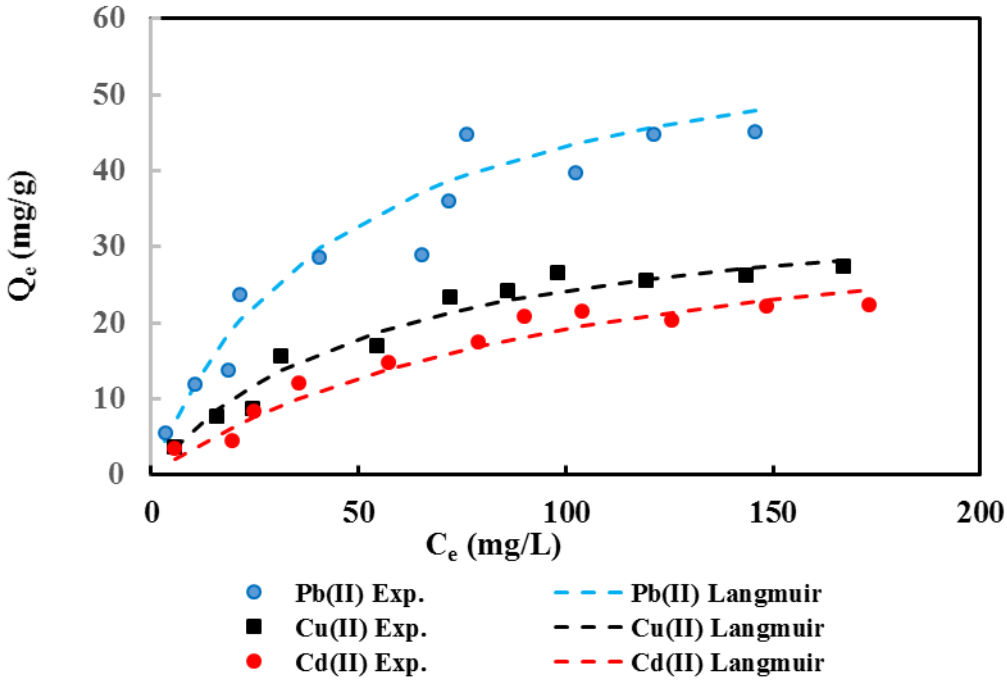

Figure 4.28: Experimental and Langmuir isotherms for Pb(II), Cu(II), and Cd(II) in the ternary system (m=1.2g/L, pH=6).

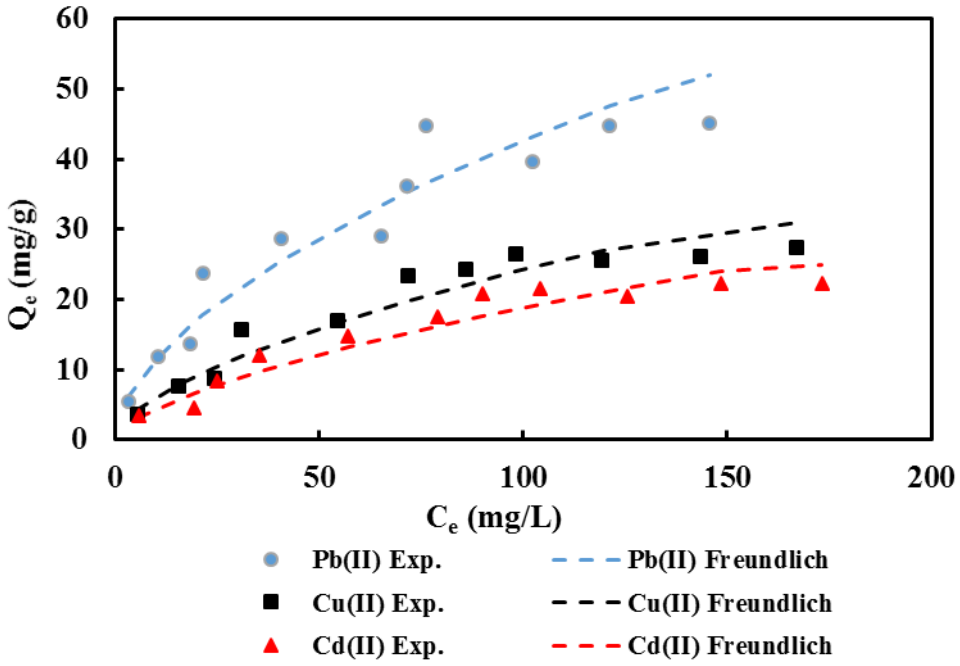

Figure 4.29: Experimental and Freundlich isotherms for Pb(II), Cu(II) and Cd(II) in ternary system (m=1.2g/L, pH=6).

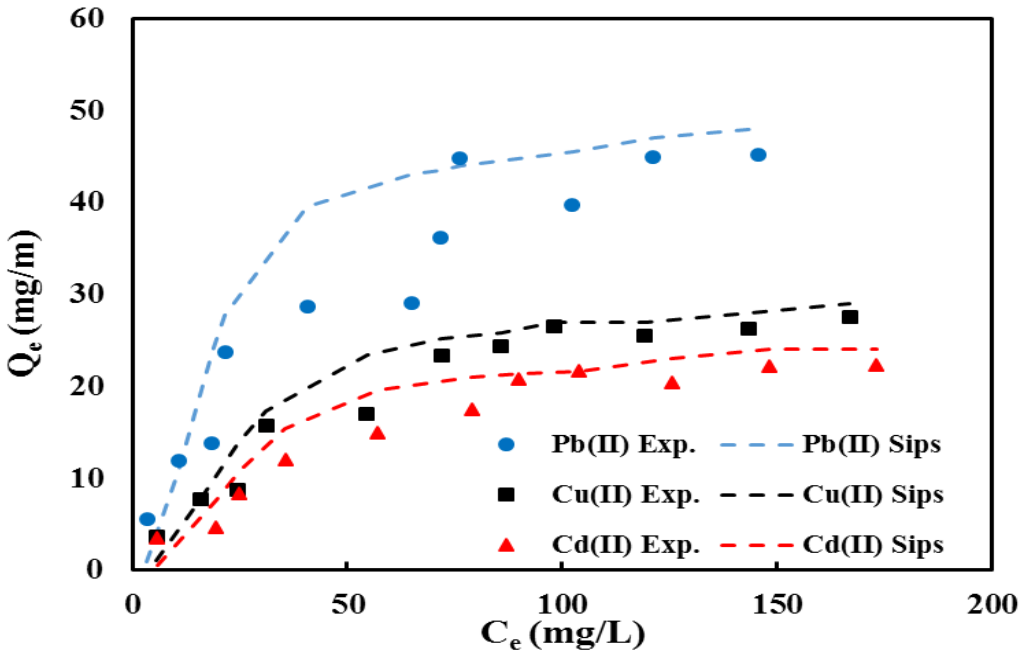

Figure 4.30: Experimental and Sips isotherms for Pb(II), Cu(II), and Cd(II) in the ternary system (m=1.2g/L, pH=6).

This outcome is supported by the values of the correlation coefficient (R^2) listed in Tables (4.4) and (4.5) for each tested system. Low values of m in the sips model for multi-ions system indicate the heterogeneity of the system with a poor correlation of the experimental data because of the interaction effects between ions coexisting in the system, however, these effect grows with increasing the concentration but the adsorption capacity increased which may be ascribed to the repulsive forces between the same charge ions forced them to penetrate to more voids and reach new adsorbing sites.

4.3.6 Adsorption mechanism

To illustrate the mechanism of the removal of Pb(II), Cu(II), and Cd(II) ions by grafted MOF adsorbent, FT-IR analysis was also conducted. The similarity in the IR spectrums of lead, copper, and cadmium ions can be seen from (Figures 4.31 to 4.34). After adsorption of metal ions, new peaks appeared for Pb(II), Cu(II), and Cd(II) ions at 540, 530, and 550 cm^{-1}, respectively. These stretching vibration peaks may be attributed to the formation of new chemical bonds corresponding to Pb-N, Cu-N, and Cd-N. Additionally, 1261,1258 and 1266 cm^{-1} appeared after the adsorption of Pb(II), Cu(II), and Cd(II) ions respectively, indicating the interaction with $Pb(OH)^+$, $Cu(OH)^+$ or $Cd(OH)^+$.

Table 4.3: Isotherm models parameters and regression coefficients for the adsorption of Pb(II), Cu(II), and Cd(II) ions on ED-MIL-101 in single ions systems.

Isotherm Model	Parameter	Pb(II)	Cu(II)	Cd(II)
Langmuir	Q_m(mg/L)	90.90	89.29	77.519
	b (L/mg)	0.0534	0.0349	0.0296
	R^2	0.983	0.962	0.9814
Freundlich	K_f	8.8227	5.914	3.264
	n	2.10	1.89	1.509
	R^2	0.8718	0.8926	0.9510
Sips	Q_m(mg/L)	87.52	79.54	72.85
	K_s ($\times 10^{-2}$) (L/mg)	4.13	2.41	1.80
	m	0.8204	0.8604	0.8839
	R^2	0.9405	0.946	0.9675

Table 4.4: Isotherm models parameters and regression coefficients for the adsorption of Pb(II), Cu(II), and Cd(II) ions on ED-MIL-101 in binary-ion systems.

Isotherm Model	Parameter	Binary system		Binary system		Binary system	
		Pb(II)	Cu(II)	Pb(II)	Cd(II)	Cu(II)	Cd(II)
Langmuir	Q_m(mg/L)	69.45	45.61	74.3358	41.2477	51.01	35.25
	b (L/mg)	0.0259	0.02237	0.03649	0.014592	0.007	0.0139
	R^2	0.9184	0.959	0.9533	0.9193	0.646	0.9195
Freundlich	K_f	5.9593	1.0011	4.3853	2.2542	1.161	0.983
	n	1.9430	1.408	1.8542	1.7167	1.155	1.384
	R^2	0.9622	0.9636	0.9618	0.9357	0.933	0.9404
Sips	Q_m(mg/L)	65.85	48.65	70.24	36.76	49.05	33.17
	K_s ($\times 10^2$) (L/mg)	3.7	2.3	5.4	1.9	1.9	2.6
	m	0.68	0.73	0.46	0.376	0.475	0.547
	R^2	0.8347	0.8571	0.722	0.739	0.793	0.7153

Table 4.5: Isotherm models parameters and regression coefficients for the adsorption of Pb(II), Cu(II), and Cd(II) ions on ED-MIL-101 in ternary ion systems.

Isotherm Model	Parameter	Pb(II)	Cu(II)	Cd(II)
Langmuir	Q_m(mg/L)	56.88	34.31	35.75
	b (L/mg)	0.0248	0.0202	0.0106
	R^2	0.9701	0.9775	0.8802
Freundlich	K_f	3.0634	1.5048	1.4408
	n	1.7376	1.6570	1.3893
	R^2	0.9626	0.9673	0.9566
Sips	Q_m(mg/L)	60.15	38.26	39.65
	K_s ($\times 10^2$) (L/mg)	0.0288	0.0196	0.0379
	m	0.432	0.463	0.416
	R^2	0.592	0.719	0.710

Split of the peak at 1385,1382 or 1392 cm^{-1} possibly due to the coordination between the adsorbed ions, and the O atom of C=O unit in the carboxylate group which may produce as a secondary functional group. According to FT-IR results, it is possible to postulate

that ion exchange and chemical adsorption (surface complexation) are both govern the interaction between the ions and ED-MIL-101 [179]. The letter (X) was used to represent the adsorbed ion (Pb/Cu/Cd) in the equations (4.1) and (4.2) to describe the interaction between the adsorbent and the adsorbate ion (X):

$$-\mathrm{N}H_2 + X^{+2} \rightleftharpoons -\mathrm{N}H_2X^{+2} \tag{4.1}$$

$$-\mathrm{N}H_2 + X^{+2} + H_2O \rightleftharpoons -\mathrm{N}H_2X(OH)^{+} \tag{4.2}$$

Adsorption was suggested to occur due to heavy metal ions coordinating with amino groups grafted on CUS on MIL-101(Cr) as shown in the schematic (Figure 4.35). The amino groups act as chelated sites for Pb(II), Cu(II), and Cd(I) ions. This interaction was also proved by the -NH bond stretching in FT-IR spectrums after Pb^{2+}, $Cu^{2+,}$ and Cd^{2+} adsorption on ED-MIL-101(Cr). Similar results are found in the literature about the action of the amine group in the adsorption process of Cu(II) ions on amino-functionalized magnetic nanoparticles [180], [181]. Furthermore, the suggested mechanism was adopted by some researchers in the encapsulation of noble metals [53] such as Pd, Pt, and Au over the amine-grafted MIL-101.

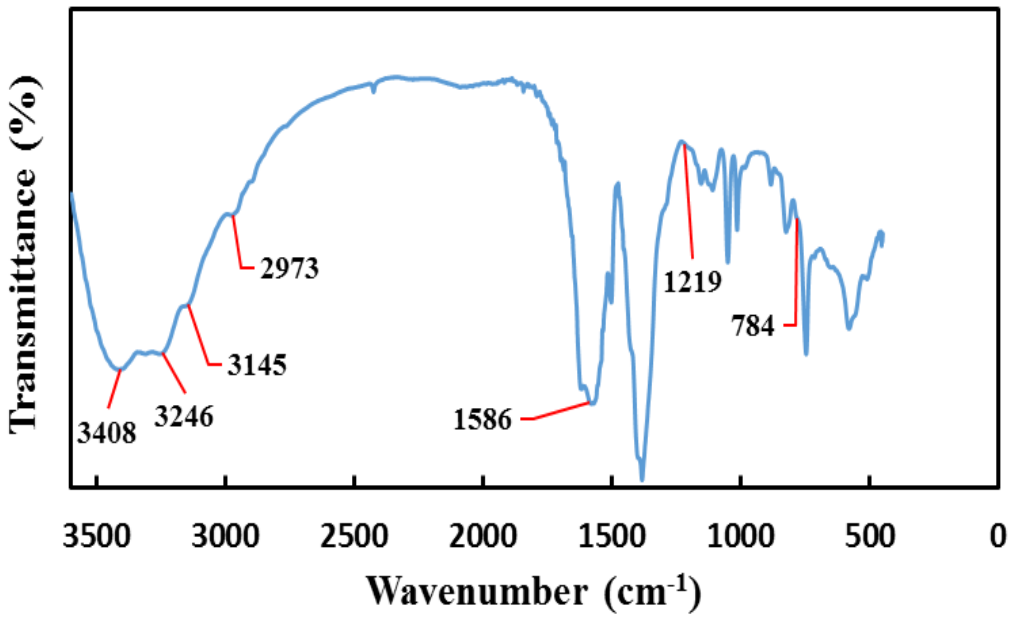

Figure 4.31: FT-IR spectrums of ED-MIL-101 before adsorption.

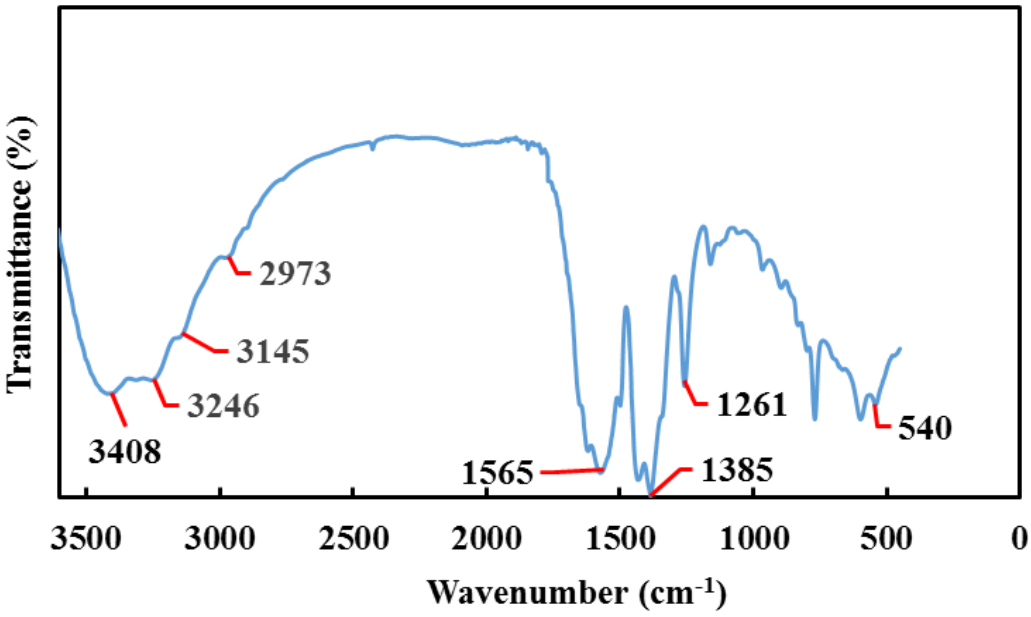

Figure 4.32: FT-IR spectrums of ED-MIL-101 after Pb (II) adsorption.

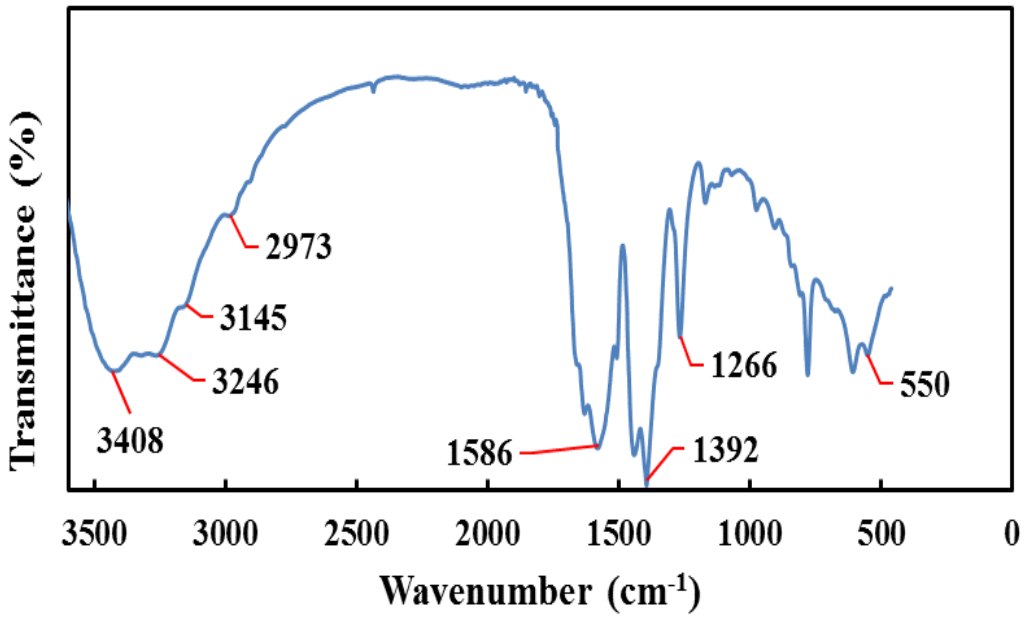

Figure 4.33: FT-IR spectrums of ED-MIL-101 after Cu(II) adsorption**.**

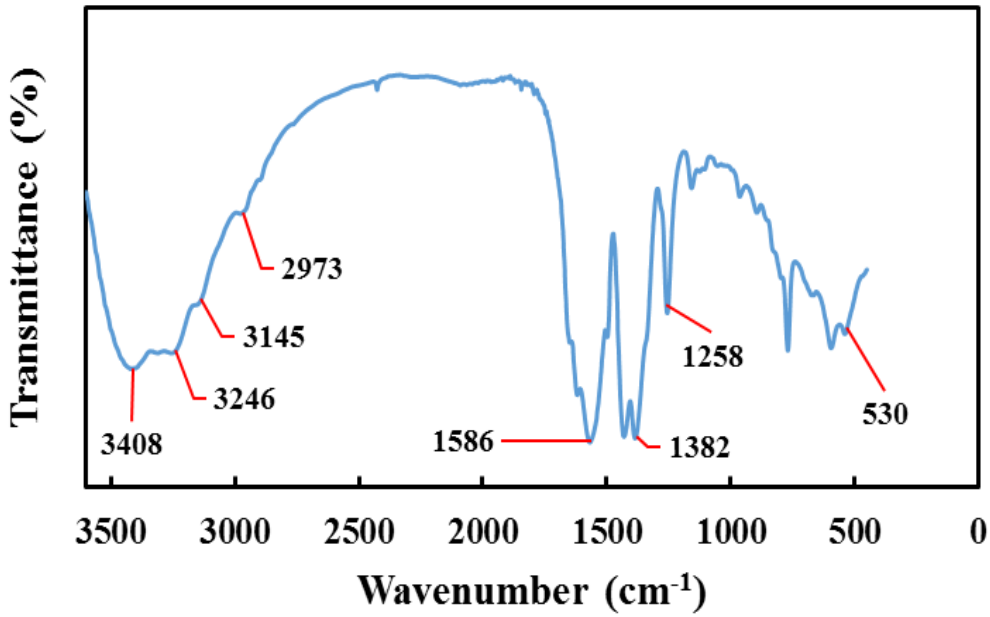

Figure 4.34: FT-IR spectrums of ED-MIL-101 after Cd(II) adsorption**.**

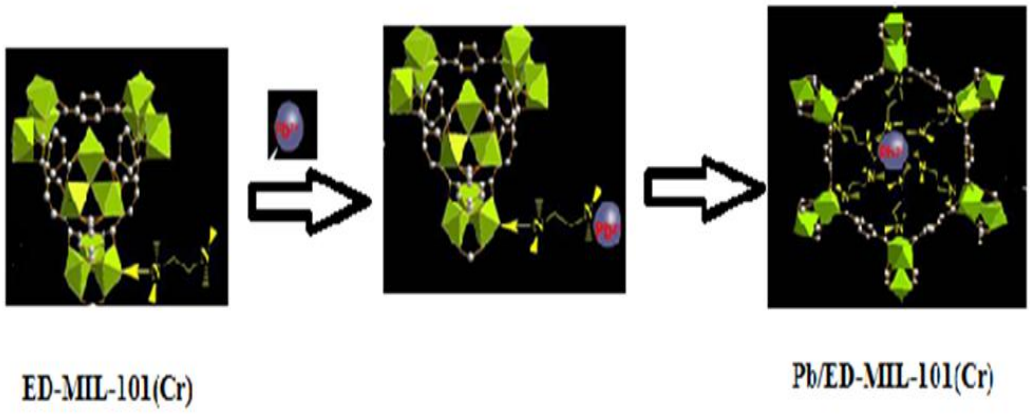

Figure 4.35: Schematic mechanism for Pb(II) adsorption in ED-MIL-101(Cr)

4.3.7 Kinetic experiments

Kinetics models applied to further investigate Pb(II), Cu(II), and Cd(II) ions adsorption mechanism on ED-MIL-101(Cr) and determination rate-control steps, so the kinetic data were fitted to the linear forms of pseudo-first order, pseudo-second order, and intra-particle diffusion equations. The models were shown in (Figures 4.36 to 4.38). The results for the rate constants and regression coefficients are summarized in Table (4.6). The Qe values theoretically calculated from the first-order model are closer for the experimental

values than those for second-order, however, the value of (R^2) for the second-order model is close to 1, so it can be concluded that the pseudo-second-order model is more reliable to describe the kinetics of lead, copper, and cadmium ions adsorption by ED-MIL-101(Cr). According to the intra-particle diffusion model, the plot of Qt versus $t^{1/2}$ doesn't give a straight line, then the adsorption process isn't influenced by intra-particle diffusion [181]. Herein, the plots exhibit multi-linearity (Figure 4.38), this confirms that intra-particle diffusion participated in lead, Copper, and Cadmium ions adsorption onto ED-MIL-101(Cr), but it was not the only rate-controlling step.

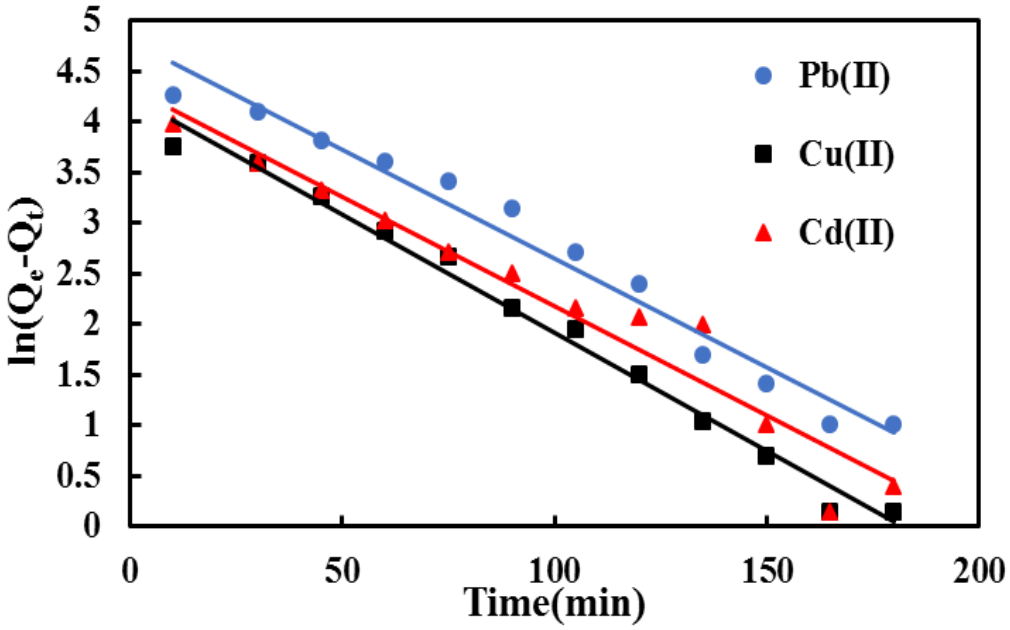

Figure 4.36: Pseudo-first order kinetics for Pb(II), Cu(II) and Cd(II) ions in single adsorption on ED-MIL-101(Cr) (m= 600 mg, v=500 ml).

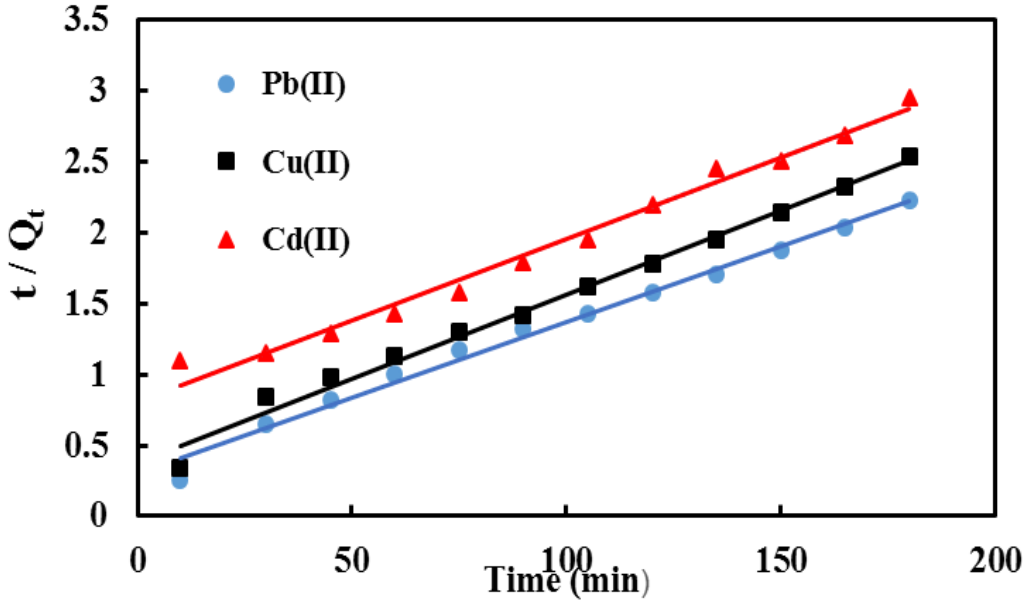

Figure 4.37: Pseudo-second order kinetics for Pb(II), Cu(II), and Cd(II) ions in single adsorption on ED-MIL-101(Cr).

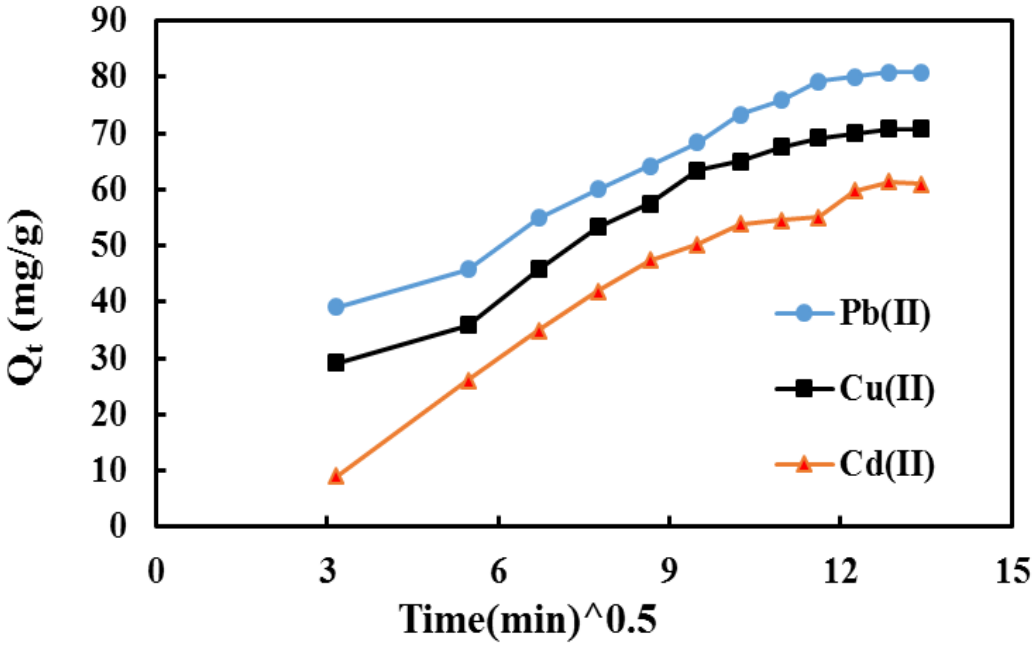

Figure 4.38: Intra-particle diffusion model for Pb(II), Cu(II), and Cd(II) ions in single adsorption on ED-MIL-101(Cr).

Table 4.6: Kinetic adsorption parameters for Pb(II), Cu(II), and Cd(II) onto ED-MIL-101(Cr).

Metal Ion	Pseudo-first Order			Pseudo-second Order			Weber and Morris	
	K_1 (min^{-1})	Q_e (mg/g)	R^2	K_2 (mg/g.min)	Q_e (mg/g)	R^2	Kid ($mg/g.min^{1/2}$)	R^2
Pb(II)	0.0214	73.8	0.97	3.8×10^{-4}	93.5	0.99	4.49	0.96
Cu(II)	0.0234	70.5	0.97	3×10^{-4}	84	0.99	4.44	0.95
Cd(II)	0.0216	76.7	0.94	1.6×10^{-4}	86.9	0.98	4.93	0.94

4.3.8 The adsorbent recycling

The regeneration process for exhausting ED–MIL–101(Cr) was carried out to assess the recyclability of ED-MIL-101(Cr) for lead, copper, and cadmium ions adsorption. This process was performed via rinsing the exhausted adsorbent using deionized water for 2 h and drying tonight at 100 ° C. There is a slight decrease in the removing efficiency of regenerated ED–MIL–101(Cr) compared with the initial removing percent as shown in (Figure 4.39). This reduction in the uptake efficiency of approximately 3% after three regeneration cycles might be attributed to the sequence influence of the inadequate desorption process.

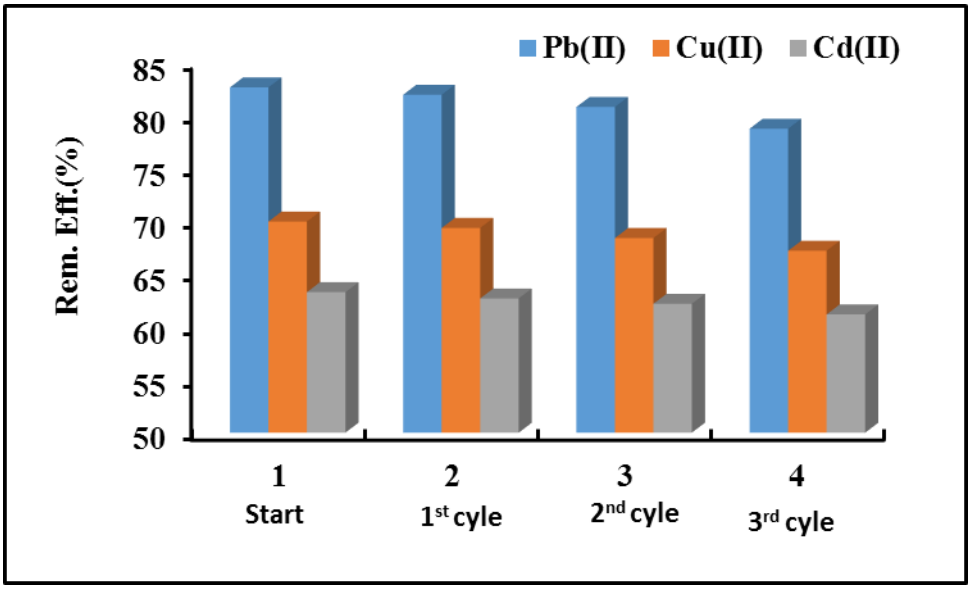

Figure 4.39: Regeneration cycles on the removing efficiency for Pb(II), Cu(II), and Cd(II) ions in single adsorption on ED-MIL-101(Cr).

Also, this insignificant change in efficiency, proving the high stability of functionalized MIL-101(Cr) under operating adsorption conditions.

4.4 Flow System Adsorption Experiments:

4.4.1 Effect of bed height:

The removal amounts of the adsorbed ions were increased with increasing the packed height within the column, this attributed to the increasing in adsorbent mass which provides the system with more active sites besides increasing the contact time between the adsorbent and the ions in the flowing solution. Consequently, the breakthrough curves will be rather gradual with increasing the bed height resulting in a broadened mass transfer zone. However, we expected that the metal adsorption per unit mass (QE) of ED-MIL–101(Cr) would be relatively constant for different bed heights, but in fact, the bed with 4 cm height showed the highest value of q_e in comparison to other values of 2 cm and 6 cm height, indicating that the q_e was not directly proportional to the amount of adsorbent available in the bed. Maybe this behavior relates to the distribution way was not sufficient to ensure the optimum contact way between the adsorbent with ions which reduces the capacity and losing some free active sites on the adsorbent surface at the given condition (Q= 15 ml/min and C_0 = 75mg/l). As revealed by (Figures 4.40 to 4.42) Pb(II) shows more adsorption capacity in the same bed height than the other metals, owing to a higher affinity of Pb(II) to the functional group of the ED-MIL–101(Cr), consequently required the longest period to reach the exhaustion time compared to the other metals in the same column condition. Moreover, the maximum obtained adsorption capacity was in the order of Pb(II) > Cu(II) > Cd(II).

4.4.2 Effect of flow rate

The results of the effect of flow rate also reveal that at the same flow rate, the adsorption capacity of ED-MIL-101(Cr) for Pb(II) is higher than for Cu(II) and Cd(II) due to a greater affinity of Pb(II) compared to Cu(II) and Cd(II). As shown in (Figures 4.41, 4.43, and 4.44).

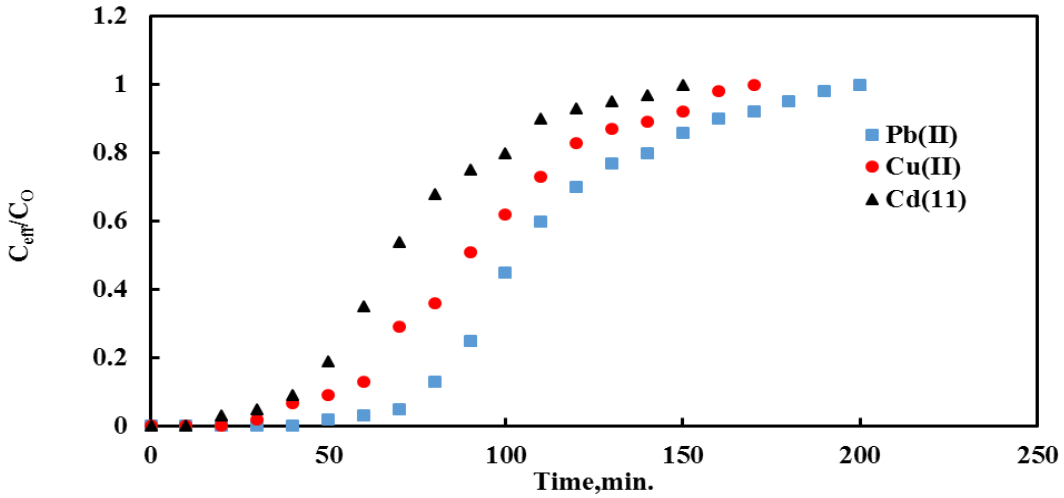

Figure 4.40: Experimental breakthrough curve at 2 cm bed height, 15 ml/min flow rate, and 75 mg/L initial concentrations for Pb(II), Cu(II), and Cd(II) removal on ED-MIL-101(Cr).

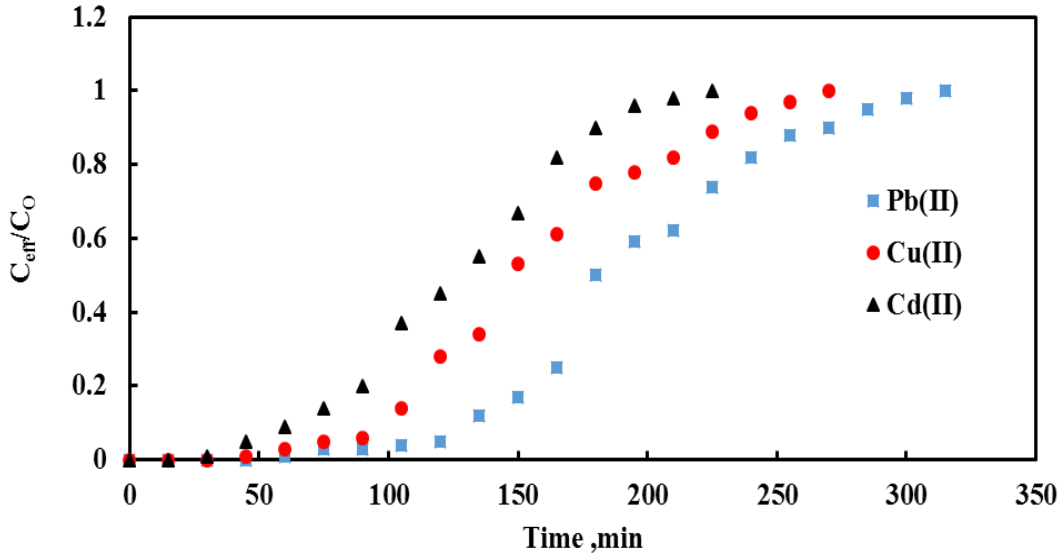

Figure 4.41: Experimental breakthrough curve at 4 cm bed height,15 ml/min flow rate, and 75 mg/L initial concentrations for Pb(II), Cu(II), and Cd(II) removal by the ED-MIL-101(Cr).

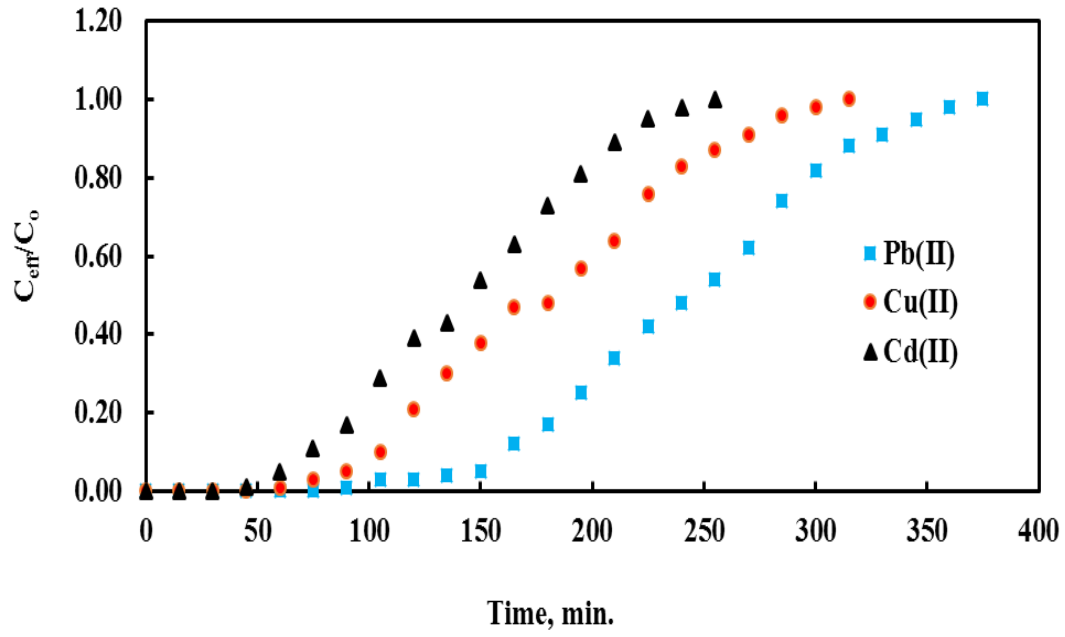

Figure 4.42: Experimental breakthrough curve at 6 cm bed height,15 ml/min flow rate, and 75 mg/L initial concentrations for Pb(II), Cu(II), and Cd(II) removal by the ED-MIL-101(Cr).

Moreover, The results show that with increasing the flow rate from 10 to 15 ml/min the breakthrough curves shift towards a slower time scale then the breakthrough and exhaustion time decrease because if the flow rate increases, not all the metal ions will have enough time to penetrate from the solution to ED-MIL-101(Cr) pores and bind with amino functional groups, which consequently results in a lower removal percentage of Pb(II), Cu(II), and Cd(II) in the column.

4.4.3 Effect of influent metal ions concentration

The effect of the influent metal ions concentration on the adsorption of Pb(II), Cu(II), and Cd(II) was investigated using various concentrations of 50, 75, and 100 mg/L at a constant bed height of 4 cm and flow rate of 15 ml/min.

The difference between the metal ions concentration of the aqueous phase and the water film around the ED-MIL–101(Cr) creates a driving force to diffuse the metal ions into this film and causes an axial dispersion along the column, as well.

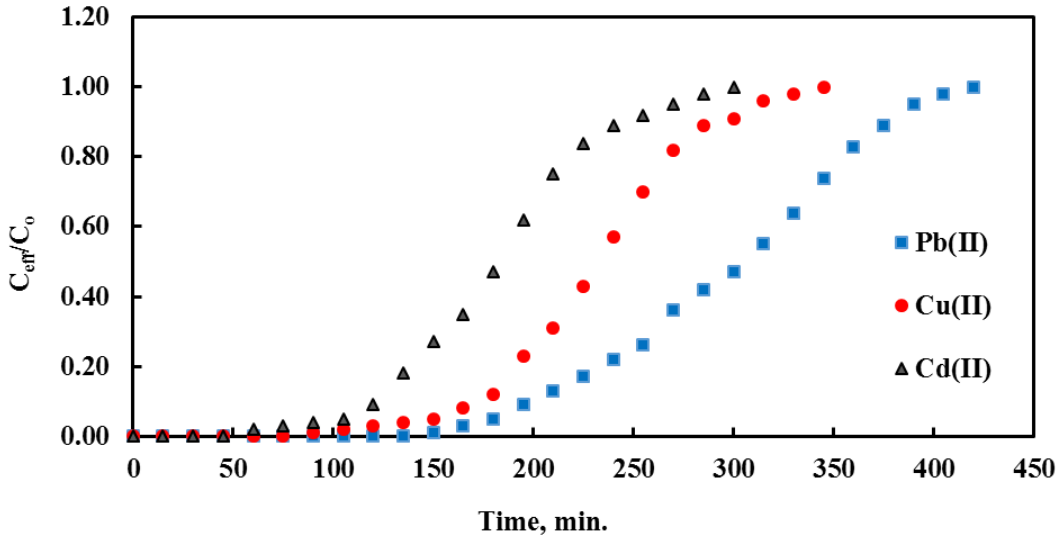

Figure 4.43: Experimental breakthrough curve at 10 ml/min flow rate, 4 cm bed height, and 75 mg/L initial concentrations for Pb(II), Cu(II), and Cd(II) removal by the ED-MIL-101(Cr).

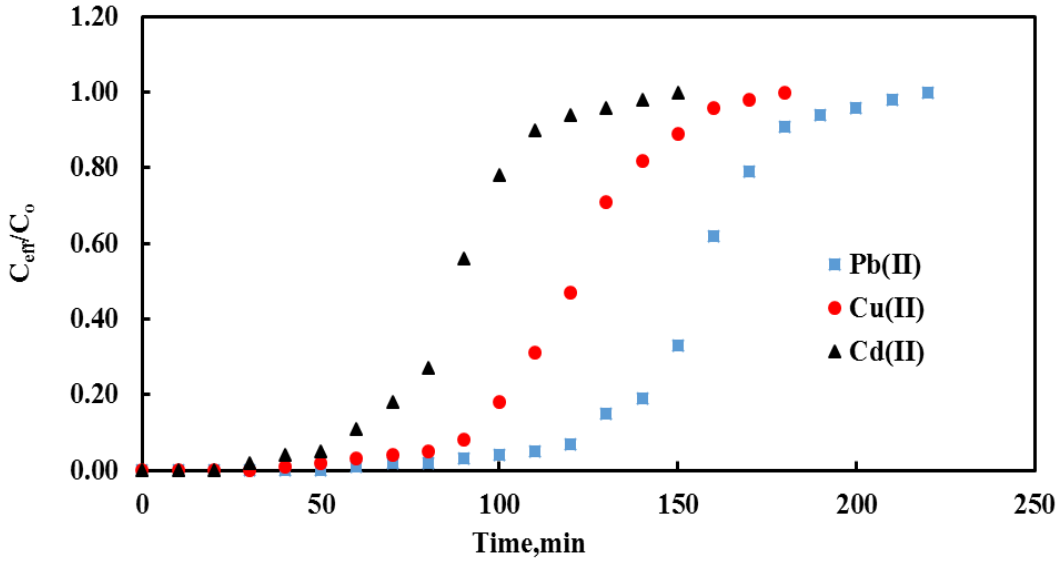

Figure 4.44: Experimental breakthrough curve at 20 ml/min flow rate, 4 cm bed height, and 75 mg/L initial concentrations for Pb(II), Cu(II), and Cd(II) removal by the ED-MIL-101(Cr).

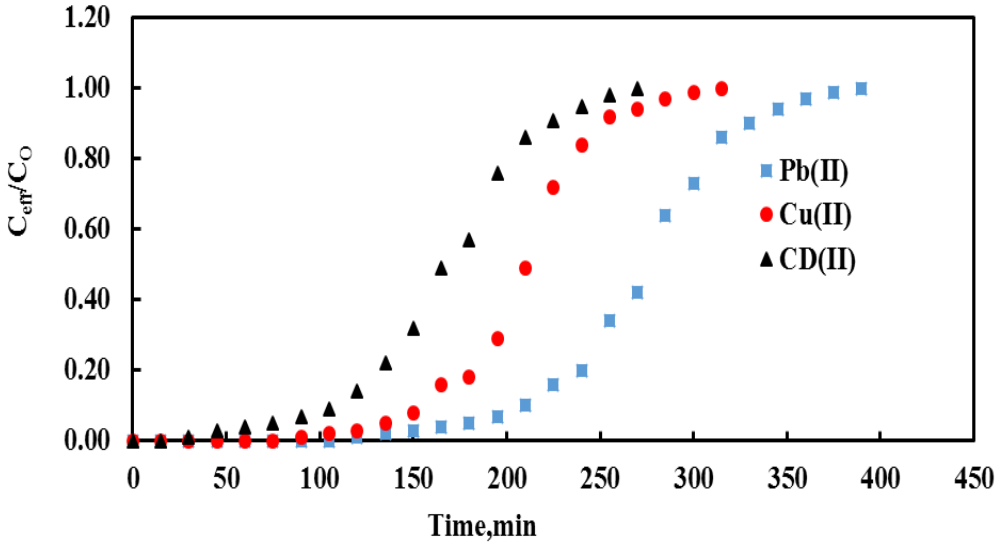

Figure 4.45: Experimental breakthrough curve at 15 ml/min flow rate, 4 cm bed height, and 50 mg/L initial concentrations for Pb(II), Cu(II), and Cd(II) removal by the ED-MIL-101(Cr).

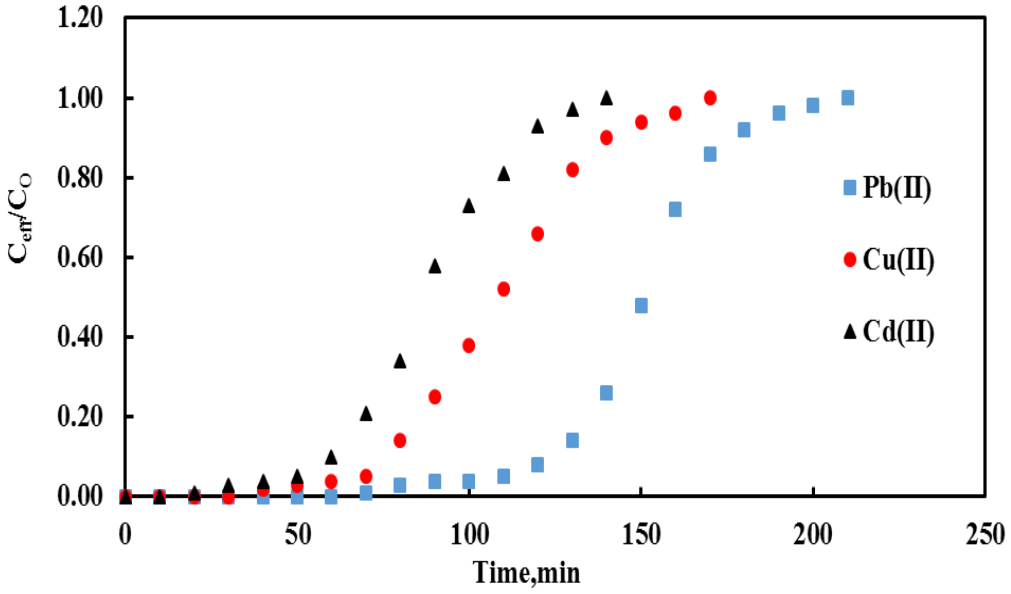

Figure 4.46: Experimental breakthrough curve at 15 ml/min flow rate, 4 cm bed height, and 100 mg/L initial concentrations for Pb(II), Cu(II), and Cd(II) removal by the ED-MIL-101(Cr).

Hence, as the influent concentration increases twice (from 50 to 100 mg/L), it provides a high concentration difference and the mass transferee zone will increase and the

breakthrough curve will be rather steep resulting in an earlier t_b and t_e, as shown in Figures (4.41,4.45, and 4.46).

4.4.4 Effect of binary and ternary ions system

The majority of contaminated effluents contain more than one type of detrimental heavy metal ions. Consequently, removal adsorption in packed bed columns involves competitive ion exchange whereby several toxic heavy metals compete for a limited number of binding sites on an adsorbent. In real and practical applications, the service time of adsorption removing columns has to be terminated as soon as the content of one of the toxic species in the column effluent exceeds the acceptable limit.

It is well known from the basic practice principles of the ion exchange and adsorption treatment process that the species which first breaks through the column is the one with the lowest affinity towards the resin or adsorbent. Hence the service time of adsorption columns is determined by the toxic metal with the lowest affinity present in the feed streams. Experimental breakthrough curves for the competitive system (binary and ternary system) are depicted in (Figures 4.47 to 4.50). The moderate operating conditions of the experiments were selected as (4 cm, 15 ml/min, and 75 mg/L) for bed height of the adsorbent, flow rate, and concentration of feed solution for Pb(II), Cu(II), and Cd(II) respectively. It is clear from these Figures:

- Due to competition effects that occur between the co-existence ions the lower affinity pollutant will have a much steeper style in its breakthrough curves.
- Cd(II) is the weakest adsorbed ion while Pb(II) is the strongest one among the present adsorbed ions adsorbed. It can be seen that the uptake capacity order for the ternary system onto ED-MIL-(101Cr) was: Pb(II)> Cu(II)> Cd(II), this sequence order coincide with that obtained from the equilibrium adsorption isotherm for each solute in a single system.
- At the initial stage, there are a lot of active sites on the MOF adsorbent; these sites remain vacant till the ions are flowing within the adsorbent. These active sites are freely available for each ion regardless of their affinity. The higher affinity component bonded with the active sites at a greater rate than the lower affinity species. With increasing time, the lower affinity component is not easily adsorbed but moves away with the bulk fluid.

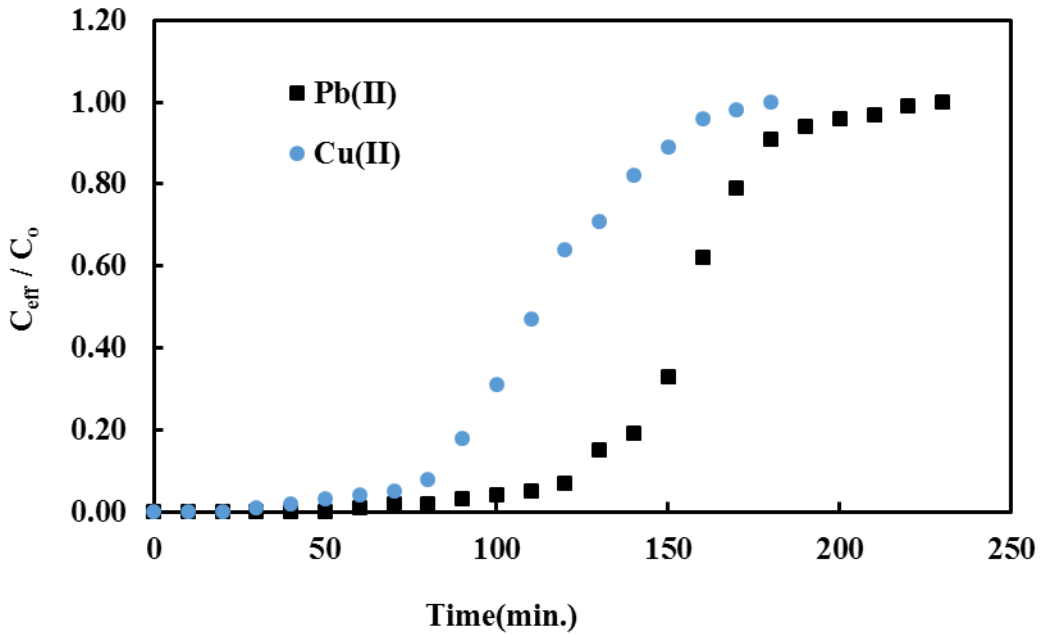

Figure 4.47: Experimental breakthrough curve at 15 ml/min flow rate, 4 cm bed height, and 75 mg/L of binary solution for Pb(II) and Cu(II) ions removal by the ED-MIL-101(Cr).

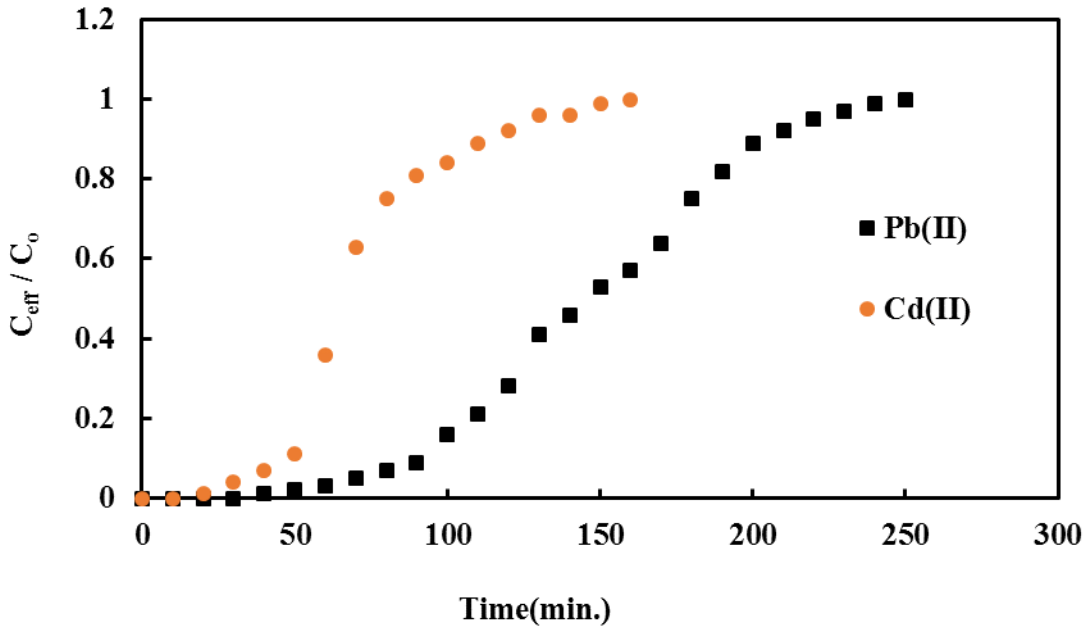

Figure 4.48: Experimental breakthrough curve at 15 ml/min flow rate, 4 cm bed height, and 75 mg/L of binary solution for Pb(II) and Cd(II) ions removal by the ED-MIL-101(Cr).

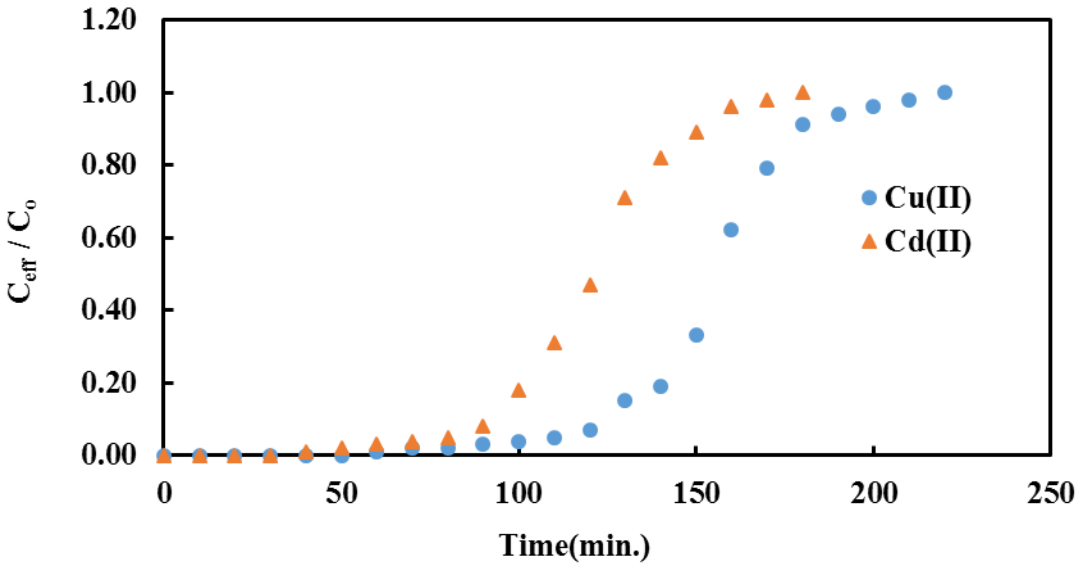

Figure 4.49: Experimental breakthrough curve at 15 ml/min flow rate, 4 cm bed height, and 75 mg/L of binary solution for Cu(II) and Cd(II) ions removal by the ED-MIL-101(Cr).

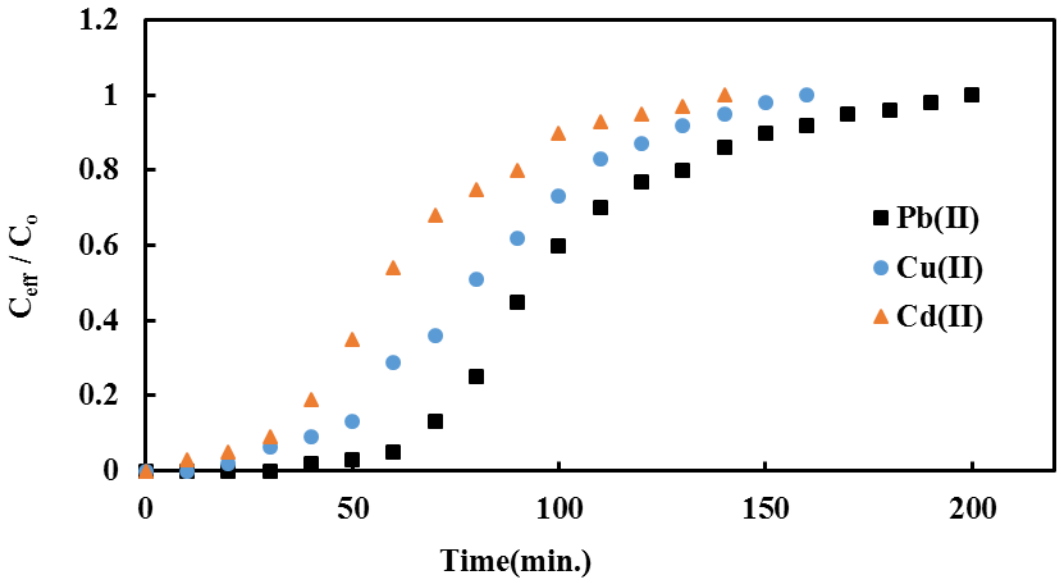

Figure 4.50: Experimental breakthrough curve at 15 ml/min flow rate, 4 cm bed height, and 75 mg/L of ternary solution for Pb(II), Cu(II), and Cd(II) ions removal by the ED-MIL-101(Cr).

4.4.5 Fixed bed column modeling

-Thomas model

Kinetic adsorption models were matched to the results of the dynamic experimental studies to analyze the performance of the fixed bed column. Thomas model was used to evaluate the breakthrough curves owing to their high reliability and acceptable confidence to analyze the dynamic data. Thomas rate constant (K_{th}) and equilibrium maximum solid phase adsorption capacity q_o (mg/g) of the metal ions were calculated to compare their values in different adsorption aqueous media.

The breakthrough curves, predicted by the Thomas model at 4 cm bed height, 15 ml/min flow rate, and at 75 mg/L initial concentrations for Pb(II), Cu(II), and Cd(II), are shown in (Figure 4.51).

The Thomas parameters from the linearized plots for single solutions results are listed in Table 4.7. From the obtained non-linear regression correlation coefficients (R^2) of the Thomas model (range from 0.960 to 0.990) in almost cases and statistically, they were the insignificant difference between the experimental adsorption capacity (qe) of Pb(II), Cu(II) and Cd(II) and the value predicted from the Thomas model (q_o) Hence, in this study the Thomas model can be considered a suitable kinetic model to describe Pb(II), Cu(II) and Cd(II) adsorption in a fixed bed column of ED-MIL-101(Cr).

The results from Thomas models suggest that the maximum solid phase adsorption capacity of the studied heavy ions from single aqueous solutions is in the order of Pb(II) > Cu(II) > Cd(II), approved by the experimental data.

According to Table 4.7, by increasing both the influent concentration and the bed height, the Thomas rate constant (k_{Th}), which characterize the rate of metal ions transfer from the fluid to the MOF adsorbent and q_o, rise due to the increase in driving force for the mass transfer process. With increasing the flow rate, the value of k_{Th} increased but the value of q_o decreased.

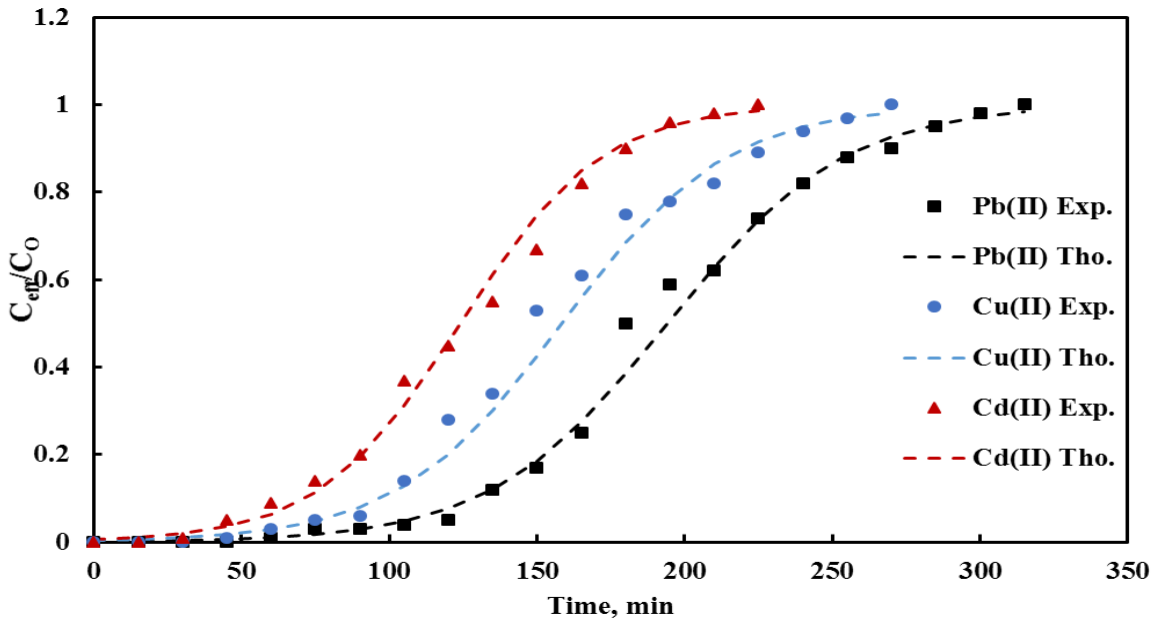

Figure 4.51: Experimental and theoretical Thomas model breakthrough curves at 15 ml/min flow rate, 4 cm bed height, and 75 mg/L for Pb(II), Cu(II), and Cd(II) ions removal by the ED-MIL-101(Cr).

Yoon–Nelson model

The Yoon–Nelson model is used to predict the breakthrough performance in the current study. This model needs less column data is for the determination of the model parameters, and it is proper for the single ion system [182,183]. The values of K_{YN} and τ were attained from the linearized Yoon–Nelson equation to predict the rate constant and time required for 50% adsorbate breakthrough and summarized in Table 4.7.

The breakthrough curves are depicted in (Figure 4.52)**.** are obtained by the Yoon–Nelson model at 4 cm bed height, 15 ml/min flow rate, and at 75 mg/L initial concentrations for Pb(II), Cu(II), and Cd(II). The Yoon–Nelson predicted that the 50% breakthrough for Pb(II), Cu(II), and Cd(II) in the previously mentioned operating conditions were at 194,148 and 124 min, respectively, see Table 4.7 With high values of the corresponding correlation coefficient range from (0.969 to 0.985), the breakthrough time can be estimated by the prediction of this model. Also by inspected the correlation coefficient for different bed lengths, the results revealed that this model is suitable for the adsorption of the metal in a longer fixed bed column.

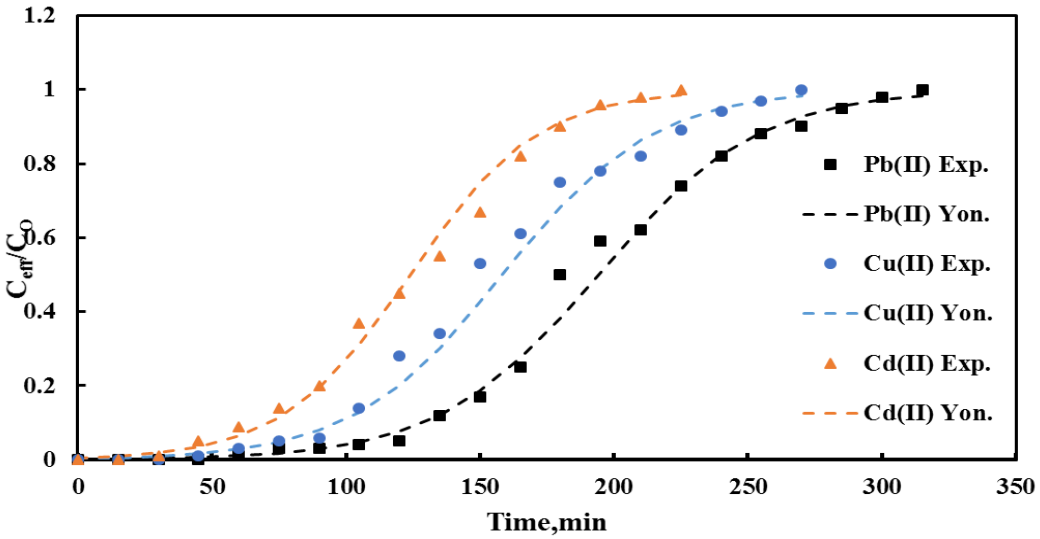

Figure 5.52: Experimental and theoretical Yoon-nelson model breakthrough curves at15 ml/min flow rate, 4 cm bed height, and 75 mg/L of Pb(II), Cu(II), and Cd(II) ions by ED-MIL(Cr).

Table 4.7: Parameters predicted by the Thomas and Yoon-Nelson models at different bed heights, flow rates, and initial concentrations.

Metal	Column condition			Breakthrough analysis		Thomas model			Yoon-Nelson model		
	H	Q	Con.	q_e	R%	$K_{th}\times10^4$	q_o	R^2	$K_{YN}\times10^2$	τ	R^2
Pb(II)	2	15	75	37.65	55.45	3.79	34.92	0.97	3.06	115	0.967
	4	15	75	40.06	61.05	4.47	40.44	0.99	3.35	194	0.969
	6	15	75	43.79	67.52	7.09	43.14	0.99	5.32	243	0.974
	4	10	75	44.56	62.1	3.68	46.70	0.97	2.65	293	*0.965*
	4	20	75	32.75	49.4	7.83	35.78	0.96	5.80	152	0.963
	4	15	50	37.56	56.75	3.78	38.81	0.98	2.95	265	0.982
	4	15	100	42.47	69.35	6.51	45.33	0.96	6.51	147	0.975
Cu(II)	2	15	75	28.31	52.09	4.07	25.32	0.98	3.58	93	0.962
	4	15	75	32.19	57.22	4.77	33.01	0.98	4.94	148	0.971
	6	15	75	36.71	62.19	7.07	38.92	0.97	5.30	158	0.985
	4	10	75	34.69	64.83	3.91	35.18	0.99	3.58	234	*0.972*
	4	20	75	26.19	49.39	8.73	29.61	0.98	6.55	117	0.981
	4	15	50	26.65	51.45	3.58	28.29	0.99	3.29	204	0.990
	4	15	100	35.15	65.76	6.30	36.96	0.99	6.30	108	0.992
Cd(II)	2	15	75	21.29	48.47	4.83	19.99	0.98	3.62	75	0.966
	4	15	75	25.97	55.40	5.59	25.82	0.98	4.19	124	0.963
	6	15	75	29.88	58.94	7.81	28.25	0.97	5.86	144	0.980
	4	10	75	31.45	44.56	4.61	32.09	0.99	2.76	193	0.973
	4	20	75	22.42	32.75	9.96	23.96	0.99	7.54	86	0.986
	4	15	50	22.94	47.15	4.04	23.40	0.98	3.52	161	0.983
	4	15	100	29.85	61.17	7.12	32.94	0.98	7.12	86	0.964

5. CONCLUSIONS

5.1 General Conclusions

This present study revealed the following outcomes and conclusions, concerning the batch and continuous (fixed bed) processes of adsorption removal of Pb(II), Cu(II), and Cd(II) ions using functionalized MOF ED-MIL-101(Cr):

5.1.1 Batch adsorption system

- The results of the present investigation have proved that the amino-functionalized MIL-101(Cr) can be considered as a promising candidate for removing divalent metal ions from single and binary contaminated solutions.
- In single batch system; optimum operation condition of adsorption for Pb(II), Cu(II) and Cd(II) ions onto ED-MIL-101(Cr) were: pH=6, adsorbent dosage= 1.2 g/L of solution, initial heavy metal concentration= 100 mg/L, contact time= 180 min.
- The adsorption uptake efficiencies for the metal ions under inspection were sensibly reduced in the multi ions systems compared with a single system at the same operating condition. This is due to the interaction effects between the co-existence ions, and the competition among them that minimize the numbers of free active sites at the sorbent surface available for the adsorption process.
- In single and multi-ions systems; Pb(II) ions were the most favorable species rather than the other ions. This can be attributed to its physiochemical characteristics that make the most favorable adsorbed component. Results for the three adsorbed ions concerning removal efficiency values were in the sequence Pb(II)>Cu(II)>Cd(II).

- Using grafted MOF adsorbent, the Langmuir model and the extended Freundlich model were the best models for single and multi-ion systems from their solutions. Respectively. These findings indicate the homogeneity of the adsorbent surface in the absence of competitive ions.
- The experimental kinetic outcomes of the adsorption process for Pb(II), Cu(II), and Cd(II) ions onto ED-MIL-101(Cr), was well described with hypothetical assumptions of the pseudo-second-order rate law.

5.1.2 Fixed bed system:

- The obtained experimental breakthrough data of three studied metal ions were consistently matched the theoretical data obtained by applying two models of Thomas and Yoon-Nelson models for kinetic data.
- The breakthrough curves were plotted for each metal, when compared to Cu(II) and d(II) ions, Pb (II) shows the longest period for the breakthrough time, while Cd(II) had the shortest one.

- The recovery capacity order for the ternary ions system is Pb(II)>Cu(II)>Cd(II) this sequence order agreed with that obtained from the equilibrium isotherm for the ternary system in batch mode.

- In small bed height, the smallest breakthrough times were recorded for all metals, which due to a finite number of vacant active sites were available for metals onto MOF adsorbent.
- Increasing the influent concentration of heavy metal ions will result in decreasing the service time for the fixed column.

REFERENCES

[1] **Mohan, D., Pittman Jr, C. U., and Steele, P. H.** (2006). Single, binary and multi-component adsorption of copper and cadmium from aqueous solutions on Kraft lignin a biosorbent, *J. Colloid Interface Sci.*, vol. *297*, no. 2, pp. 489–504.

[2] **Chiban, M., Soudani, A., Sinan, F., and M. Persin, M.** (2011). Single, binary and multi-component adsorption of some anions and heavy metals on environmentally friendly Carpobrotus edulis plant, *Colloids Surfaces B Biointerfaces*, vol. *82*, no. 2, pp. 267–276.

[3] **Chmielewská, E., and Medved, J.** (2001). Bioaccumulation of heavy metals by green algae Cladophora glomerata in a refinery sewage lagoon, *Croat. Chem. Acta*, vol. *74*, no. 1, pp. 135–145.

[4] **Chowdhury, T.** (2017). Adsorptive removal of arsenic(III), nickel(II) and lead(II) from aqueous solution using metal organic framework-graphene oxide nanocomposite, ProQuest Dissertations Publishing, vol. *11*, pp. 1–85.

[5] **Wu, B., Lin, X., Ge, L., Wu, L., and Xu,T.** (2013). A novel route for preparing highly proton conductive membrane materials with metal-organic frameworks, *Chem. Commun.*, vol. *49*, no. 2, pp. 143–145.

[6] **Kamar, F. H., Nechifor, A. C., Mohammed, A. A., Albu, P. C., and Craciun, M. E.** (2015). Removal of lead and cadmium ions from aqueous solution using walnut shells as low-cost adsorbent materials, *Rev. Chim.*, vol. *66*, no. 5, pp. 615-620.

[7] **Wang, C., Singer, P. C., and Coronell, O.** (2016). Removal of copper and lead ions from aqueous solution using brass granular media, vol. *67*, no. 7, pp. 1276–1280.

[8] **Denizli, A., Büyüktuncel, E., Tuncel, A., Bektas, S., and Genç, Ö.** (2000). Batch removal of lead ions from aquatic solutions by polyethyleneglycol-methacrylate gel beads carrying Cibacron Blue F3GA, *Environ. Technol.*, vol. *21*, no. 6, pp. 609–614.

[9] **Sekar, M., Sakthi, V., and Rengaraj, S.** (2004). Kinetics and equilibrium adsorption study of lead (II) onto activated carbon prepared from coconut shell, *J. Colloid Interface Sci.*, vol. *279*, no. 2, pp. 307–313.

[10] **Nosier, S. A.** (2003). Removal of cadmium ions from industrial wastewater by cementation, *Chem. Biochem. Eng. Q.*, vol. *17*, no. 3, pp. 219–224, 2003.

[11] **Fu, F., and Wang, Q.** (2011).Removal of heavy metal ions from wastewaters: a review, *J. Environ. Manage.*, vol. *92*, no. 3, pp. 407–418.

[12] **Kalibantonga, P. D.** (2004). Adsorption of heavy metals from solution by a South African Industrial clay., Ph.D. thesis. Tshwane University of Technology, South Africa.

[13] **Muhaisn, L. F.** (2014). Competitive removal of heavy metal ions from simulated wastewater by sorptive flotation using Punica Granatum. Thesis master, Env. Eng. Dep. College of Eng., University of Baghdad.

[14] **Aslam, M. M. Hassan, I., Malik, M., and Matin, A.** (2004). Removal of copper from industrial effluent by adsorption with economical viable material, *Electron. J. Environ. Agric. Food Chem*, vol. *3*, no. 2, pp. 658–664.

[15] **Ali, I.** (2014). New generation adsorbents for water treatment, *Chem. Rev.*, vol. *112*, no. 10, pp. 5073–5091.

[16] **Khan, N. A. Hasan, Z., and Jhung, S. H.** (2013). Adsorptive removal of hazardous materials using metal-organic frameworks (MOFs): a review, *J. Hazard. Mater.*, vol. *244*, pp. 444–456.

[17] **Mohan, D., and Pittman, Jr C. U.** (2007). Arsenic removal from water/wastewater using adsorbents—a critical review, *J. Hazard. Mater.*, vol. *142*, no. 1–2, pp. 1–53.

[18] **Kobielska, P. A., Howarth, A. J., Farha O. K., and Nayak S.** (2018). Metal–organic frameworks for heavy metal removal from water, *Coord. Chem. Rev.*, vol. *358*, pp. 92–107.

[19] **Hwang, Y. K., Hong, D. Y., and Chang, J.** (2008). Amine grafting on coordinatively unsaturated metal centers of MOFs: consequences for catalysis and metal encapsulation, *Angew. Chemie*, vol. *120*, no. 22, pp. 4212–4216.

[20] **Yaghi, O. M., O'keeffe, M., Ockwig, N. W., Chae, Eddaoudi, H. K., Kim, M., and J.** (2003). Reticular synthesis and the design of new materials, *Nature*, vol. *423*, no. 6941, p. 705.

[21] **Eddaoudi, M. Kim, J., and Rosi, N.** (2002). Systematic design of pore size and functionality in isoreticular MOFs and their application in methane storage, *Science*, vol. *295*, no. 5554, pp. 469–472.

[22] **Chen, B., Xiang, S., and Qian, G.** (2010). Metal-organic frameworks with functional pores for recognition of small molecules, *Acc. Chem. Res.*, vol. *43*, no. 8, pp. 1115–1124.

[23] **Horcajada, P., Russell E. Morris, and Christian Serre .** (2011). Metal–organic frameworks in biomedicine, *Chem. Rev.*, vol. *112*, no. 2, pp. 1232–1268.

[24]**Aijaz, A., Karkamkar A., and Autrey T.** (2012). Immobilizing highly catalytically active Pt nanoparticles inside the pores of metal-organic framework: a double solvents approach, *J. Am. Chem. Soc.*, vol. *134*, no. 34, pp. 13926–13929, 2012.

[25] **Ricco, R.,Kristina K., and Mark J.** (2015). Lead(II) uptake by aluminium based magnetic framework composites (MFCs) in water, *J. Mater. Chem. A*, vol. *3*, no. 39, pp. 19822–1983.

[26] **Sumida, K., David, L., Jarad A., and Thomas M.** (2011). Carbon dioxide capture in metal–organic frameworks, *Chem. Rev.*, vol. *112*, no. 2, pp. 724–781.

[27] **Minh Thanh, Phuong T., and Hang P.,** (2018). Comparative study of Pb(II) adsorption onto MIL-101 and Fe-MIL-101 from aqueous solutions, *J. Environ. Chem. Eng.*, vol. *6*, no. 4, pp. 4093–4102.

[28] **Haque, E. Lee j., and Jang I, .** (2011). Adsorptive removal of methyl orange from aqueous solution with metal-organic frameworks, porous chromium-benzenedicarboxylates, *J. Hazard. Mater.*, vol. *181*, no. 1–3, pp. 535–542.

[29] **Zhou, M. Wu Y, and Qiao J.,** (2013). The removal of bisphenol A from aqueous solutions by MIL-53 (Al) and mesostructured MIL-53 (Al), *J. Colloid Interface Sci.*, vol. *405*, pp. 157–163.

[30] **Cychosz, K. A., and Matzger, A. J.** (2010). Water stability of microporous coordination polymers and the adsorption of pharmaceuticals from water, *Langmuir*, vol. *26*, no. 22, pp. 17198–17202.

[31] **Férey, G., Mellot-Draznieks C., C Serre C., and F Millange F.** (2005). A chromium terephthalate-based solid with unusually large pore volumes and surface area," *Science*, vol. *309*, no. 5743, pp. 2040–2042.

[32] **Sung, B. J Lee J., and Yoon J,** (2007). Microwave Synthesis of Chromium Terephthalate MIL-101 and Its Benzene Sorption Ability , Advanced Materials, vol., *19*, no.1, pp. 121–124.

[33]**Burrows, A. D., Jiang, D. L., Keenan, L., Burrows, A. D., and Edler, K. J.** (2012). "ChemComm Synthesis and post-synthetic modification of MIL-101(Cr) -NH_2 via a tandem diazotisation process w," vol. *48*, no. 99, pp. 99–102.

[34] **Kumar, K. V., Subanandam, K., Ramamurthi, V., and Sivanesan, S.** (2004). "Solid-liquid adsorption for wastewater treatment: principle design and operation," *Anna Univ. Coll. Technol.Chennai, India*.

[35] **Dąbrowski, A. Adsorption—from theory to practice**, (2001). *Adv. Colloid Interface Sci.*, vol. *93*, no. 1–3, pp. 135–224.

[36] **Osman M. A., and Faust, S. D.** (1987). Adsorption Processes for Water Treatment. Butterworth Publisher, Boston, MA, USA.

[37] **Khan, N. A., Hasan, Z., and Jhung, S. H.** (2013). Adsorptive removal of hazardous materials using metal-organic frameworks (MOFs): A review, *J. Hazard. Mater.*, vol. *244–245*, pp. 444–456.

[38] **Seader, D., and Henley, E. J. (**1998.). SEPARATION PROCESS RINCIPLES. Wiley, New York, USA

[39] **Sulaymon, A. H., Abid, B. A., and Al Najar, J. A.** (2009). Removal of Lead and Copper Ions onto Granular Activated Carbon in Batch and Fixed Bed A Dsorber', Eng. and Tech. J., Vol. *27*, No.131, pp. 2336-2337.

[40] **Tan, K.** (19893). Adsorption and desorption of chromium on clayey soils Copyright Warning & Restrictions,.

[41] **Parvathi, K., Nagendran, R., and Nareshkumar, R.** (2007). Lead biosorption onto waste beer yeast by-product: a means to decontaminate effluent generated from battery manufacturing industry, *Electron. J. Biotechnol.*, vol. *10*, no. 1, pp. 92–105.

[42] **Villaescusa, I., Fiol, N., Martínez, M., Miralles, N., Poch, J., and Serarols,J.** (2004). Removal of copper and nickel ions from aqueous solutions by grape stalks wastes, *Water Res.*, vol. *38*, no. 4, pp. 992–1002.

[43] **Alley, E. R.** (2000) *WATER QUALITY CONTROL HANDBOOK*. The McGraw-Hill Companies, Inc

[44] **Seader, J. D., Henley, E. J., and Roper, D. K.** 1998. Separation process principles, Wiley, New York, USA.

[45] **Weber, J. R., and Walter, J.** (1972). Physicochemical process for Water Quality Control', New York, John Willey and Sons, Inc., pp. 199-206.

[46] **Tabrez, A. K., and Ved**, **V.** (2010). Removal of cadmium(II), lead(II), and chromium(VI) ions from aqueous solution using clay, Toxicological & Environmental Chemistry, Vol. 92, pp. 1435 – 1446.

[47] **Alley, E. R.** (2006). Water quality control handbook, 2nd ED., McGraw-Hill Companies, Inc., USA.

[48] **Inglezakis V. J., and Poulopoulos, S. G.** (2006). Adsorption, ion exchange and catalysis: design of operations and Environmental Applications, Elsevier B.V., Netherlands.

[49] **Hsieh, H. N.** (1989). Adsorption and Desorption of Chromium on Clayey Soills, Thesis, MSC / Feng- Chai University/ Taiwan, R.0.C.

[50] **Kumar, K. V., Subanandam, K. Ramamurthi, V., and Sivanesan,S.** (2004). Solid Liquid Adsorption for Wastewater Treatment*: Principle Design and Operation , College Technology, Anna University, Chennai-India, Feb*.

[51]**Barakat, M. A.** (2011). New trends in removing heavy metals from industrial wastewater, *Arab. J. Chem.*, vol. *4*, no. 4, pp. 361–377.

[52]**Du, R., Ssenyange, Aktary, S. M., and McDermott, M. T.** (2009). Fabrication and characterization of graphitic carbon nanostructures with controllable size, shape, and position, *Small*, vol. *5*, no. 10, pp. 1162–1168.

[53] **Pollard, S. J. T., Fowler, G. D., Sollars, C. J., and Perry, R.** (1992). Low-cost adsorbents for waste and wastewater treatment: a review. Sci. Total Environ., vol. *116*, pp. 31-39.

[54] **Onundi,Y. B., Mamun, A. A., Al Khatib, M. F., and Ahmed,Y. M.** (2010). Adsorption of copper, nickel and lead ions from synthetic semiconductor industrial wastewater by palm shell activated carbon, Int. J. Environ. Sci. Tech.,vol. *7*,no. 4, pp. 751-758.

[55] **Badmus, M. A. O., Audu, T. O. K., and B. U. Anyata,** (2007). Removal of Lead Ion from Industrial Wastewaters by Activated Carbon Prepared from Periwinkle Shells (Typanotonus fuscatus)', Turkish J. Eng. Env. Sci., vol. *31*, pp. 251-263.

[56]**Kongsuwan, A., Patnukao, P. and Pavasant,P.** (2009). Binary component sorption of Cu(II) and Pb(II) with activated carbon from Eucalyptus camaldulensis Dehn bark. Journal of Industrial and Engineering Chemistry, vol. *15* no.4 pp. 465-470.

[57] **Wang, H., Zhou A., and Peng F.**, (2007). Mechanism study on adsorption of acidified multiwalled carbon nanotubes to Pb(II). Journal of Colloid and Interface Science. vol., *316*, no. 2, pp. 277-283.

[58] **Csefalvay, E., V. Pauer, and P. Mizsey,** (2009). Recovery of copper from process waters by nanofiltration and reverse osmosis. Desalination, vol., *240*, no. 1, pp. 132-142.

[59] **Apiratikul, R. and Pavasant, P.** (2013). Batch and column studies o f biosorption of heavy metals by Caulerpa lentillifera. Bioresource Technology, vol., *99*, no. 8, pp. 2766-2777.

[60] **Ajjabi, L.C. and Chouba, L.** (2009). Biosorption o f Cu^{2+} and Zn^{2+} from aqueous solutions by dried marine green macroalga Chaetomorpha linum. Journal of Environmental Management, 2009. vol., *90*,no,11, pp. 3485-3489.

[61] **Pavasant, P., Apiratikul R., and Sungkhum V.**, (2006). Biosorption o f Cu^{2+}, Cd^{2+}, Pb^{2+}, and Zn^{2+} using dried marine green macroalga Caulerpa lentillifera. Bioresource Technology, vol., *97*,no.,18, pp. 2321-2329.

[62] **Bhainsa, K.C. and D'Souza, S.F.** (2008). Removal of copper ions by the filamentous fungus, Rhizopus oryzae from aqueous solution. Bioresource Technology, vol., *99*, no. 9, pp. 3829-3835.

[63] **Wang, S., and Peng, Y.** (2010). Natural zeolites as effective adsorbents in water and wastewater treatment. Chem. Eng. J., vol., *156*, pp 11.

[64] **Erdem, E., Karapinar N., and Donat R.,** (2004). The removal of heavy metal cations by natural zeolites. Journal of Colloid and Interface Science, vol., *280* ,no.2, pp. 309-314.

[65] **Huang K. J., Niu D., and Sun J.,** (2011). Novel electrochemical sensor based on functionalized graphene for simultaneous determination of adenine and guanine in DNA, *Colloids Surfaces B Biointerfaces*, vol. 82, no. 2, pp. 543–549.

[66]**Butova V. V, Soldatov M. A., Guda A. A., Lomachenko K. A., and C.** (2014). Metal-organic frameworks : structure, properties, methods of synthesis and characterization, vol. *85*, no. 12, pp. 280–307.

[67] **Wang, Y., Ye, G., Chen, H., Hu, X., Niu, Z., and Lamberti S. Ma.** (2015). Functionalized metal–organic framework as a new platform for efficient and selective removal of cadmium (II) from aqueous solution, *J. Mater. Chem. A*, vol. *3*, no. 29, pp. 15292–15298.

[68] **Chakraborty, A., Bhattacharyya, S., Hazra, Ghosh, A., A., C., and Maji, T. K.** (2016). Post-synthetic metalation in an anionic MOF for efficient catalytic activity and removal of heavy metal ions from aqueous solution, *Chem. Commun.*, vol. *52*, no. 13, pp. 2831–2834.

[69] **Cornelius O. Audu, Huong Giang,and SonBinh T. Nguyen**, (2016). The dual capture of AsV and AsIII by UiO-66 and analogues, *Chem. Sci*., vol.7, pp. 6492-6498.

[70] **Vu T. A.,GH Le, Dao C., Dang L., and Nguyen K. .,** (2015). Arsenic removal from aqueous solutions by adsorption using novel MIL-53(Fe) as a highly efficient adsorbent, *RSC Adv.*, vol. *5*, no. 7, pp. 5261–5268.

[71] **Li, Z. Q., Yang, J. C., Sui, K. W., and Yin, N.** (2015). Facile synthesis of metal-organic framework MOF-808 for arsenic removal, *Mater. Lett.*, vol. *160*, pp. 412–414.

[72] **Chen, Y., and Tang**, **S.** (2019). Solvothermal synthesis of porous hydrangea-like zeolitic imidazole framework-8 (ZIF-8) crystals, *J. Solid State Chem.*, vol. *276*, pp. 68–74.

[73] **Moradpour, T**., **and K. V. H. Alireza Abbasi,** (2015). A new 3D cobalt (II) metal-organic framework nanostructure for heavy metal adsorption, *INORGANICA Chim. ACTA.*, vol. *430*, pp. 261–267.

[74] **Li, J., Wu, Y., Li, Z., Zhu, M., and Li, F.** (2014). Characteristics of arsenate removal from water by metal-organic frameworks (MOFs), *Water Sci. Technol.*, vol. *70*, no. 8, pp. 1391–1397.

[75] **Jian, M., Liu, B., Zhang, G., Liu, R., and Zhang, X.** (2015). Colloids and Surfaces A : Physicochemical and Engineering Aspects Adsorptive removal of arsenic from aqueous solution by zeolitic imidazolate framework-8 (ZIF-8) nanoparticles, *Colloids Surfaces A Physicochem. Eng. Asp.*, vol. *465*, pp. 67–76.

[76] **Qin, Q., Wang, Q., Fu, D., and Ma, J.** (2011). An efficient approach for Pb (II) and Cd (II) removal using manganese dioxide formed in situ, *Chem. Eng. J.*, vol. *172*, no. 1, pp. 68–74.

[77] **Zou, F., Yu, R., Li, R., and Li, W.** (2013). Microwave-assisted synthesis of HKUST-1 and functionalized HKUST-1-@ H3PW12O40: selective adsorption of heavy metal ions in water analyzed with synchrotron radiation, *ChemPhysChem*, vol. *14*, no. 12, pp. 2825–2832.

[78] **Tahmasebi, E., Masoomi, M. Y., and Morsali**, **A.** (2013). Application of mechanosynthesized azine-decorated zinc (II) metal–organic frameworks for highly efficient removal and extraction of some heavy-metal ions from aqueous samples: a comparative study, *Inorg. Chem.*, vol. *54*, no. 2, pp. 425–433.

[79] **Saleem, H., Ra, U., and Davies**, **R. P.** (2016). Microporous and Mesoporous Materials Investigations on post-synthetically modified UiO-66-NH_2 for the adsorptive removal of heavy metal ions from aqueous solution, Microporous and Mesoporous Materials vol. *221*, pp. 238–244.

[80] **Rahimi, E., and Mohaghegh**, **N.** (2015). Removal of Toxic Metal Ions from Sungun Acid Rock Drainage Using Mordenite Zeolite, Graphene Nanosheets, and a Novel Metal-Organic Framework, Mine Water and Environment,vol. *35*, pp 18-28.

[81] **Fang, Q. R., Yuan, D. Q., Sculley, J., Li, J. R., Han, Z. B., and Zhou**, **H. C.** (2010). Functional mesoporous metal-organic frameworks for the capture of heavy metal ions and size-selective catalysis, *Inorg. Chem.*, vol. *49*, no. 24, pp. 11637–11642.

[82] **Yang, Q., Zhao, Q., Ren, S., Lu, Q., Guo, X., and Chen, Z.** (2016). Fabrication of core-shell Fe3O4@ MIL-100 (Fe) magnetic microspheres for the removal of Cr (VI) in aqueous solution, *J. Solid State Chem.*, vol. *244*, pp. 25–30.

[83] **Zhang, J., Xiong, Z., Li, C., and Wu, C.**(2016). Exploring a thiol-functionalized MOF for elimination of lead and cadmium from aqueous solution, *J. Mol. Liq.*, vol. *221*, pp. 43–50.

[84] **Wang, C. C., Du, X. D., Li, J., Guo, X. X., Wang, P., and Zhang, J.** (2016). Photocatalytic Cr (VI) reduction in metal-organic frameworks: A mini-review, *Appl. Catal. B Environ.*, vol. *193*, pp. 198–216.

[85] **Li, X., Gao, X., Ai, L., and Jiang**, **J.** (2015). Mechanistic insight into the interaction and adsorption of Cr (VI) with zeolitic imidazolate framework-67 microcrystals from aqueous solution, *Chem. Eng. J.*, vol. *274*, pp. 238–246.

[86] **Rapti S., Pournara A., and Sarma D..,** (2016). Rapid, green and inexpensive synthesis of high quality UiO-66 amino-functionalized materials with exceptional capability for removal of hexavalent chromium from industrial waste, *Inorg. Chem. Front.*, vol. *3*, no. 5, pp. 635–644.

[87] **Wang, C., Liu, X., Chen, J. P., and Li**, **K.** (2015). Superior removal of arsenic from water with zirconium metal-organic framework UiO-66, *Sci. Rep.*, vol. *5*, p. 16613.

[88] **Maleki, A., Hayati, B., Naghizadeh, M., and Joo, S. W.** (2015). Adsorption of hexavalent chromium by metal organic frameworks from aqueous solution, *J. Ind. Eng. Chem.*, vol. *28*, pp. 211–216.

[89] **Li, L. L., Feng, X. Q., Han, R. P., Zang, S. Q., and Yang, G.,** (2017). Cr (VI) removal via anion exchange on a silver-triazolate MOF, *J. Hazard. Mater.*, vol. *321*, pp. 622–628.

[90] **Zhang Q., Yu J., J Cai J., and Zhang L.,** (2015). A porous Zr-cluster-based cationic metal–organic framework for highly efficient Cr 2 O 7 2− removal from water, *Chem. Commun.*, vol. *51*, no. 79, pp. 14732–14734.

[91] **Wang, K., Tao, X., Xu, J., and Yin**, **N.** (2016). Novel chitosan-MOF composite adsorbent for the removal of heavy metal ions, *Chem. Lett.*, vol. *45*, no. 12, pp. 1365–1368.

[92] **Aboutorabi, L., Morsali, A., Tahmasebi, E., and Buyukgungor, O.** (2016). Metal-organic framework based on isonicotinate N-oxide for fast and highly efficient aqueous phase Cr (VI) adsorption, *Inorg. Chem.*, vol. *55*, no. 11, pp. 5507–5513.

[93] **Rivera, J. M., Rincón, S., Ben Youssef, C., and Zepeda, A.** (2016). Highly efficient adsorption of aqueous Pb (II) with mesoporous metal-organic framework-5: an equilibrium and kinetic study, *J. Nanomater.*, vol. ***2016***.

[94] **Ricco R., Konstas K., and Styles M.,** (2015). Lead (II) uptake by aluminium based magnetic framework composites (MFCs) in water, *J. Mater. Chem. A*, vol. *3*, no. 39, pp. 19822–19831.

[95] **Jamali, A., Tehrani, A. A., Shemirani, F., and Morsali, A.** (2016). Lanthanide metal–organic frameworks as selective microporous materials for adsorption of heavy metal ions, *Dalt. Trans.*, vol. *45*, no. 22, pp. 9193–9200.

[96] **Zhang, J., Xiong, Z., Li, C., and Wu**, **C.** (2016). Exploring a thiol-functionalized MOF for elimination of lead and cadmium from aqueous solution, *J. Mol. Liq.* vol. *221*, September , pp. 43-50.

[97] **Mon, M., Lloret, F., Ferrando-Soria, J., Martí-Gastaldo, C., Armentano, D., and Pardo,E.** (2016). Selective and efficient removal of mercury from aqueous media with the highly flexible arms of a BioMOF, *Angew. Chemie Int. Ed.*, vol. *55*, no. 37, pp. 11167–11172.

[98] **Ke, F., Qiu L., and Yuan Y.,** (2011). Thiol-functionalization of metal-organic framework by a facile coordination-based postsynthetic strategy and enhanced removal of Hg^{2+} from water, *J. Hazard. Mater.*, vol. *196*, pp. 36–43.

[99] **Halder, S., Mondal, J., Ortega-Castro, J., Frontera, A., and Roy, P.,** (2017). A Ni-based MOF for selective detection and removal of Hg^{2+} in aqueous medium: a facile strategy, *Dalt. Trans.*, vol. *46*, no. 6, pp. 1943–1950.

[100] **Liang, L. Chen Q., and Jiang F.,** (2016). In situ large-scale construction of sulfur-functionalized metal–organic framework and its efficient removal of Hg (II) from water, *J. Mater. Chem. A*, vol. *4*, no. 40, pp. 15370–15374.

[101] **Rudd, N. D., Wang H., and Erika M.,** (2016). Highly efficient luminescent metal–organic framework for the simultaneous detection and removal of heavy metals from water, *ACS Appl. Mater. Interfaces*, vol. *8*, no. 44, pp. 30294–30303.

[102] **Luo, F. Chen J., and Dang L.,** (2015). High-performance Hg 2+ removal from ultra-low-concentration aqueous solution using both acylamide-and hydroxyl-functionalized metal–organic framework, *J. Mater. Chem. A*, vol. *3*, no. 18, pp. 9616–9620.

[103] **Huang, L., He, M., Chen, B., and Hu**, **B.** (2015). A designable magnetic MOF composite and facile coordination-based post-synthetic strategy for the enhanced removal of Hg^{2+} from water, *J. Mater. Chem. A*, vol. *3*, no. 21, pp. 11587–11595.

[104] **Sohrabi**, **M. R.,** (2014). Preconcentration of mercury (II) using a thiol-functionalized metal-organic framework nanocomposite as a sorbent, *Microchim. Acta*, vol. *181*, no. 3–4, pp. 435–444.

[105] **Xiong, Y. Y., JQ Li J., and Feng X.,** (2017). Using MOF-74 for Hg^{2+} removal from ultra-low concentration aqueous solution, *J. Solid State Chem.*, vol. *246*, pp. 16–22.

[106] **Luo, X., Shen, T., Ding, L., Zhong, W., Luo, J., and Luo, S.** (2016). Novel thymine-functionalized MIL-101 prepared by post-synthesis and enhanced removal of Hg2+ from water, *J. Hazard. Mater.*, vol. *306*, pp. 313–322.

[107] **Bhattacharjee, S., Lee, Y. R., and Ahn, W. S.** (2015).Post-synthesis functionalization of a zeolitic imidazolate structure ZIF-90: a study on removal of Hg (II) from water and epoxidation of alkenes, *Cryst EngComm*, vol. *17*, no. 12, pp. 2575–2582.

[108] **Yee, K. K., Reimer N., and Liu J.,** (2013). Effective mercury sorption by thiol-laced metal–organic frameworks: in strong acid and the vapor phase, *J. Am. Chem. Soc.*, vol. *135*, no. 21, pp. 7795–7798.

[109] **Liu, T., Che, J., Hu, Y., Dong, X., Liu, X., and Che, C.** (2014). Alkenyl/Thiol-Derived Metal-Organic Frameworks (MOFs) by Means of Postsynthetic Modification for Effective Mercury Adsorption, *Chem. Eur. J.*, vol. *20*, no. 43, pp. 14090–14095.

[110] **Zou, F., Yu, R., Li, R., and Li, W.** (2013). Microwave-assisted synthesis of HKUST-1 and functionalized HKUST-1-@H 3PW12O40: Selective adsorption of heavy metal ions in water analyzed with synchrotron radiation, *ChemPhysChem*, vol. *14*, no. 12, pp. 2825–2832.

[111] **Cheng, X., Zhang A., and Song C.,** (2015). Size-controlled silver nanoparticles stabilized on thiol-functionalized MIL-53 (Al) frameworks, *Nanoscale*, vol. *7*, no. 21, pp. 9738–9745.

[112] **Conde-González, J. E., Peña-Méndez, E. M., Rybáková, S., Pasán, J., Ruiz-Pérez, C., and Havel**, **J.** (2016). Adsorption of silver nanoparticles from aqueous solution on copper-based metal organic frameworks (HKUST-1), *Chemosphere*, vol. *150*, pp. 659–666.

[113]**Zhang, Y., Xie, Z., Wang, Z., Feng, X., Wang, Y., and Wu**, **A.** (2016). Unveiling the adsorption mechanism of zeolitic imidazolate framework-8 with high efficiency for removal of copper ions from aqueous solutions, *Dalt. Trans.*, vol. *45*, no. 32, pp. 12653–12660.

[114] **Bakhtiari N., and Azizian**, S. (2015). Adsorption of copper ion from aqueous solution by nanoporous MOF-5: a kinetic and equilibrium study, *J. Mol. Liq.*, vol. *206*, pp. 114–118.

[115] **Zheng, T. T., Shi S., and Li J. .,** (2017). Aluminescent metal-organic framework with high sensitivity for detecting and removing copper ions from simulated biological fluids, *Dalt. Trans.*, vol. *46*, no. 8, pp. 2456–2461, 2017.

[116] **Ding, L., Shao P., and Yu Luo Y.**, (2020). Functionalization of UiO-66-NH_2 with rhodanine via amidation: Towarding a robust adsorbent with dual coordination sites for selective capture of Ag (I) from wastewater, *Chem. Eng. J.*, vol. *382*, p. 123009.

[117] **Zhao, Y., Pan, Y., Liu, W., and Zhang, L.** (2015). Removal of heavy metal ions from aqueous solutions by adsorption onto ZIF-8 nanocrystals, *Chem. Lett.*, vol. *44*, no. 6, pp. 758–760.

[118]**Fang, Q. R., Yuan, D. Q., Sculley, J., Li, J. R., Han, Z. B., and Zhou, H. C.** (2010).Inorg. Chem. vol. *49*, 11637–11642.

[119] **Saleem, H., Rafique, U., and Davies, R. P.** (2016). Investigations on post-synthetically modified UiO-66-NH2for the adsorptive removal of heavy metal ions from aqueous solution, *Microporous Mesoporous Mater.*, vol. *221*, pp. 238–244.

[120]**Tahmasebi, E., Masoomi, M. Y., Yamini, Y., and Morsali**, **A.** (2015). Application of mechanosynthesized azine-decorated zinc(II) metal-organic frameworks for highly efficient removal and extraction of some heavy-metal ions from aqueous samples: A comparative study, *Inorg. Chem.*, vol. *54*, no. 2, pp. 425–433.

[121]**Yang, Q., Zhao, Q., Ren, S., Lu, Q., Guo, X., and Chen**, **Z.** (2016). Journal of Solid State Chemistry Fabrication of core-shell Fe_3 O_4 @ MIL-100 (Fe) magnetic microspheres for the removal of Cr (VI) in aqueous solution, *J. Solid State Chem.*, vol. *244*, pp. 25–30.

[122] **Schmuhl, R., Krieg, H. M., and Keizer, K.** (2001). Adsorption of Cu (II) and Cr (VI) ions by chitosan: Kinetics and equilibrium studies, *Water Sa*, vol. *27*, no. 1, pp. 1–8.

[123] **Zhu, Y., Hu, J., and Wang, J.** (2012). Competitive adsorption of Pb (II), Cu (II) and Zn (II) onto xanthate-modified magnetic chitosan, *J. Hazard. Mater.*, vol. *221*, pp. 155–161.

[124] **Zhou, L., Wang, Y., Liu, Z., and Huang, Q.** (2009). Characteristics of equilibrium, kinetics studies for adsorption of Hg (II), Cu (II), and Ni (II) ions by thiourea-modified magnetic chitosan microspheres, *J. Hazard. Mater.*, vol. *161*, no. 2–3, pp. 995–1002, 2009.

[125] **Cheetham, A. K., Férey, G., and Loiseau, T.** (1999). Open-framework inorganic materials, *Angew. Chemie Int. Ed.*, vol. *38*, no. 22, pp. 3268–3292.

[126] **Hong, B. D., Hwang, Y. K., Serre, C., and Chang, J.** (2009). Porous Chromium Terephthalate MIL-101 with Coordinatively Unsaturated Sites : Surface Functionalization, Encapsulation, Sorption and Catalysis, pp. 1537–1552.

[127] **Ferey G., and Draznieks, M., Serre, C.; Millange, F,** (2005). *Acc. Chem. Res*, vol. *38*, p. 217.

[128] **LoiseauT., and Férey, G.,** (2007). Crystalline oxyfluorinated open-framework compounds: Silicates, metal phosphates, metal fluorides and metal-organic frameworks (MOF), *J. Fluor. Chem.*, vol. *128*, no. 4, pp. 413–422.

[129]**Ingleson, M. J., Barrio, J. P., Guilbaud, J., Khimyak, Y. Z., and Rosseinsky, M. J.** (2008). Framework functionalization triggers metal complex binding, *Chemical Communications*, vol. *23*, pp.2680–2682.

[130] **Yong, K., Do-Yong, H., Jong-San C., and Sung, H**. (2008). Amine Grafting on Coordinatively Unsaturated Metal Centers of MOFs, Consequences for Catalysis and Metal Encapsulation, *Angewandte chemie*, vol. *120*, no. 22, pp. 4212–4216.

[131] **Wang Z., and Cohen, S. M.,** (2007). Postsynthetic Covalent Modification of a Neutral Metal−Organic Framework. *Journal of the American Chemical Society*, *vol.129*, no.41, pp 12368–12369.

[132] **Wang, X., Tseng, Y., Chan, J. C. C., and Cheng, S.** (2005). Catalytic applications of aminopropylated mesoporous silica prepared by a template-free route in flavanones synthesis, *Journal of Catalysis***.** Vol. *233*, no. 2, pp 266-275.

[133] **Cooney, D. O.,** (1999). *Adsorption Design for Wastewater Treatment*, Boca Raton. Lewis publishers.

[134] **Tchobanoglous D. H. S. G., and F. L. B.** (2002). *Wastewater Engineering Treatment and Reuse*, 4th Edition. McGraw- Hill professional.

[135] **Yu, Z., Qi, T., Qu, J., Wang, L.,and Chu, J.** (2009). Removal of Ca (II) and Mg (II) from potassium chromate solution on Amberlite IRC 748 synthetic resin by ion exchange, *Journal of Hazardous Materials*,Vol. *167*, no.(1–3), pp. 406-412.

[136] **D. W. Green**, **and Perry, R. H.** (1999). *Perry's Chemical Engineering Handbook*, 7th Editio. New York: McGrew-Hill.

[137] **Harriot, P. and L. W. (**1993) *Unit operation of Chemical Engineering*. McGrow-Hill,.

[138] **Smith**, **J. C., and W. L. M.** (1985). *Unit Operation of Chemical Engineering*. McGraw-Hill, 1985.

[139] **Ho, Y. S.** (2003). Removal of Copper Ions from Aqueous Solution by Tree Fern, *Wat. Res.*, vol. *37*, pp. 2323–2330.

[140] **Langmuir**, **I.** (2016). The constitution and fundamental properties of solids and liquids. Part I solids, *J. Am. Chem. Soc.*, vol. *38*, pp. 2221–2295, 1916.

[141] **Limousin, G. Gaudet, J. P., Charlet, L., Szenknect, S., Barthes, V., and Krimissa, M. (**2007). Sorption isotherms: a review on physical bases, modeling, and measurement, *Appl. geochemistry*, vol. *22*, no. 2, pp. 249–275.

[142] **Muhammad, N., and J. Parr, (**1998). Adsorption of Heavy Metals in Slow Sand Filters, , Islamabad, Pakistan, *Proc. 24th WEDC Int. Conf. Water Treat.*, pp. 346–349.

[143] **Kumara, N. T. R. N., Hamdan, N., Petra, M. I., Tennakoon, K. U. and Ekanayake, P. (**2014). Equilibrium Isotherm Studies of Adsorption of Pigments Extracted from Kuduk-kuduk (Melastoma malabathricum L . Pulp onto TiO_2 Nanoparticles, *Journal of Chemistry*, Vol. *2014*, pp. 1-6.

[144] **Soto, J. C. P. M. L., A. Moure, Domínguez,H. (**2011). Recovery, concentration, and purification of phenolic compounds by adsorption: a review, *J. Food Eng.*, vol. *105*, no. 1, pp. 1–27,

[145] **Mirzaei, P. K. A., and Ebadi, A. (**2013). Kinetic and equilibrium modeling of single and binary adsorption of methyl tert-butyl ether (MTBE) and tert-butyl alcohol (TBA) onto nano- perfluorooctyl alumina, *Chem. Eng. J.*, no. *231*, pp. 550–560 .

[146] **Weber Jr, W. J., McGinley, P. M., and Katz, L. E.** (1991) Sorption phenomena in subsurface systems: concepts, models and effects on contaminant fate and transport, *Water Res.*, vol. *25*, no. 5, pp. 499–528.

[147] **Pagnanelli, F., Trifoni, M., Beolchini, F., Esposito, A., Toro, L.,and Veglio, F. (**2001). Equilibrium biosorption studies in single and multi-metal systems, *Process Biochem.*, vol. *37*, no. 2, pp. 115–124,.

[148] **Puranik, K. P. P., and Modak, J.** (2005) A comparative study of the mass transfer kinetics of metal biosorption by microbial biomass, *Hydrometallurgy*, vol. *52*, pp. 189–197.

[149] **Lagergren, S.** (1989) About the theory of so-called adsorption of soluble substances, *K. Seventeen Hand*, vol. *24*, pp. 1–39, 1989.

[150] **Ho Y. S., and McKay, G. (**1999) Pseudo-second order model for sorption processes, *Process Biochem.*, vol. *34*, no. 5, pp. 451–465.

[151] **Weber , W. J., and Morris, J. C.** (1963) Kinetics of adsorption on carbon from solution, *J. Sanit. Eng. Div.*, vol. *89*, no. 2, pp. 31–60.

[152] **Srivastava, S. K., Tyagi, R., Pant N., and Pal, N**. (1989) The application of nature absorbents for heavy metals uptake from contaminated water, *Environ. Technol.*, vol. *10*, pp. 275–282.

[153] **Markovska, V. N. L., and Meshko, V.,** (2001) Adsorption of basic dyes in a fixed bed column, *Korean J. Chem. Eng.*, vol. *18*, pp. 190–195.

[154] **Muhamad, H., Doan, H., and Lohi, A.** (2010) Batch and continuous fixed-bed column biosorption of Cd2+ and Cu2+, *Chem. Eng. J.*, vol. *158*, no. 3, pp. 369–377.

[155] **Thomas, H. C.** (1944) Heterogeneous ion exchange in a flowing system, *J. Am. Chem. Soc.*, vol. *66*, no. 10, pp. 1664–1666, 1944.

[156] **C. Tien,** *Fixed-Bed Adsorption Models, and Fixed-Bed Design Calculations*. 2019.

[157] **Ahnfeldt, T., Guillou N., and Gunzelmann D.,** (2009). Organic Framework with an Unprecedented Aluminum-Containing, Angew. Chem. Int. Ed, vol. *4*, pp. 5163–5166.

[158] **Lin, Y., Kong, C., and Chen, L.,** (2012). Direct synthesis of amine-functionalized MIL-101 (Cr) nanoparticles and application for CO_2 capture, *RSC Adv.*, vol. *2*, no. 16, pp. 6417–6419, 2012.

[159] **Wei, H., Teo, B., Chakraborty, A., and Kayal, S.** (2017). Evaluation of CH_4 and CO_2 Adsorption on HKUST-1 and MIL-101(Cr) MOFs Employing Monte Carlo Simulation and Comparison with Experimental Data, *Appl. Therm. Eng.*, vol. *101*. pp. 891-900.

[160] **Hu, T.**,**Jia Q., and He S.**, (2017). Novel functionalized metal-organic framework MIL-101 adsorbent for capturing oxytetracycline, *J. Alloys Compd.*, vol. 727, pp. 114–122.

[161] **Luo, X., Ding, L., and Luo, J.** (2015). Adsorptive removal of Pb(II) ions from aqueous samples with amino-functionalization of metal-organic frameworks MIL-101(Cr), *J. Chem. Eng. Data*, vol. 60, no. 6, pp. 1732–1743.

[162] **Murugesan, S., Myers, K., and Subramanian, V. R.** (2011). Amino-functionalized and acid-treated multi-walled carbon nanotubes as supports for electrochemical oxidation of formic acid, *Appl. Catal. B Environ.*, vol. *103*, no. 3–4, pp. 266–274.

[163] **Ramanathan, T., Fisher, F. T., Ruoff, R. S., and Brinson, L. C.,** (2005). Amino-functionalized carbon nanotubes for binding to polymers and biological systems, *Chem. Mater.*, vol. *17*, no. 6, pp. 1290–1295.

[164] **Hwang, Y. K., Do-Young H., and Jong-San C.,** (2008). Amine grafting on coordinatively unsaturated metal centers of MOFs: Consequences for catalysis and metal encapsulation, *Angew. Chemie - Int. Ed.*, vol. *47*, no. 22, pp. 4144–4148.

[165] **Liu, Y., Shen, X., Xian, Q., Chen, H., Zou, H., and Gao**, **S.** (2006). Adsorption of copper and lead in aqueous solution onto bentonite modified by 4′-methylbenzo-15-crown-5, *J. Hazard. Mater.*, vol. *137*, no. 2, pp. 1149–1155.

[166] **Imamoglu, M., and Tekir, O.** (2008). Removal of copper (II) and lead (II) ions from aqueous solutions by adsorption on activated carbon from a new precursor hazelnut husks, *Desalination*, vol. *228*, no. 1–3, pp. 108–113.

[167] **Jha, V. K., Matsuda, M., and Miyake, M.** (2008). Sorption properties of the activated carbon-zeolite composite prepared from coal fly ash for Ni^{2+}, Cu^{2+}, Cd^{2+}, and Pb^{2+}, *J. Hazard. Mater.*, vol. *160*, no. 1, pp. 148–153.

[168] **Melichová, Z., and Hromada, L.** (2013). Adsorption of Pb^{2+} and Cu^{2+} ions from aqueous solutions on natural bentonite, *Pol. J. Environ. Stud*, vol. *22*, no. 2, pp. 457–464.

[169] **Baek, M. H., Ijagbemi, C. O., Se-Jin, O., and Kim, D. S.** (2010). Removal of Malachite Green from aqueous solution using degreased coffee bean, *J. Hazard. Mater.*, vol. *176*, no. 1–3, pp. 820–828, .

[170] **Sprynskyy, M., Buszewski, B., Terzyk, A. P., and Namieśnik, J.,** (2006). Study of the selection mechanism of heavy metal (Pb^{2+}, Cu^{2+}, Ni^{2+}, and Cd^{2+}) adsorption on clinoptilolite, *J. Colloid Interface Sci.*, vol. *304*, no. 1, pp. 21–28.

[171] **Malamis, S., and Katsou, E.,** (2013). A review on zinc and nickel adsorption on natural and modified zeolite, bentonite and vermiculite: Examination of process parameters, kinetics, and isotherms, *J. Hazard. Mater.*, vol. *252*, pp. 428–461.

[172]**Zhang, M.** (2011). Adsorption study of Pb (II), Cu (II) and Zn (II) from simulated acid mine drainage using dairy manure compost, *Chem. Eng. J.*, vol. *172*, no. 1, pp. 361–368,.

[173]**Padilla-Ortega, E., Leyva-Ramos, R., and Flores-Cano, J. V.** (2013). Binary adsorption of heavy metals from aqueous solution onto natural clays, *Chem. Eng. J.*, vol. *225*, pp. 535–546.

[174]**Chakravarty S.,Ashok M., and Sudha T.,** (2010). Removal of Pb (II) ions from aqueous solution by adsorption using bael leaves (Aegle marmelos), *J. Hazard. Mater.*, vol. *173*, no. 1–3, pp. 502–509.

[175]**Jang, A., Seo, Y., and Bishop, P. L.** (2005). The removal of heavy metals in urban runoff by sorption on mulch, *Environ. Pollut.*, vol. *133*, no. 1, pp. 117–127.

[176]**Kadirvelu, K., Goel, J., and Rajagopal**, **C.** (2008). Sorption of lead, mercury and cadmium ions in multi-component system using carbon aerogel as adsorbent, *J. Hazard. Mater.*, vol. *153*, no. 1–2, pp. 502–507.

[177] **Futalan, C. M., Kan, C. C. , Dalida, M. L., Hsien, K. J., Pascua, C., and Wan, M. W.** (2011). Comparative and competitive adsorption of copper, lead, and nickel using chitosan immobilized on bentonite, *Carbohydr. Polym.*, vol. *83*, no. 2, pp. 528–536.

[178] **Mohan, D., and Singh, K. P.** (2002). Single-and multi-component adsorption of cadmium and zinc using activated carbon derived from bagasse an agricultural waste, *Water Res.*, vol. *36*, no. 9, pp. 2304–2318.

[179] **Lyubchik, S. I. *et al.*,** (2004). Kinetics and thermodynamics of the Cr (III) adsorption on the activated carbon from co-mingled wastes, *Colloids Surfaces A Physicochem. Eng. Asp.*, vol. *242*, no. 1–3, pp. 151–158.

[180] **Li, H., Xiao, D. L., He, H., Lin, R., and Zuo, P. L.** (2013) . Adsorption behavior and adsorption mechanism of Cu(II) ions on amino-functionalized magnetic nanoparticles, *Trans. Nonferrous Met. Soc. China (English Ed.*, vol. *23*, no. 9, pp. 2657–2665.

[181] **Yao, Z. Y., Qi, J. H., and Wang, L. H.** (2010). Equilibrium, kinetic and thermodynamic studies on the biosorption of Cu(II) onto chestnut shell, *J. Hazard. Mater.*, vol. *174*, no. 1–3, pp. 137–143.

[182] **Taylor, P., Pilli, S. R., Goud, V. V., and Mohanty, K.** (2012) Biosorption of Cr (VI) on immobilized Hydrilla verticillata in a continuous up-flow packed bed : prediction of kinetic parameters and breakthrough curves, Desalination and Water Treatment, vol. *15*, no.5, pp. 115-124.

[183] **Abustan, I., and Bello O. S.,** (2011). Fixed-bed column study for Cu (II) removal from aqueous solutions using rice husk based activated carbon, International Journal of Engineering & Technology vol. *11*, no.1, pp. 248-252.

CURRICULUM VITAE

Name Surname **:** FADHIL ABID ELAIWI

EDUCATION

- **B.Sc.** **:** 1999, Iraq-Baghdad University, College of Engineering, Chemical Engineering Department
- **M.Sc.** **:** 2002, Iraq-Baghdad University, College of Engineering, Chemical Engineering Department

PROFESSIONAL EXPERIENCE:

- **2003-2005** Supervising Engineer In Al-Nahar Company for Production of Detergent And chemical Acids, Baghdad, Iraq.
- **Since 2005** A lecturer In Al-Furat Al-Awsat Technical University / Technical College /al-Mussiab, Iraq.
- **2015-2019 Ph.D.** Candidate at ISTANBUL Technical University, Chemical Engineering Department.

PUBLICATIONS, PRESENTATIONS, AND PATENTS ON THE THESIS

- **ELAIWI, F. A.,** and SIRKECIOGLU, A. (2020)**.** Amine-functionalized metal-organic frameworks MIL-101(Cr) adsorbent for copper and cadmium ions in single and binary solution, separation science and technology, vol. *55*, no.18, pp.3362-3374.